Polarimetry of the peculiar elliptical galaxy, NGC 5128

Berry, David Stuart

Polarimetry of the Peculiar Elliptical Galaxy, NGC 5128

by

David Stuart Berry

A thesis submitted to the University of Durham for the degree of Doctor of Philosophy

May, 1985

ABSTRACT

A high resolution linear polarization map is presented of the peculiar elliptical galaxy NGC5128 (= Centaurus A) and is used to investigate the polarizing mechanism at work in the dust lane.

The spatial distribution and orientation of the polarization, together with a possible correlation between the degree of polarization and the extinction through the dust, suggest scattering from aligned non-spherical grains as the probable cause of the polarization.

A computer model of the passage of light from an extended source, through a dust cloud of arbitrary shape, has been developed, using a backward Monte-Carlo method. This model has been applied to an NGC5128-like system and it is found that in order to obtain the structure and degree of polarization observed in NGC5128, the dust needs to be aligned by a toroidal magnetic field of about the same strength as that in our Galaxy.

It is suggested that the magnetic field could have originally belonged to a spiral galaxy which subsequently collided with NGC5128.

CONTENTS

CONTENTS

CONTENTS

CONTENTS

CHAPTER 1

THE POLARIZATION OF LIGHT

This chapter looks at the nature of polarized light and the physical processes which produce it.

1.1 The nature of polarized light

Light is an electro-magnetic wave and can be described by two sinusoidal vectors, namely the electric (E) and magnetic (H) vectors. These vectors are normal to each other and their amplitudes vary with position and time in such a way as to produce a wave which travels in a direction normal to both the E and the H vectors (fig. 1.1). To characterize the wave it is only necessary to specify its propagation vector and its E vector, since given these two it is possible to determine the H vector.

Fig. 1.1
An electro-magnetic wave.

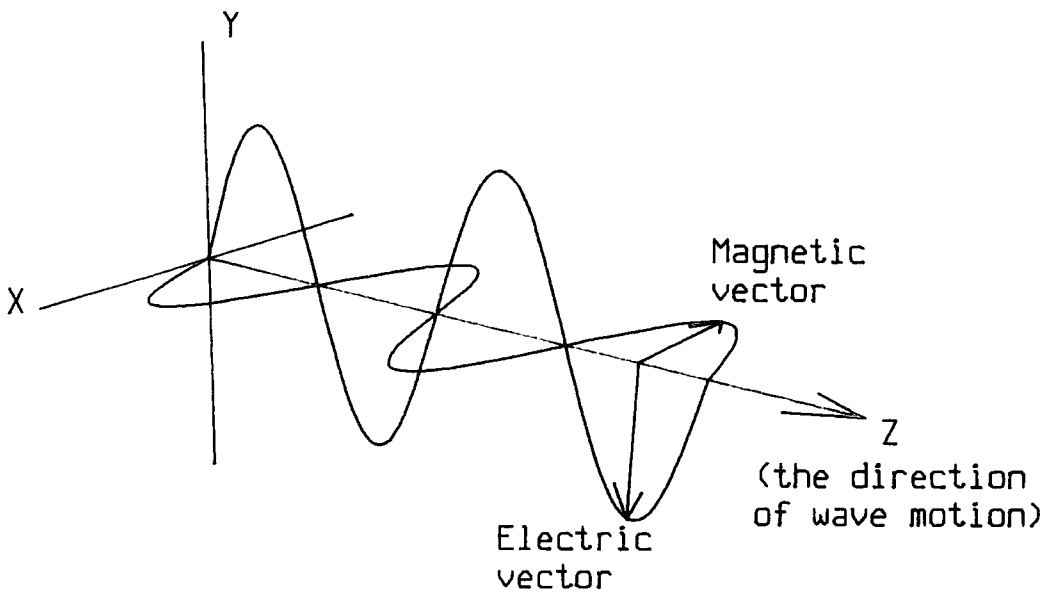

There are several parameters connected with these two vectors that produce observable properties in light. For instance the square of the amplitude of the E vector determines the intensity of the light, and the wavelength of the E vector wave determines the colour of the light. One such parameter, namely the orientation of the E vector, gives rise to the phenomenon of polarization.

Given a particular propagation vector, the direction of the E vector is fixed to lie within the plane which is normal to the propagation vector. However, if we fix a reference direction in this plane, then the angle the E vector makes with this reference direction is not normally fixed and it can take any value. In natural, or unpolarized light, the orientation of the E vector varies in a random way with time and position, showing no preference for any particular direction. If, however, the orientation of the E vector is not uniformly random, but shows some order or preference for particular values, then the light is said to be polarized. There are two basic types of polarization, plane and circular.

1.1.1 Plane polarization

Light is said to be completely plane (or linearly) polarized if the orientation of the E vector is constant. Consider a wave travelling along the z axis of a

Cartesian co-ordinate system. The plane which is normal to the direction of propagation is the xy plane, and the E vector is thus constrained to lie in the xy plane. If θ is the angle between the E vector and the y axis, then for completely plane polarized light, θ is fixed. For an arbitrary value of θ, the E vector can be resolved into two components, E_x parallel to the x axis, and E_y parallel to the y axis. In fig. 1.2 the E vector of a plane polarized beam is shown, resolved into x and y components. The resultants vectors are indicated by arrows for various positions in the wave, and the envelope of all such resultant vectors shown as a dashed line. Fig. 1.3 is the same as fig. 1.2 except that the viewpoint has been changed to look down the z axis. The resultant vectors of fig 1.2 are consequently shown superimposed and can be seen to be parallel (as would be expected since θ is constant). Each component of the E vector varies as a wave, the waves being in phase.

1.1.2 Circular polarization

If the two components of the E vector are not in phase, then the resultant vector does not have a constant orientation, but rotates. In addition, if the phase difference between the two components is exactly one quarter of a wavelength, and the two E vector components

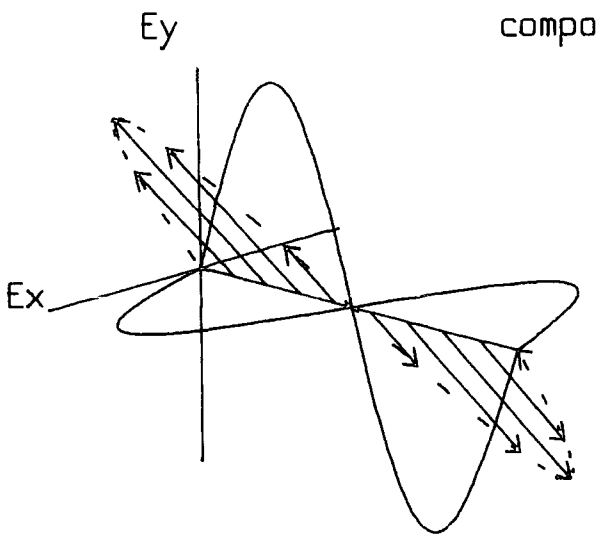

Fig. 1.2

The electric vector of a plane polarized beam resolved into X and Y components.

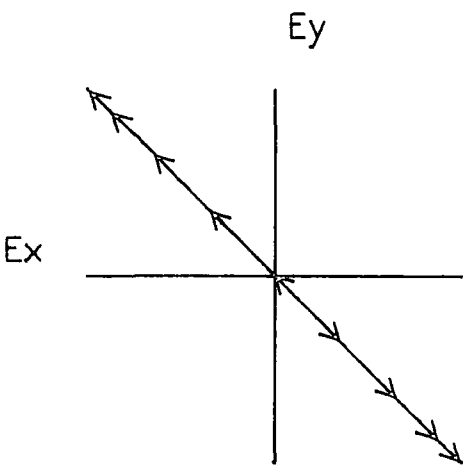

Fig. 1.3

A view down the direction of propagation of fig. 1.2.

are of equal amplitude, then the resultant E vector will be of constant amplitude and so will describe a circle (fig.s 1.4 and 1.5). Light with this property is circularly polarized.

If two light beams with different polarization are combined, then the resultant polarization can be found by the vector addition of the two original E vectors. Thus if we combine a circularly polarized beam, described by

$$\underline{E}=(A.\mathrm{Sin}(u),\ A.\mathrm{Cos}(u))$$

where $u=\omega t+z/\lambda$ and A is a constant

with a linearly polarized beam, described by

$$\underline{E}=(B.\mathrm{Sin}(u+\alpha)\ ,\ C.\mathrm{Sin}(u+\alpha)\ )$$

where B,C and α are constants

then the resultant E vector is

$$\underline{E}=(A.\mathrm{Sin}(u)+B.\mathrm{Sin}(u+\alpha)\ ,\ A.\mathrm{Cos}(u)+C.\mathrm{Sin}(u+\alpha)\ )$$

It can be shown that this represents an ellipse in E_x and E_y.

Thus the resultant vector describes an ellipse and the resultant light beam is said to have elliptical polarization. By a reverse argument it can be shown that any elliptically polarized beam can be separated into a linearly polarized beam and a circularly polarized beam. In practice, elliptically polarized light is formed in the

Fig. 1.4

The electric vector of a circularly polarized resolved into X and Y components.

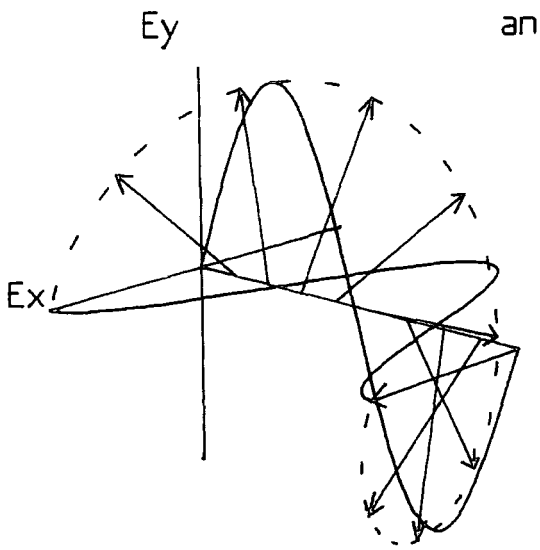

Fig. 1.5

A view down the direction of propagation of fig. 1.4.

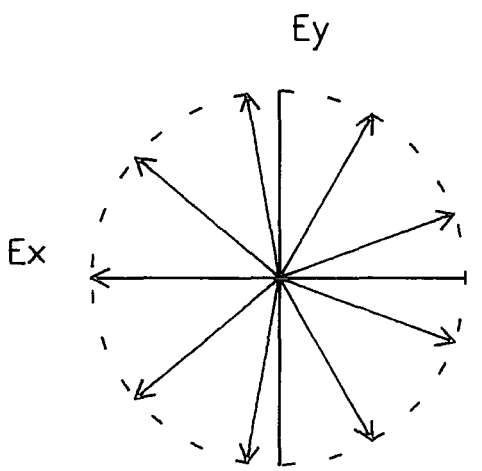

same way as circularly polarized light, by the retardation of one component of the E vector. Elliptical rather than circular polarization, is obtained if the two components of the E vector are not of equal amplitude, or the phase retardation is not exactly half a wavelength (fig.s 1.6 and 1.7). Both linear and circular polarization are extremal cases of elliptical polarization. Linear polarization can be described as elliptical polarization where the eccentricity of the ellipse (formed by the E vector as it rotates), is unity, and circular polarization can be described as elliptical polarization with eccentricity of zero.

Light with any form of polarization can be combined with unpolarized light to form partially polarized light.

1.1.3 Partial polarization

The polarization of a light beam can be investigated by the use of polarizers. An ideal polarizer passes only the component of the E vector which is parallel to its preferred axis, the orthogonal component being absorbed by the polarizer. The physical quantity which is measured in such a situation is the light intensity which is proportional to the mean squared E vector amplitude.

Fig. 1.6

The electric vector of an elliptically polarized beam resolved into X and Y components.

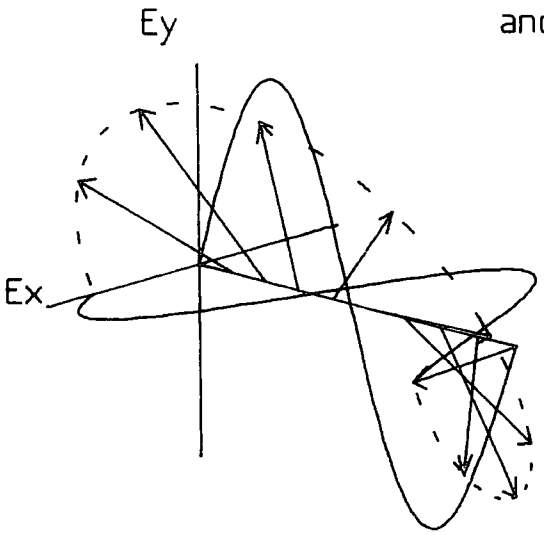

Fig. 1.7

A view down the direction of propagation of fig. 1.6.

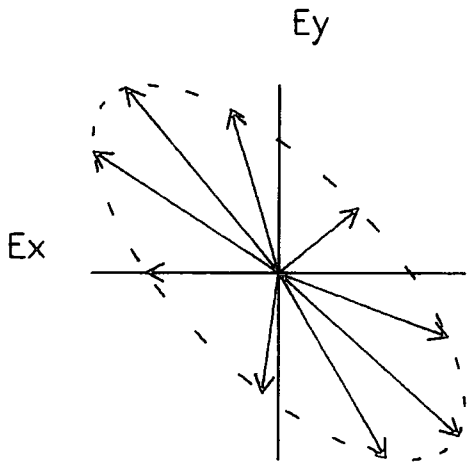

THE POLARIZATION OF LIGHT

If a completely plane polarized light beam is incident on an ideal polarizer which is then rotated, then a particular orientation of the polarizer can be found at which no light emerges. At this point the preferred axis of the polarizer is normal to the E vector of the incoming light and so all the light is absorbed. Likewise, if the polarizer is positioned with its preferred axis parallel to the incoming E vector, then no light is absorbed. The relationship between the intensity passed, and the orientation of the incoming E vector is given by Malus' law,

$$I_{out} = I_{in} . Cos^2(\theta)$$

where I_{in} and I_{out} are the total intensities of the incoming and the outgoing light respectively, and θ is the angle between the incoming E vector and the polarizer's preferred axis.

In unpolarized light, the E vector has no preferred direction and consequently the time averaged component of the E vector has the same amplitude in all directions. Thus, if the E vector is resolved into two orthogonal components, equal intensity is carried by each component, so if unpolarized light is passed through a polarizer, the intensity of the light is halved irrespective of the orientation of the polarizer.

If partially plane polarised light (that is,

plane polarized light combined with unpolarized light) is passed through a polarizer, the emergent intensity will be the sum of the intensities due to the polarized and unpolarized light taken separately. That is

$$I_{out} = \frac{I_u}{2} + I_p \cdot \cos^2(\theta)$$

where I_u is the intensity of the unpolarized light. Thus there will be no orientation of the polarizer at which all the light is absorbed.

A point to be noted is that there is no way to distinguish between unpolarized and circularly polarized light by the use of a polarizer alone. This is because the E vector of a circularly polarized beam has equal components in all directions, as does unpolarized light. Likewise, elliptical and partial plane polarization are indistinguishable without resorting to more complicated techniques.

1.1.4 Stokes parameters

As the above general introduction to the nature of polarized light was more qualitative than quantitative, in this section we shall look at a way of quantitatively describing polarized light.This is most easily done by describing the light in terms of four quantities called the Stokes parameters. Firstly, we shall consider a simple

wave solution of Maxwell's equation, and then deal with real light which is a superposition of many such simple waves.

1.1.4.1 Simple waves

Consider a simple wave travelling along the Z axis. Define some reference direction Y, perpendicular to Z and let the normal to both Y and Z be X. By E_x we shall refer to the component of the E vector parallel to X, and by E_y to the component parallel to Y. These components are complex oscillating quantities:

$$E_j = a_j \cdot e^{-\varepsilon_j} \cdot e^{-kz+i\theta} \qquad \text{---- 1.1}$$

where a_j is the amplitude, and ε_j is the phase of each component, j=X or Y.

The Stokes parameters are defined as

$$\left.\begin{aligned} I &= \langle E_y \cdot E_y^* + E_x \cdot E_x^* \rangle \\ Q &= \langle E_y \cdot E_y^* - E_x \cdot E_x^* \rangle \\ U &= \langle E_y \cdot E_x^* + E_y^* \cdot E_x \rangle \\ V &= i\langle E_y \cdot E_x^* - E_y^* \cdot E_x \rangle \end{aligned}\right\} \qquad \text{---- 1.2}$$

where * ≡ complex conjugation

and $\langle\rangle$ ≡ time averaging

(a constant factor common to them all has, for convenience, been omitted). They are real and satisfy the

relationship

$$I^2 = Q^2 + U^2 + V^2 \qquad \text{---- 1.3}$$

The Stokes parameter I, is the square of the resultant E vector amplitude, and is thus the total intensity of the wave. The other parameters have the same dimension and describe the way the intensity is distributed between E_x and E_y. The Stokes parameters can be described in terms of real quantities by substituting the above definitions of Ex and Ey (equation 1.1), into the Stokes parameter definitions (equations 1.2), to get:

$$\left.\begin{aligned} I &= a_y^2 + a_x^2 \\ Q &= a_y^2 - a_x^2 \\ U &= 2.a_y.a_x.\mathrm{Cos}\ \delta \\ V &= 2.a_y.a_x.\mathrm{Sin}\ \delta \end{aligned}\right\} \qquad \text{---- 1.4}$$

where $\delta = \varepsilon_y - \varepsilon_x$

We can relate the Stokes parameter description of polarization, to the geometric picture developed earlier, by considering a general elliptically polarized beam with E vector components described by:

$$E_x = a.(\mathrm{Cos}(\theta).\mathrm{Cos}(\alpha).\mathrm{Cos}(\beta) + \mathrm{Sin}(\theta).\mathrm{Sin}(\alpha).\mathrm{Sin}(\beta))$$

$$E_y = a.(\mathrm{Sin}(\theta).\mathrm{Cos}(\alpha).\mathrm{Sin}(\beta) - \mathrm{Cos}(\theta).\mathrm{Sin}(\alpha).\mathrm{Cos}(\beta))$$

where $\theta = \omega t + kz$

α= inclination of the major axis to the Y axis

$\mathrm{Tan}(\beta)$= ellipticity (the ratio of major to minor axis)

which can be re-written as

$$E_x = a_x . Sin(\theta+\varepsilon_x)$$

$$E_y = a_y . Sin(\theta+\varepsilon_y)$$

where $a_x^2 = a^2 . (Cos^2(\alpha).Cos^2(\beta)+Sin^2(\alpha).Sin^2(\beta))$

$$a_y^2 = a^2 . (Cos^2(\beta).Sin^2(\alpha)+Cos^2(\alpha).Sin^2(\beta))$$

$$Tan(\varepsilon_x) = -Cot(\alpha).Cot(\beta)$$

$$Tan(\varepsilon_y) = Tan(\alpha).Cot(\beta)$$

So in terms of a, α and β, the Stokes parameters are

$$\left.\begin{aligned} I &= a^2 \\ Q &= a^2 . Cos(2\beta).Cos(2\alpha) \\ U &= a^2 . Cos(2\beta).Sin(2\alpha) \\ V &= a^2 . Sin(2\beta) \end{aligned}\right\} \qquad 1.5$$

Note that since Q contains a $Cos(2\alpha)$ factor, it measures the intensity parallel to the X axis, and since U contains a $Sin(2\alpha)$ factor, it measures the intensity parallel to the Y axis. V measures the circularly polarized component, since if $Tan(\beta)=0$ (linear polarization) then V=0, and if $Tan(\beta)=1$ (circular polarization), then $V=a^2$.

The four Stokes parameters I,Q,U and V can be described as a Stokes vector (I,Q,U,V). In order to interpret the numbers in a Stokes vector, the reference

direction used in the definition of the Stokes parameters (in this case, the Y direction) must be known. A Stokes vector given with respect to one reference direction, can be transformed to refer to another reference direction by changing the value of α in equations 1.5. I and V are unaffected by this transformation, as would be expected since they refer to physical quantities (total intensity and circularly polarized intensity) which should not depend on the particular frame of reference used to measure them in.

1.1.4.2 Real light

Real light consists of many (generally incoherent) simple waves combined together. The Stokes parameters of real light are defined to be the sum of the corresponding Stokes parameters of all the component simple waves. i.e.

$$\left.\begin{aligned} I &= \sum_i I_i \\ Q &= \sum_i Q_i \\ U &= \sum_i U_i \\ V &= \sum_i V_i \end{aligned}\right\} \qquad \text{1.6}$$

It can be shown (see Van De Hulst, 1957) that it is impossible by means of any instruments to distinguish between various incoherent sums of simple waves that may

together form a beam with the same Stokes parameters. This is known as the Principal of Optical Equivalence. It should be noted that the above definitions are not useful if the individual simple waves which make up the real light have not got a random phase distribution. Each Stokes parameter represents a light intensity and in order to add them together correctly, interference effects must be taken into account. Two simple waves of equal intensity might, for instance, add together to give zero intensity if their phase difference is suitable. The simple algebraic addition of intensities used in the above definitions (equations 1.6) would in this case be wrong. However, if the phases of the component simple waves are randomly distributed, then the effects of interference will tend to cancel out so that the intensities can be simply added. This assumption can be made for most astronomical situations and consequently Stokes vectors can be added or subtracted simply. For instance, if light originating in some star has Stokes vector S1, and the general night sky background light has Stokes vector S2, then the Stokes vector measured for light coming from the direction of the star will be S3=S1+S2 . If S3 is measured and S2 can be estimated, then the polarization of the star light can be calculated by subtracting the Stokes vector for the night sky light, S2 , from the total observed Stokes vector S3, to give S1. A situation in which the

above assumption cannot be made is if the E vector of a simple wave is resolved into two components to form two coherent simple waves. If each simple wave undergoes a different process (such as happens in scattering from non-spherical particles) then the sum of the resultant Stokes vectors will not correctly describe the resultant wave, since the simple algebraic addition used, will not take into account the interference effects caused by the original two waves being coherent.

1.1.4.3 Polarized intensity

Given that the above assumption of a random phase distribution among the component simple waves is satisfied, then it can be seen that

$$I^2 = (\sum_i I_i)^2$$

$$= \sum_i I_i^2 + 2.\sum_{i \neq j} (I_i . I_j)$$

Likewise

$$Q^2 = \sum_i Q_i^2 + 2.\sum_{i \neq j} (Q_i . Q_j)$$

$$U^2 = \sum_i U_i^2 + 2.\sum_{i \neq j} (U_i . U_j)$$

$$V^2 = \sum_i V_i^2 + 2.\sum_{i \neq j} (V_i . V_j)$$

so

$$I^2 - Q^2 - U^2 - V^2 = \sum_i (I_i^2 - Q_i^2 - U_i^2 - V_i^2) + 2.\sum_{i \neq j} (I_i . I_j - Q_i . Q_j - U_i . U_j - V_i . V_j)$$

but for simple waves we know that

$$I_i^2 = Q_i^2 + U_i^2 + V_i^2 \qquad \text{1.7}$$

so

$$I^2 - Q^2 - U^2 - V^2 = 2.\sum_{i \neq j}(I_i . I_j - (Q_i . Q_j + U_i . U_j + V_i . V_j)) \qquad 1.8$$

Considering (Q ,U ,V) as a vector in three dimensional space, equation 1.7 implies that I_i is the modulus of this vector. Taking the dot product of two such vectors gives

$$Q_i . Q_j + U_i . U_j + V_i . V_j = I_i . I_j . \mathrm{Cos}(\theta_{ij}) \qquad 1.9$$

where θ_{ij} is the angle between the two vectors. Substituting equation 1.9 in 1.8 gives

$$I^2 - Q^2 - U^2 - V^2 = 2.\sum_{i \neq j}(I_i . I_j - I_i . I_j . \mathrm{Cos}(\theta_{ij}))$$

$$= 2.\sum_{i \neq j} I_i . I_j (1 - \mathrm{Cos}(\theta_{ij}))$$

Now

$0 \leqslant 1 - \mathrm{Cos}(\theta_{ij}) \leqslant 2$ and $I_i \geqslant 0$ for all i, so

$2.\sum_{i \neq j} I_i . I_j . (1 - \mathrm{Cos}(\theta_{ij})) \geqslant 0$ and

therefore

$$\underline{I^2 \geqslant Q^2 + U^2 + V^2} \qquad 1.10$$

The quantity on the right hand side of the inequality sign in equation 1.10, is the square of the polarized intensity. The difference between the polarized intensity and the total intensity is called the unpolarized intensity, and the polarization of light described by a stokes vector (I,Q,U,V) is defined to be

$$P=\frac{I_p}{I} = \frac{\sqrt{(Q^2+U^2+V^2)}}{I}$$

(P is usually given as a percentage), while the degree of linear polarization is defined to be

$$P=\frac{I_p}{I} = \frac{\sqrt{(Q^2+U^2)}}{I}$$

As an example of the description of polarization using Stokes vectors, consider a Stokes vector S, given by

$$S=(I,Q,U,V)=(10,3,4,0)$$

This says that the light beam which it describes has a total intensity of 10 units (whatever units are being used to measure intensity), the polarized intensity is

$$I_p=\sqrt{(9+16+0)}=5$$

Consequently the light is polarized by 50% , i.e. half the intensity in the light beam is carried by the polarized components and half by the unpolarized component. From the expression for V given in equation 1.5, it is apparent that if V is to be zero, it is necessary for $\mathrm{Sin}(2\beta)$ to be zero, so $\beta=0°$ or $90°$ and $\mathrm{Tan}(\beta)=0$ or infinity.

For either of these conditions to be true, one of the axes of the ellipse must be zero, which implies that the polarization is linear. The orientation of this linear polarization is given by the angle α in equations 1.5, where α is the angle between the linear polarization

and the reference direction used to define the Stokes vector. From equation 1.5 it can be seen that

$$\text{Tan}(2\alpha) = \frac{U}{Q} = \frac{4}{3} \quad \Rightarrow \quad \alpha = 26^{\circ}$$

If V had not been zero, then the light would have had a circularly polarized component and the result of adding this to the linear polarization would have been to produce elliptically polarized light.

1.1.4.4 Matrix transformations

When light passes through an optical system, the Stokes vector of the light undergos a transformation. This transformation can be described by a four by four matrix which when applied to the incoming Stokes vector produces the outgoing Stokes vector. The matrices which describe a rotation of the reference direction, and the action of an ideal polarizer, are derived in appendix A as examples of such matrices. We shall see that the scattering of a photon by a small particle can also be described by such a matrix.

Having described polarization in general and introduced the concept of the Stokes vector to describe it, we can now move on to examine various mechanisms which produce polarized light.

1.2 The production of polarized light

There are many ways in which polarized light can be produced but we here restrict our attention to those mechanisms which are important in astronomical situations.

1.2.1 The scattering of light by small particles

When light is scattered by a small particle, its state of polarization is altered. With reference to fig. 1.8 let light be incident on a particle P, and let a detector be positioned to measure the intensity scattered through an angle α at some arbitrary azimuthal angle. The plane containing the incident and scattered rays is called the scattering plane and is used to define the reference direction for the incident and scattered Stokes vectors. Let the component of the incident E vector which is parallel to the scattering plane be E_l and the component which is perpendicular be E_r. Let the equivalent components of the scattered E vector be E_l' and E_r' respectively. Assuming that the processes involved in the scattering are linear, we can write:

$$\begin{pmatrix} E_l' \\ E_r' \end{pmatrix} = \begin{pmatrix} S_2 & S_3 \\ S_4 & S_1 \end{pmatrix} \cdot \begin{pmatrix} E_l \\ E_r \end{pmatrix}$$

Given this transformation of the E vector components, it

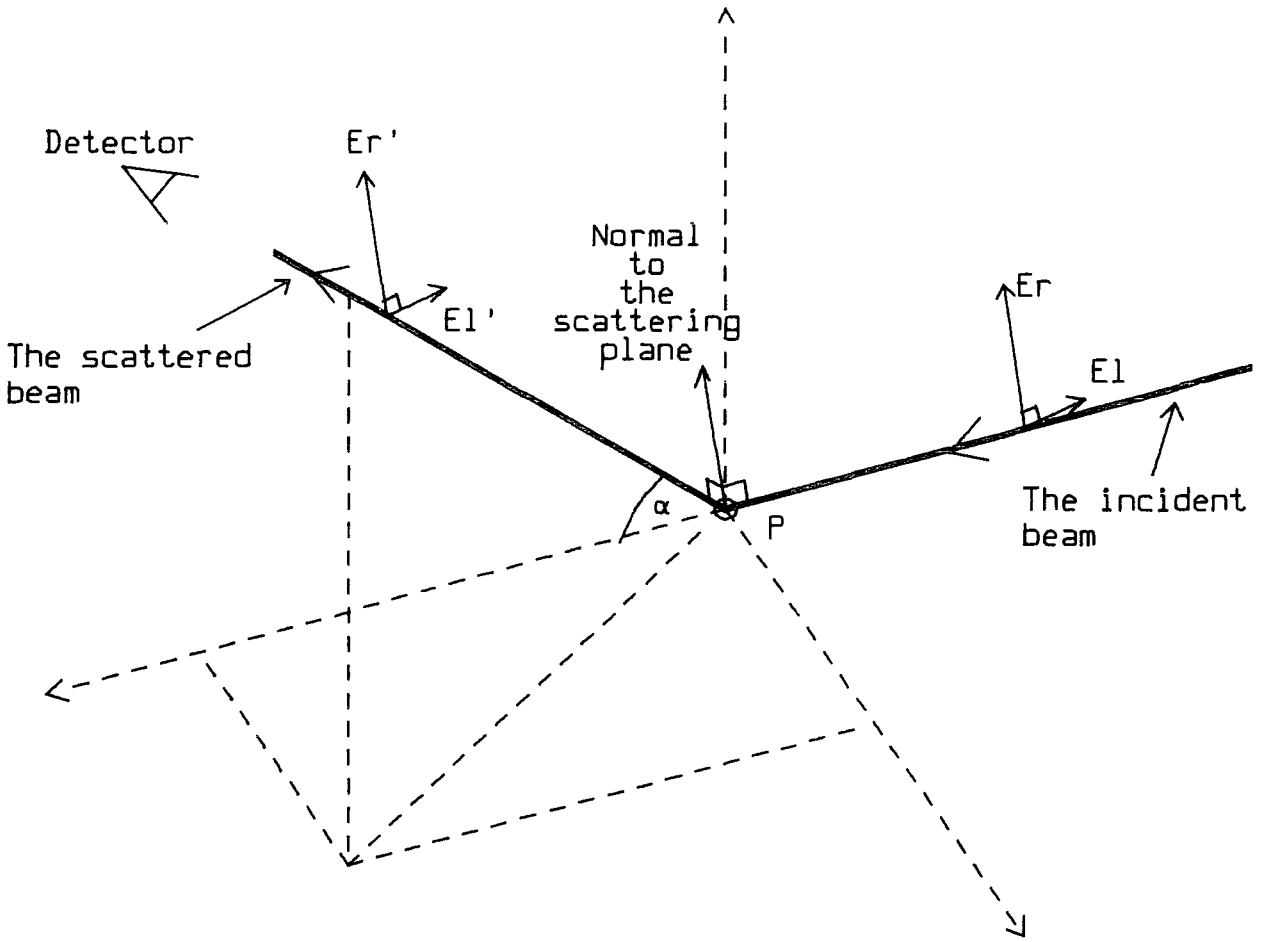

Fig. 1.8

The geometry of light scattering from a small particle. The incident beam is scattered through an angle α , to form the scattered beam. The incident and scattered beams together define the scattering plane, and the E vector components Er and El are respectively, parallel and perpendicular to it.

is possible to calculate the 4 x 4 matrix which transforms the Stokes vectors. If the particles are spherical then by symmetry considerations

$$S_3 = S_4 = 0$$

and in this case

$$\underline{S}' = \begin{pmatrix} C & D & 0 & 0 \\ D & C & 0 & 0 \\ 0 & 0 & E & -F \\ 0 & 0 & F & E \end{pmatrix} \underline{S} \qquad \text{1.11}$$

where $\underline{S}$ and $\underline{S}'$ are the Stokes vectors of the incident and scattered beams respectively, both given with respect to the perpendicular to the scattering plane. Thus if an unpolarized beam is scattered by a small particle, the scattered beam will be polarized with Stokes vector $\underline{S}'(\alpha)$

$$\underline{S}'(\alpha) = \begin{pmatrix} C(\alpha) \\ D(\alpha) \\ 0 \\ 0 \end{pmatrix}$$

The forms of the functions C,D,E and F depend (amongst other things) on the size of the particle. It is relatively straight forward to calculate them for the cases of particles either much larger or much smaller then

the wavelength of the light, but is more difficult for the case of particles with linear dimensions similar to the wavelength of the light.

1.2.2 Rayleigh scattering

In 1871 Lord Rayleigh published a paper (Rayleigh 1871) which described the theory of light scattering by "very small particles" (i.e. the diameter of the scattering particle is much smaller than the wavelength of the incident light). In his theory the scattering particle absorbs energy from the incident beam which is then re-radiated in all directions as light of the same wavelength.

The form of the scattering matrix of equation 1.11 is shown by Van De Hulst (1956) to be (for spherical particles)

$$\frac{1}{2}\begin{pmatrix} \cos^2(\alpha)+1 & \cos^2(\alpha)-1 & 0 & 0 \\ \cos^2(\alpha)-1 & \cos^2(\alpha)+1 & 0 & 0 \\ 0 & 0 & 2.\cos(\alpha) & 0 \\ 0 & 0 & 0 & 2.\cos(\alpha) \end{pmatrix}$$

Thus, unpolarized incident light aquires a polarization of

$$P(\theta)=\frac{\cos^2(\alpha)-1}{\cos^2(\alpha)+1} * 100\%$$

This function is symmetrical about $\alpha=90°$ and has a maximum

value of 100% at that angle. The total intensity scattered by α, into a unit solid angle, is proportional to

$$\mathrm{Cos}^2(\alpha)+1$$

which is again symmetric about $\alpha=90°$ implying that as much light is back scattered as is forward scattered.

1.2.3 Mie Scattering

The evaluation of the scattering functions for grains comparable in size to the wavelength of the incident light, is much more complicated requiring the solution of Maxwell's equations both inside and outside the particle with suitable boundary conditions. This problem was first solved by Mie (1908) for the case of homogenous spheres and his solution is described by van der Hulst (1956). Due to the difficulty of finding such solutions of Maxwell's equations, the case of spherical particles remains the best studied, and most useful solution. A practical method of computing the Mie scattering functions for spherical particles of any size and refractive index, has been produced by Warren-Smith (1979) amongst others, based on a scheme of Wickramasinghe (1973). In general, the scattering functions for a single particle, comparable in size to that the the wavelength of

the incident light, show oscillations as the scattering angle is varied. These oscillations are attributed to resonances within the particle and are generally removed when the more realistic situation is considered of light scattering from a cloud containing particles of many different sizes.

1.2.4 Scattering by a Cloud of Particles

Let incident light be scattered by spherical particles within a small volume element dV of a cloud, such that no light is scattered more than once within the volume element (i.e. the volume element is optically thin). The scattered light has a total Stokes vector equal to the sum of all the individual Stokes vectors scattered from each particle. If the grains within the cloud have a distribution of different sizes described by the size distribution function n(a) such that the number of grains with sizes between a and a+da is n(a)da, then the total scattered Stokes vector can be derived from the incident Stokes vector by a matrix similar to that of equation 1.11 but using the integrated scattering functions A'_{ij}, defined by

$$A'_{ij} = \int_{a=0}^{\infty} n(a).A_{ij}.da$$

where A_{ij} is a scattering function

Integrating over a distribution of sizes removes certain resonance features found in the scattering functions of single size particles.

The curves of scattered intensity and polarization (for unpolarized incident light) against scattering angle for such distributions of spherical particle sizes show that:

1) No polarization is produced for scattering through 0° or 180° .
2) The maximum polarization generaly decreases with increasing mean grain size.
3) The maximum polarization occurs for a scattering angle dependant on the mean grain size and the refractive index, generally being higher than 90° for small refractive indeces and lower than 90° for high refractive indices
4) The grains are always forward throwing, i.e. more light is scattered by less than 90° than is scattered by more than 90° .

Fig.s 1.9 and 1.10 show curves of polarization and scattered intensity for a power law size distribution

$$n(a)=a^{-\gamma}$$

where γ is the power law index. This form of size distribution is thought to describe the dust of the

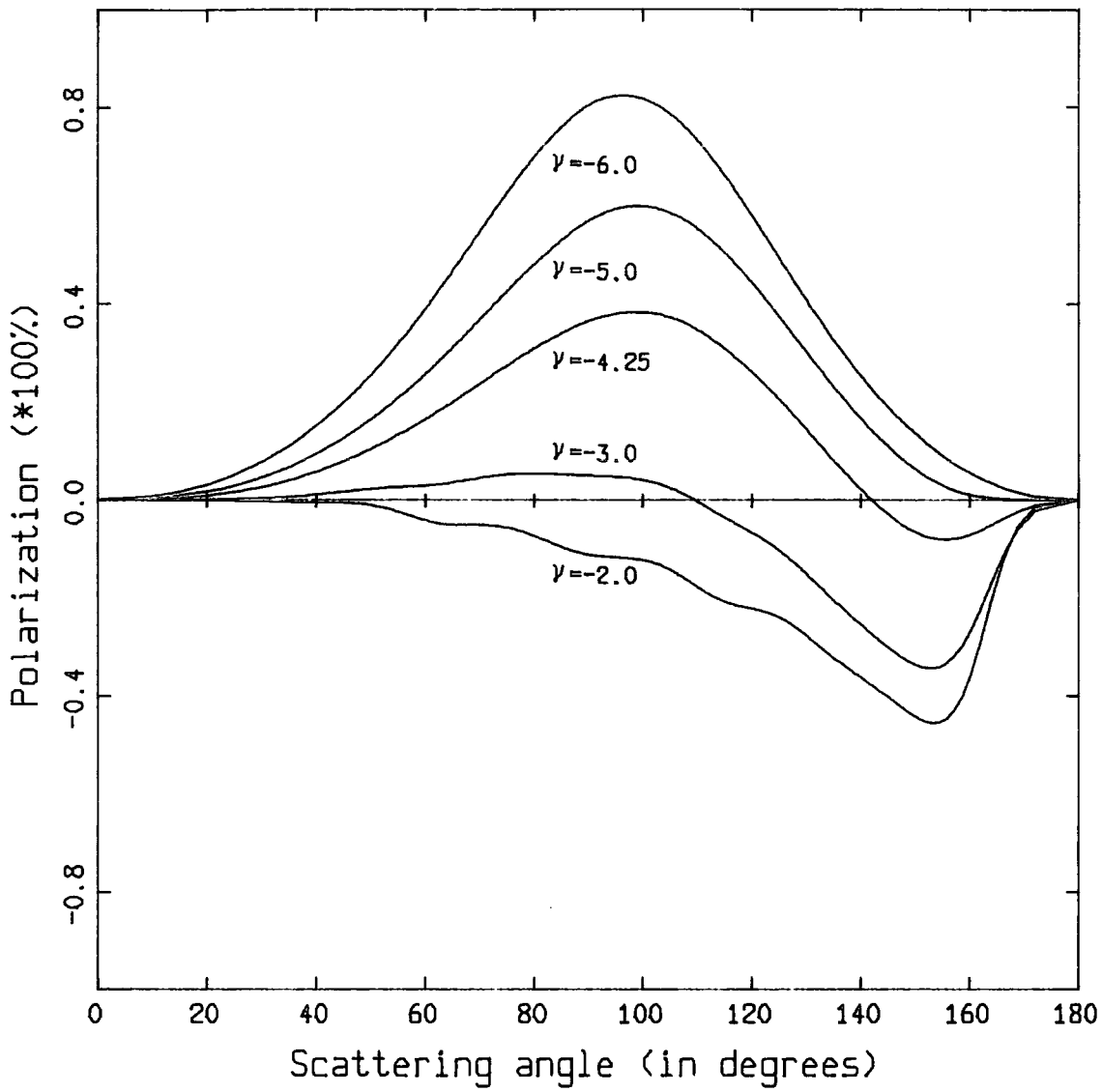

Fig. 1.9
Curves of the polarization produced by the scattering of unpolarized light in a cloud of Mie scatterers with a power law distribution of particle sizes (index γ). The refractive index used to produce these plots was 1.65-0.05i (silicates).

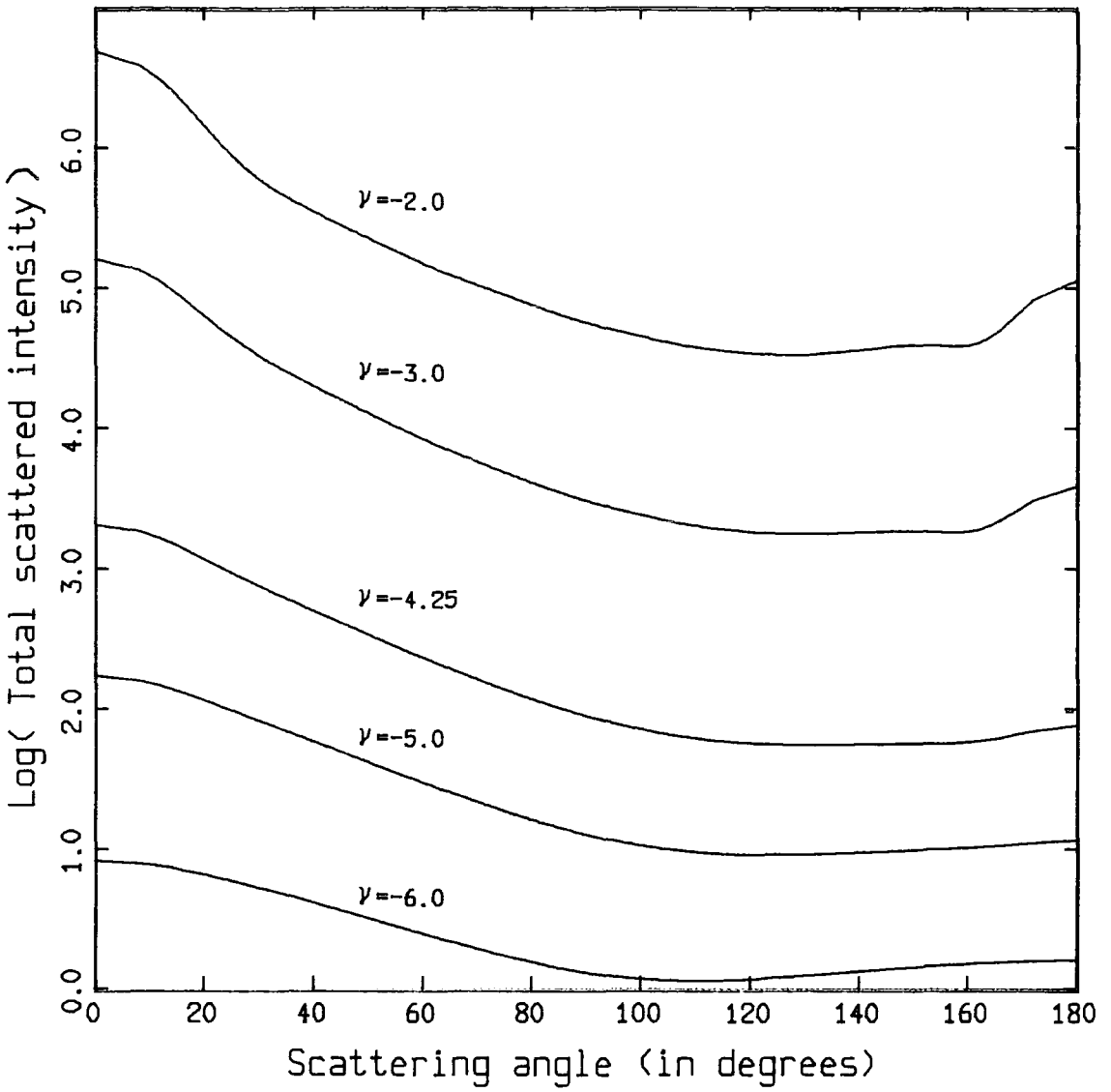

Fig. 1.10
Curves of the total intensity scattered (for unit incident intensity) by a cloud of Mie scatterers with a power law distribution of particle sizes (index= γ). The refractive index used to produce these plots was 1.65-0.05i (silicates).

interstellar medium (Mathis et al, 1977; Warren-Smith 1983).

1.2.5 Aligned Non-Spherical Grains

It is known from the exitence of interstellar polarization (discovered by Hiltner,1949, and Hall, 1949) that the dust grains in the interstellar medium must be non-spherical and that the particles must be aligned by some mechanism. This produces a difference in the scattering cross section for light polarized parallel and perpendicular to the overall axis of alignment. Consequently light polarized in one sense is not extinguished as much as light polarized in the other sense, and a net polarization is thus introduced. Data on the interstellar polarization has now been obtained for several thousand stars and it is found that the polarization can be roughly uniform over sizable fractions of the galaxy implying some large scale alignment mechanism. Various possibilities for the alignment process exist, but the most favoured is that the alignment is determined by the galactic magnetic field. The theory of such alignment was initially developed by Davies and Greenstein (1951) but their theory is thought to require too large a magnetic field to produce the observed polarizaton (Purcell and Spitzer, 1971). Various

modifications have been made and alternatives suggested to this mechanism to produce more efficient alignment (see Greenberg, 1978; review by Johnson, 1982) but, although the exact nature of the alignment mechanism is in debate, it is genarally accepted that in certain situations, non-spherical grains can be aligned by a weak magnetic field (a few micro-Gauss) in such a way as to produce polarization parallel to the projection of the magnetic field. In particular, the optical interstellar polarization is thought to be a useful tracer of the Galactic magnetic field and possibly of the magnetic field in external galaxies (see Heiles, 1976).

1.2.6 Synchrotron Radiation

When charged particles travel through a magnetic field, the resulting Lorentz force causes the particles to spiral around the magnetic field lines, radiating electro-magnetic energy as they do so. This radiation is known as synchrotron radiation and is a common source of radio emission. To produce radiation in the optical region, the charged particles must have much higher energies and consequently, optical synchrotron radiation is found much more infrequently than its radio counterpart. Light produced by the synchrotron mechanism is characterized by a high degree of linear polarization

(70% in the case of the Crab nebula; McLean et al, 1983) perpendicular to the projection of the magnetic field onto the plane normal to the direction of propagation. For an analysis of the synchrotron process, see Longair (1981).

The concepts introduced in this chapter will be used later in the description and modelling of the polarization of the perculiar elliptical galaxy NGC5128. The next chapter will give a general introduction to this object.

CHAPTER 2

THE PECULIAR GALAXY, NGC5128

The unusual visual appearance of the galaxy NGC5128, and its high level of activity have prompted a vast number of observations in most parts of the electro-magnetic spectrum. However, many questions still remain unresolved, not least of which is the origin of the vast amount of energy released by this galaxy. In order to set the polarimetric data studied in this thesis in perspective a brief review of the history and recent findings will be given. A more detailed review is given by Ebneter and Balick (1983).

THE PECULIAR GALAXY, NGC5128

2.1 Introduction

The history of NGC5128 (fig. 2.1) extends back to 1847 when Sir John Herschel, observing from the Cape of Good Hope, noted the dark lane that divides it in two. Observations of this object were slow to arrive owing to its southern declination (RA= 13h 22.4m, DEC= -42° 45', 1950 co-ordinates) but in 1922 Edwin Hubble obtained a spectrum of NGC5128 and classified it as a diffuse galactic nebula. The extra-galactic nature of this "large patch of structureless and possibly gaseous nebulosity" (Gregory 1921) was the subject of debate for many years. In 1949 Evans suggested that NGC5128 might be a perculiar form of planetary nebula, but in 1954 Baade and Minkowsky established the it was in fact a galaxy by obtaining a mean radial velocity of +450 Km/sec, and suggested that its present appearance could be the result of a collision between an elliptical and a spiral galaxy.

Interest in NGC5128 increased in 1949 when Bolton, Stanley and Slee identified NGC5128 with the powerful radio source Centaurus-A. This identification was confirmed three years later by Mills (1952). Since then the galaxy has been found to be emitting copious amounts of radiation over the entire electro-magnetic spectrum (Grindlay 1975). In 1970 Bowyer et al found that NGC5128

Fig. 2.1

The peculiar elliptical galaxy, NGC5128.

is an X-ray source and in 1975, Grindlay et al reported the detection of very high energy gamma rays (>300Gev) at the 4.5σ level.

NGC5128 is thus a very energetic system, but in order to know just how much energy it is producing, it is necessary to know its distance from our galaxy. This, however, is something which is not known with any real accuracy. Estimates range from 2.1 Mpc (Sersic 1958 based on possible resolution of O and B stars in the dust lane) to 8.5 Mpc (using data on Hubbles constant in Sandage and Tammann 1974). The value adopted by most workers, if for no other reason than it is the mean of all the others, is 5 Mpc, first suggested by Burbidge and Burbidge in 1959.

Adopting this value, the size and absolute magnitude can be calculated. Using the results of Sersic (1958) gives a standard diameter Do=30Kpc. (The standard diameter is the diameter the 25 mag/arcsec^2 contour would have if unobscured by dust). Using more recent data obtained by van den Burgh (1976) gives Do=57Kpc. The same two sets of data give absolute magnitudes (Mv) of -21.7 (Sersic) and -22.3 (van den Burgh). Thus NGC5128 is one of the biggest and brightest galaxies known. (Sandage (1973) found that the brightest galaxies in rich clusters have Mv=-21.8±0.4).

2.2 The Morphology of NGC5128

It is not clear from the two dimensional projection available to observers, what the three dimensional structure of this galaxy might be, and various models have been proposed at different times. Most of these assume that the luminous bulges seen above and below the dark dust lane constitute part of an elliptical (or S0) galaxy. Whether this elliptical component is a normal elliptical galaxy is a subject of debate.

The dust and gas which form the chaotic dark lane are most easily interpreted as a disk or annulus centred on the centre of the elliptical component. Evidence for this model comes from several sources. Graham (1979) plotted the position of seventeen HII regions associated with the dust lane and found them to lie approximately on an ellipse, as would be the case if they were actually in a circular ring, and were viewed from a position slightly out of the plane of the ring. That this is actually the case and not just a coincidence, is suggested by the radial velocities of these HII regions which show the variation one would expect if they did lie in a ring which rotates at a speed of 266Km/sec. Dufour and van den Burgh (1978a) have published pictures in Hα which show seventy HII regions with most lying in a

ring as described above, but with twenty lying inside the ring. They also found many young stars lying inside the same ring. These results suggest that the ring described by Graham is in fact a complete disk. In the same paper, Dufour and van den Burgh displayed pictures of B-V and U-B colour indices which indicate a torus like structure for the dust.

Thus the currently accepted model of the dust lane is of a solid, thick disk of HII regions, gas and young stars embedded in an elliptical distribution of stars, with a concentration of dust towards the outer rim of the disk. It should be noted that this can only be an approximation because of the many non-uniformities and warping within the visual dust distribution. Rodgers and Harding (1980) pointed out that the south east end of the dust lane is much darker than the north west end and that this would not be so if the dust was in the form of a uniform disk. They suggested a model in which the dust is confined within a tube which passes through the centre of the galaxy such that the north west end is tilted away from the observer and so has many stars from the elliptical component in front of it, and the south east end is tilted towards the observer and so has fewer stars in front of it. However, this model was found to be inconsistent with photometric observations made by Dufour et al (1979) and has been abandoned by the authors

(Harding et al, 1981) leaving the disk model as most tenable.

We shall now look in more detail at the two major components of the system, the elliptical (E) component and the disk (D) component.

2.3 The Elliptical Component

Spectroscopic observations of the E component seem to imply that its stellar population is very similar to that of normal elliptical galaxies containing mainly old population II stars, (Burbidge and Burbidge 1962, Rodgers 1978). However, its colour is slightly bluer than normal, van den Burgh (1976) found a difference of 0.15 in (U-B) between NGC5128 and normal ellipticals, becoming more noticable as the dust lane is approached. Rodgers (1978) found no reddening of the light from the E component, impling that it contains little dust. Further evidence for this comes from the close fit of the surface brightness of the E component to the de Vaucouleurs (1948) law, which states that the surface brightness of a normal elliptical galaxy is given by

$$\mathrm{LOG}\left(\frac{I}{I_e}\right) = -3.33.\left(\left(\frac{r}{r_e}\right)^{0.25}-1\right) \qquad \text{2.1}$$

where r is the distance out from the centre along a given radius, r_e is the "effective radius" (the radius of

the eliptical isophote inside which half the total luminosity is contained), and I_e is the flux at the effective radius. Sersic (1958) using photographic photometry found r_e=189 arcsec and σ_e=22.19 mag/arcsec^2 (the surface brightness at the effective radius =2.5logI_e+constant) which on integrating equation 2.1 over all radii gives a total unobscured apparent magnitude of 6.79. Van den Burgh (1976) using photoelectric photometry found r_e=330 arcsec and σ_e=22.15 giving a total apparent magnitude of 6.17. Dufour et al (1979) found r_e=305 arcsec, σ_e=22.00 and a total apparent magnitude of 6.2. The difference between these values is probably due to reddened regions near the dust lane being included in the fitting procedure. However all workers conclude that the surface brightness can be well fitted by the de Vaucouleurs law for radii between 70 and 255 arcsec.

The isophotes of NGC5128 are found to be nearly circular with increasing eccentricity at lower surface brightness (a common characteristic of elliptical galaxies, Carter 1978). Dufour et al (1979) found eccentricities varying from 0.367 at a radius of 2.6 arcmin to 0.673 at 9.0 arcmins, with intermediate values which would classify the E component of NGC5128 as an E2 system.

Various workers have found non-elliptical

features in the fainter regions. Johnson (1963) found faint optical extensions along the major axis at the 26 to 28 mag/arcsec^2 level, and Malin (1983) found a system of faint shells surrounding the galaxy.

Several attempts have been made to measure the speed of rotation of the E component by observations of absorption features in its spectrum (Burbidge and Burbidge, 1962; Graham, 1979; Appenzeller and Mollenhoff, 1980). The results of these observations indicate that there is very little, if any, rotation of the E component, as was found to be the case for many other elliptical galaxies by Illingworth (1977). This result is in marked contrast, however, to the disk component which is found to be rotating rapidly (Graham 1979). No systematic radial motion between the E and the D (disk) components has been found, so the disk is neither falling into, nor being ejected from the centre of the galaxy.

Most of the above results seem to suggest that the E component is, to all intents and purposes, a normal elliptical galaxy. The deviations from normality may well be caused by the same agency that caused the dust lane and the high level of activity.

2.4 The Disk Component

The D component is currently thought to be approximately in the form of a circular disk passing through the galactic nucleus and inclined at an angle of 72° to the plane of the sky (Graham 1979, Dufour et al 1979) so that its projection forms a highly eccentric ellipse. The disk contains gas, young stars and dust intermingled with the old stars of the E component (Harding et al 1981).

The gas is most obviously present in the form of HII regions which provide a useful tracer of the shape of the disk. The HII regions have been found to be similar in chemical composition, to those in our own galaxy (Dufour et al 1979, Phillips 1981) and are associated with vigourous star formation (Telesco 1978). Young blue stars are resolved in many areas of the dust lane, but especially along the edges (van den Burgh 1976). Dufour et al suggest that a burst of star formation is occuring within the dust lane which started 50 million years ago. By comparison they find that colours in the E component are consistent with those of globular clusters which are 10,000 million years old, (comparable to the age of the universe). There is also evidence for a component of shock ionized gas associated with areas of anomoulous dispersion

(Phillips 1981).

Photographs obtained by Dufour et al (1979) suggest that the dust is concentrated around the outer rim of the disk with a large "rift" extending as far as 10 arcmin east of the nucleus. Rodgers and Harding (1980) have pointed out asymmetry in the absorption due to the dust, there being far more absorption in the south east half of the dust lane than in the north west, suggesting that the dust is not uniformly distributed throughout the disk. Rodgers (1978) found the reddening law for the dust to be similar to that of the dust in the Perseus region of our Galaxy (Nandy 1965), which is typical of dust not associated with young stars. Grasdalen and Joyce (1976) have found the "silicate" feature in the infra-red spectrum at 10μm, a feature commonly found from dust in our galaxy. They estimate that the visual extinction to the infra-red source (situated at or near the nucleus found by Kunkel and Bradt (1971)) is 22±5 mag. In view of the much lower value of 3 to 6 magnitudes for the extinction through the dust lane at several non-nucleur locations found by Harding et al (1981), it would seem that there must be a very small area of very dense obscuring matter surrounding the infra red source. It thus seems that the interstellar medium in NGC5128 is very similar to that in our galaxy (Grasdalen and Joyce 1976).

Elvius and Hall (1964) have observed linear

polarization in the dust lane of up to 6% parallel to the direction of the dust lane. This has generally been taken as an indication of the presence of a magnetic field in the dust (Elvius 1978). However, Jura (1982) has suggested that the observed polarization could be produced by scattering alone, without the need of a magnetic field to align the grains. This suggestion will be investigated later in this thesis.

Several workers have found the D component to be rapidly rotating (Burbidge and Burbidge, 1959; Sersic, 1969; Graham, 1979; Appenzeller and Mollenhoff, 1980; Mercelin et al, 1982). The rotation curve obtained by Mercelin et al has a slope of 150 km/sec/arcmin which is very significant, in view of the fact that Graham (1979) found there to be very little if any rotation in the E component. Explaining the difference in the angular momentum of the E and the D components is a major consideration for any model of this system.

2.5 Activity within NGC5128

Balick and Heckman (1982) define an active galaxy as a galaxy in which "signs of qualitatively unusual and quantitatively energetic activity (i.e. activity not associated with the evolution of normal stars) are clearly visible and can be connected directly

or indirectly to the nucleus". In this sense NGC5128 shows several signs of activity, primarily in the associated radio, X-ray and γ-ray sources, but also in the jet which is found to extend from the nucleus.

The radio source, Centaurus-A which is associated with NGC5128 is one of the largest known extra-galactic radio sources, having a maximum diameter of 10°. Structure can be seen on scales over a factor of 10^{6}, from the giant outer radio lobes extending up to 450Kpc from the galactic centre, to the inner jet of size 1pc (Preston et al, 1982). Burns et al (1983) present a series of radio maps illustrating the structure of Cen-A at various scale sizes. Radio emission is found to be high at the nucleus and extending away from the nucleus by 20 arcsec in a jet, inclined at 65° to the dust lane, and in two lobes (the "inner" lobes) on either side of the dust lane at a distance of 6 arcmins from the nucleus, which are co-linear with the jet (fig. 2.2). Further radio emission is found at greater distances from the nucleus in the form of the "outer" lobes which again are co-linear with the inner lobes and the jet. The radio emission is found to have varying degrees of linear polarization. At 6cms, the inner lobes are polarized by 48% (north west lobe) and 12.5% (south east lobe). Burns et al (1983) suggest that this could be produced if the south east lobe was tilted away from us, and thus lay behind the galaxy,

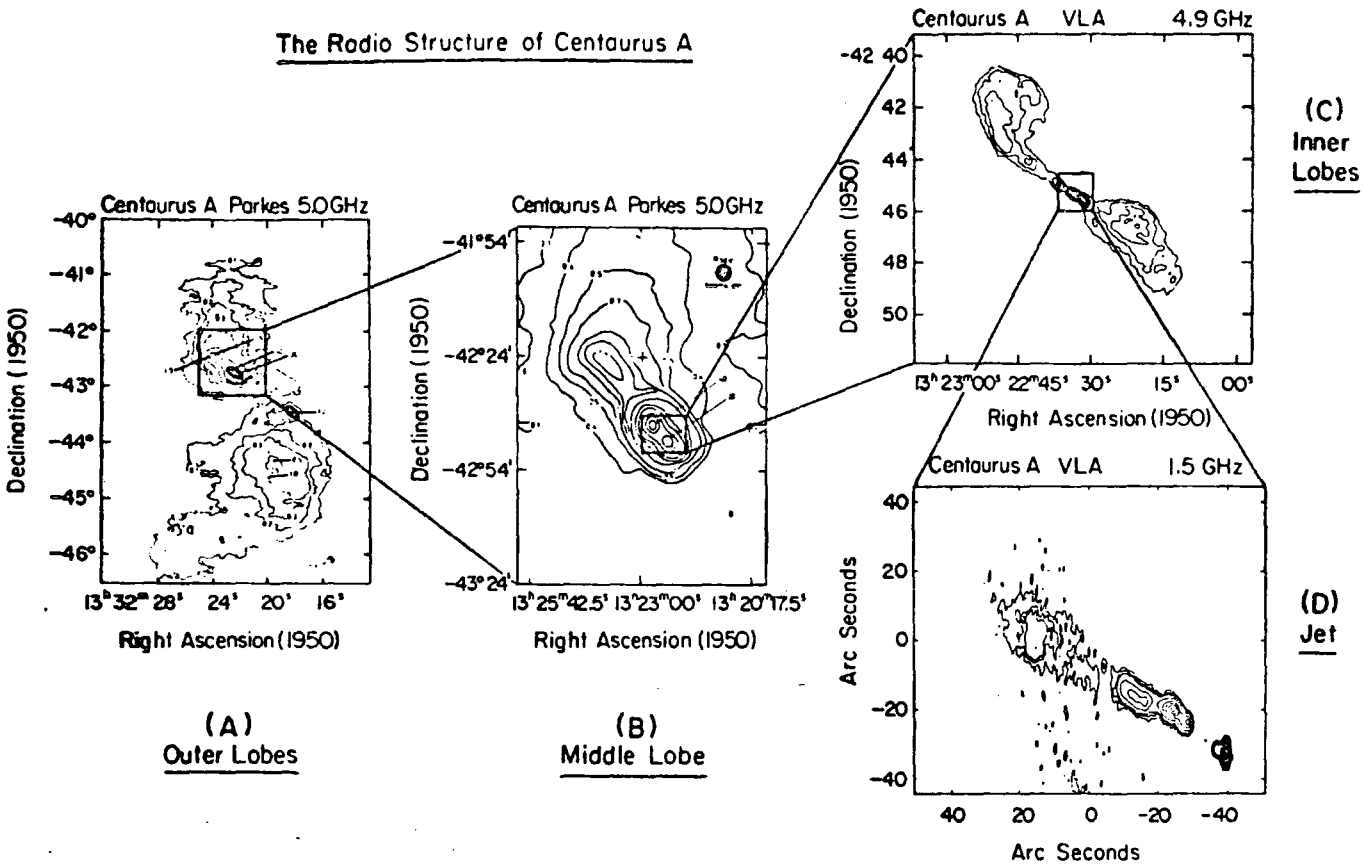

Fig. 2.2

The structure of the radio source Centaurus-A on four different scales. Reproduced from Burns et al ,1983, (see their paper for details).

so that the radio emission would be subject to more Faraday depolarization. This idea is consistent with the observations of Graham and Price (1981) that the optical jet associated with the radio jet is travelling outwards from the nucleus and towards us. The radio jet has polarization ranging from 10% to 20%. Burns et al conclude on the basis of the radio to X-ray spectrum of the jet, that they are both produced by a common synchrotron source. They thus envisage a beam of relativistic particles being emitted from the nucleus and travelling up the jet, spiralling round the lines of flux of a magnetic field to produce the observed radio and X ray jet. This jet is confined by a pressure proportional to the density of the interstellar medium (ISM) and to the square of the jet's velocity (Sersic, 1982, p129; Burns et al 1983), so that it retains its narrow jet-like appearence. As energy is removed from the jet by radiation and interaction with the ISM, its velocity is reduced and the confining pressure is thus reduced allowing the jet to expand transversely into the wide lobes. The presence of several distinct areas of radio emission at various distances from the galactic centre would suggest that ejection of relativistic particles is not a continuous process, but occurs spasmodically (Sersic, 1982, p98).

Optically, the jet is associated with various knots of diffuse emission regions, HII regions and blue

stellar objects. The first indications of this optical jet came from Blanco et al (1975), who discovered the outer jet extending from 7.8 arcmins to 28.2 arcmins from the nucleus. Dufour and van den Burgh (1978b) claimed to have found an Hα filament extending between the nucleus and the innermost end of the jet discovered by Blanco et al, but this has been questioned by Graham and Price (1981) and Brodie et al (1983) who failed to find the inner jet. The general outflow of the optical jet (Graham and Price, 1981) suggests that the material which constitutes the jet originates near the nucleus. They find high metalicity in the jet, ruling out the possibility of it being composed of unprocessed intergalactic material, and a decrease of excitation with radial distance, which they see as indicative of the cooling of the gas as it expands in a fashion similar to the plasma responsible for the radio emission. In the inner regions of the jet, Brodie et al (1983) find an optical continuum which corresponds to the form expected if it was produced by the same synchrotron process that produces the radio emission. They also find evidence for shock ionization of the gas within the jet.

The nucleus, as well as powering the jet and radio lobes,is itself an emitter of electro-magnetic radiation over a wide range of wavelengths. It was originally discovered by Kunkel and Bradt (1971) as an infra-red "hot spot" at 8000Å; at millimetre

wavelengths, it seems to show evidence of a compact, non-thermal source (Kellerman et al, 1975). It is a fairly normal X-ray source (Culhane, 1978), and seems to be emitting γ-rays as well (Grindlay et al, 1975). The source of this energy is one of the more important questions about NGC5128 still to be answered. Most workers agree that it is probably intimately connected with the peculiar morphology of the rest of the galaxy, but whether the nuclear activity was caused by the appearence of the strange morphology, or vice versa, is still to be decided.

2.6 Proposed Models for NGC5128

The first attempt to explain the peculiarities of NGC5128 was made by Baade and Minkowski (1954), who suggested that they might be the result of a collision between a giant elliptical galaxy and a small spiral. This was not favoured by many people because of energy considerations (Burbidge and Burbidge, 1957, 1959), and also because NGC5128 is seen not to be associated with a galaxy cluster, but to be in an isolated region of space without any close neighbours, thus reducing the chance of a collision occurring. An alternative proposal was made by van den Burgh (1976), who suggested that the gas and dust forming the peculiar features was ejected by evolving stars within the E component. The question of why other

elliptical galaxies show little evidence of gas or dust was answered by Gunn and Gott (1972).They proposed that since most ellipticals occur in rich clusters, the intra-cluster medium could sweep them clean of any gas or dust. Since NGC5128 is a field galaxy (i.e. not associated with a rich cluster) this process could not be active and thus the gas and dust would be left within the galaxy. However, this model fails to explain the great difference in angular momentum between the E and the D components.

Another alternative to the merger hypothesis, was provided by Mercelin et al (1982), who suggested that NGC5128 is in fact a late developing spiral galaxy in which the disk is still being accreted. Several objections to this idea have been made, foremost among which is the fact that the E component does seem to have all the characteristics of a normal elliptical galaxy, which are different from those of the bulges in S0 - Sa spirals.

The original idea of a galaxy merger has been attracting more adherents over the past few years, and seems as if it might hold an explanation to the structure of other galaxies similar to NGC5128 (Bertola and Galletta, 1978; Hawarden et al 1981).

Work has been done on numerical simulation of the dynamics of galaxy collisions (Tubbs, 1980), which suggests that if a small spiral galaxy collided with a giant elliptical in an arbitrary fashion, dissipative

cloud-cloud collisions and precesion of the orbits of the accreted material would tend to cause a relaxation of the accreted material into a disk. The existence of strong warping of the dust lane (see the photograph on p127 of Sersic, 1982) is taken as evidence that the collision was fairly recent (of the order of 10^8 years ago) and that the disk has not fully relaxed yet. Van Albada et al (1982) have produced a model of a triaxial elliptical galaxy tumbling about its minor axis, in which a warp could be a permanent feature, and would then impose no limits on the age of the disk. The merger hypothesis is, at the moment, the most favoured explanation of NGC5128. The supporting evidence for this can be summarized in three points:

1) The presence of large quantities of dust,gas and young stars in an elliptical galaxy, when normal elliptical galaxies have very little.

2) The high angular momentum of the D component compared to the E component. It is difficult to account for this if one assumes that the galaxy has always been an isolated system which has suffered no disturbances from outside.

3) The faint shells found by Malin (1983) in the faint outer regions of the galaxy. It has been shown theoretically (Quinn 1982a,b) that such shell structure could be produced in a collision between a massive elliptical and a small spiral.

The main objections which have been raised to the merger hypothesis are:

1) No remnant of the stellar like nucleus of the spiral galaxy has been found. This could be explained if the swallowed galaxy was a late type spiral, in which case its nucleus could have been faint and subject to tidal disruption (Tubbs,1980; Schweizer, 1980).

2) Lack of the turbulent motions in the gas which would be expected after a collision. Mercelin et al (1982) found no evidence for turbulent motion within the gas of the D component. However, as Mollenhoff (1981) and Graham (1979) did find turbulent motions, the issue remains in doubt. One would expect turbulent motions to die down with time so that if, in fact, there is no turbulent motion, it might be possible to explain its absence by assuming that the collision happened a long time ago.

3) The lack of near neighbours to NGC5128 make the chances of a collision very small. It is now known that NGC5128 is, in fact, a member of a loose cluster (de Vaucouleurs, 1975,1979; Webster et al, 1979) containing many dwarf galaxies which seem to be clustering around NGC5128. Calculations on the merger rate in rich clusters (e.g. Ostriker and Hausman, 1977) show that larger galaxies tend to be accreted by giant "galactic cannibals" in preference to smaller galaxies. It is possible, therefore, that the dwarf galaxies found in the neighbourhood of NGC5128 are the survivors from a previous, more substantial cluster.

2.7 Future Work

NGC5128 has recently come to be seen as the architypal member of a class of elliptical galaxies with dust lanes, of which about 90 are known (Hawarden et al, 1981). It is tempting to assume that similar processes have shaped the evolution of these galaxies. About 35 of these galaxies are known to be radio sources, and the rest have not, in general, been studied extensively. If future studies strengthen the idea of a common evolution for this galactic class, then observations of NGC5128 could be important in determining the properties of the class, due to its proximity and consequent ease of observation.

CHAPTER 3

NEW POLARIMETRIC OBSERVATIONS

In this chapter, results of new observations of the spatial distribution of polarization in NGC5128 will be presented.

3.1 The Observations

NGC5128 was observed by Dr. S.M. Scarrott and Dr. K.J. Watts on the nights of the 22nd, 23rd, 25th and 26th of March, 1979, using the 1 metre telescope of the South African Astronomical Observatory at Sutherland, South Africa. The analyzer and detector systems used were the Durham polarimeter (described by Scarrott et al, 1983, and Warren-Smith, 1979) and a 4cm MacMullan electronographic camera, the images being recorded on

Ilford L4 nuclear emulsion.

NGC5128 has a large angular size and fills the entire field (9 arcmins) of the Durham polarimeter on the telescope used. In order to obtain data for the sky areas adjacent to the object, it was thus necessary to place the object to one side of the polarimeter field, so that only half of the galaxy was visible. In this way observations were taken for each half of the object. Each set of observations was repeated twice with the object in slightly different positions within the field, in order to increase the signal-to-noise ratio. All exposures were of 30 minutes duration and were taken through a broad visual filter with FWHM of 2000Å centred at 5500Å.

3.2 The Data Reduction

The first step in the data reduction sequence was the conversion of the electronographic images into digital form, which was done using the P.D.S. micro-densitometer machine of the Royal Greenwich Observatory. The polarimeter images were scanned using an aperture size of 24 microns (equivalent to 1.3 arcsec on the sky), with a sample spacing of 25 microns, to produce images of 512 by 512 pixels. The area scanned extended beyond the actual polarimeter image into the unexposed areas of the emulsion, in order to provide a measure of

the background density of the emulsion. These digital images were then transported to Newcastle where they were further reduced on the IBM 370/168 machine of the Northern Universities Multiple Access Computer (NUMAC) system. The reduction procedure (fully described by Warren-Smith, 1979, 1982) had to carried out very carefully, due to the fact that estimates of the polarization were required in the dark dust lane where very little signal was available (the dust lane is typically half the brightness of the sky alone). Great attention was given to choosing areas on each image to be used to estimate the Stokes vector of the sky, since it was found that even at the edges of the images, there could still be a systematic gradient in the light intensity, implying that luminosity due to the galaxy was still present.

The alignment of the four final sets of data was achieved by obtaining co-ordinates for stars found on more than one image and applying a transformation to one set of data, such that the common stars lined up. If no common stars could be found then the co-ordinates of different stars were found and a transformation applied to one data set, such that the stars were in the correct relative positions. By this method, alignment to better than 4 arcsec was achieved.

A correction for the induced interstellar polarization of the Galaxy was then made. The values used

were those used by Elvius and Hall (1964) of 1.4% at position angle 70°. This figure was based on the polarization of the foreground stars near NGC5128, and could not be estimated from the new data, due to emulsion saturation in the star images, although it was found to be close to the value of the polarization found in the dust free regions of NGC5128.

3.3 The Polarization Map

The final map produced by the above reduction procedure is shown in fig. 3.1 superimposed on a negative image of NGC5128. This map was formed by binning the original data into bins of 10 by 10 pixels (eqivalent to 14 by 14 arcsec on the sky) centred on a matrix of points separated by 8 pixels in both the horizontal and the vertical directions so that adjacent bins overlap. The effect of this is to reduce the noise on the data, introduce some smoothing between adjacent values, and reduce the total number of polarization vectors displayed in order to make the final map more amenable to visual inspection.

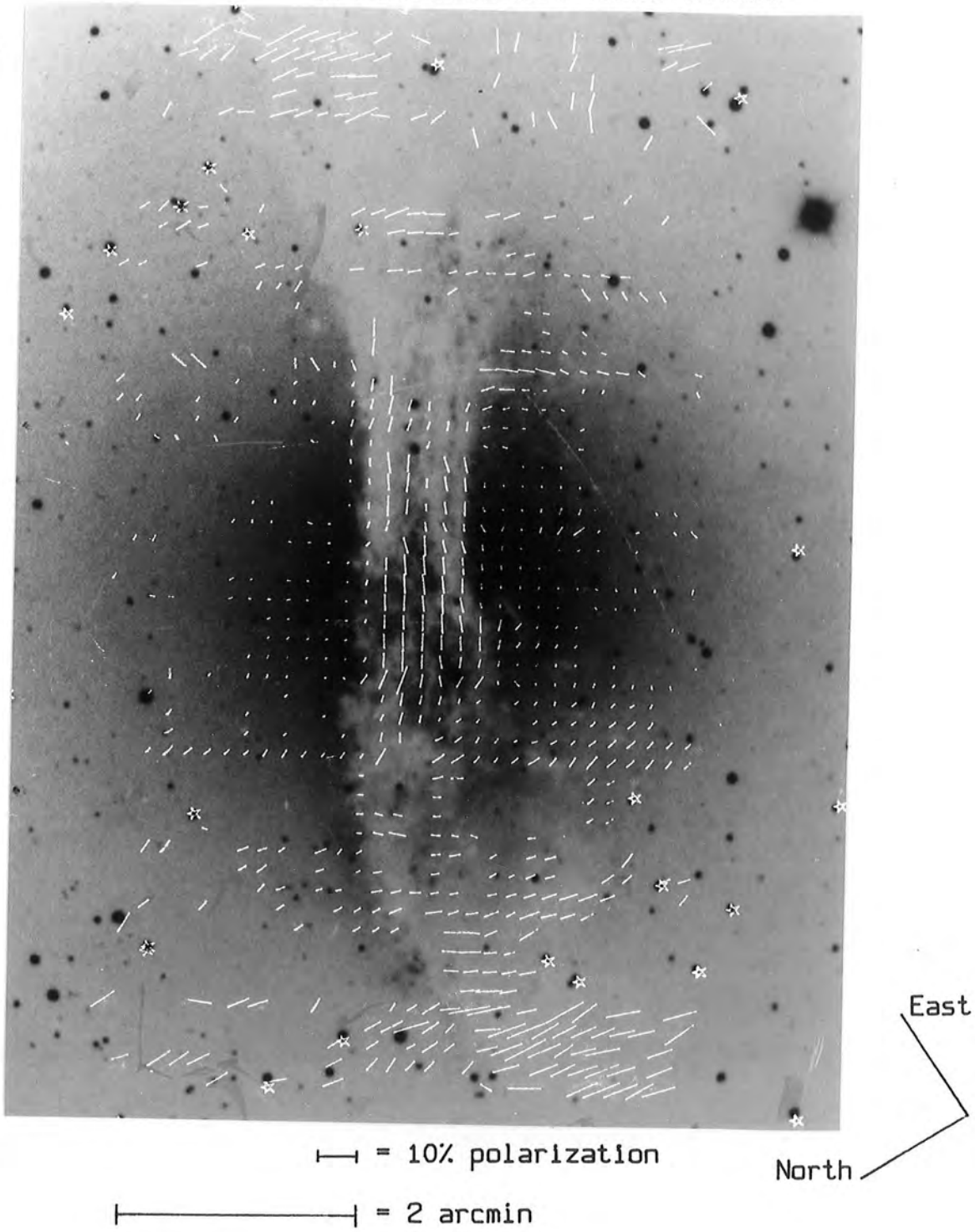

Fig. 3.1

The new polarization map of NGC5128. Each vector represents the integrated polarization in a 14x14 arcsec bin.

3.3.1 The Inner Dust Lane

Several regions of polarization can be identified, the most obvious being the region of roughly parallel vectors in the dark dust lane, where the polarization values are typically 4%. An estimate of the expected error on these values can be made (see Warren-Smith, 1979) and is found to be 0.5%. This region of well ordered vectors parallel to the dust lane extends at least 110 arcsec away from the galactic centre to the south east, and 70 arcsec to the north west. It covers the entire width of the dust lane, the polarization becoming less at the edges.

About 40 arcsec to the west of the galactic centre, on the south west edge of the dust lane, can be seen a circular arc of dust extending about 20 arcsec into the elliptical (E) component. The polarization vectors in this region change direction in such a way as to remain parallel to the dust loop. The presence of this small scale structure is significant in determining the nature of the polarizing mechanism at work in the central regions of the dust lane.

3.3.2 The Intermediate Dust Lane Regions

Further out along the dust lane, the vectors turn through 90° to become perpendicular to the dust lane, the degree of polarization remaining at between 3 and 4%. The regions of transition between the two vector orientations contain few vectors, most of the original vectors having been rejected due to high noise content and paucity of signal in these areas.

3.3.3 The Outer Dust Lane Regions

Further out still, at about 290 arcsec from the galactic centre, lying not directly along the line of the central dust lane regions, but rather in westerly and easterly directions, are two regions of higher polarization (around 10%) which are co-incident with the warped outer extremities of the dust lane. The vectors in both regions are tangential to the line joining them to the galactic centre.

3.3.4 The Elliptical component

The north west end of the dust lane can be seen to be more chaotic than the south east, with a

considerable fraction of the south west bulge of the E component obscured by dust, where polarization of around 1 to 2% is found. The vectors here show some degree of random orientation but with a definite preference for lying tangentially to a line through the galactic centre.

Elsewhere in the E component polarization is insignificant and any sizeable vectors occuring in the outer regions of the galaxy not already mentioned are probably spurious. In particular, no significant polarization is found in the region of the optical jet, where high radio polarization is found and where several workers have suggested optical synchrotron emission might be produced (see section 2.5). Elvius and Hall (1964) also found no significant polarization in this area.

3.3.5 Comparison With Previous Observations

Elvius and Hall (1964) obtained several estimates of the polarization at various positions within NGC5128, using photoelectric photometry with a circular aperture of 40 arcsec diameter. Fig 3.2 shows their polarization vectors superimposed on the new map. It can be seen that there is good agreement between the two sets of data in the inner dust lane regions, Elvius and Hall finding between 3 and 4% polarization parallel to the dust lane. There is some disagreement in orientation in the

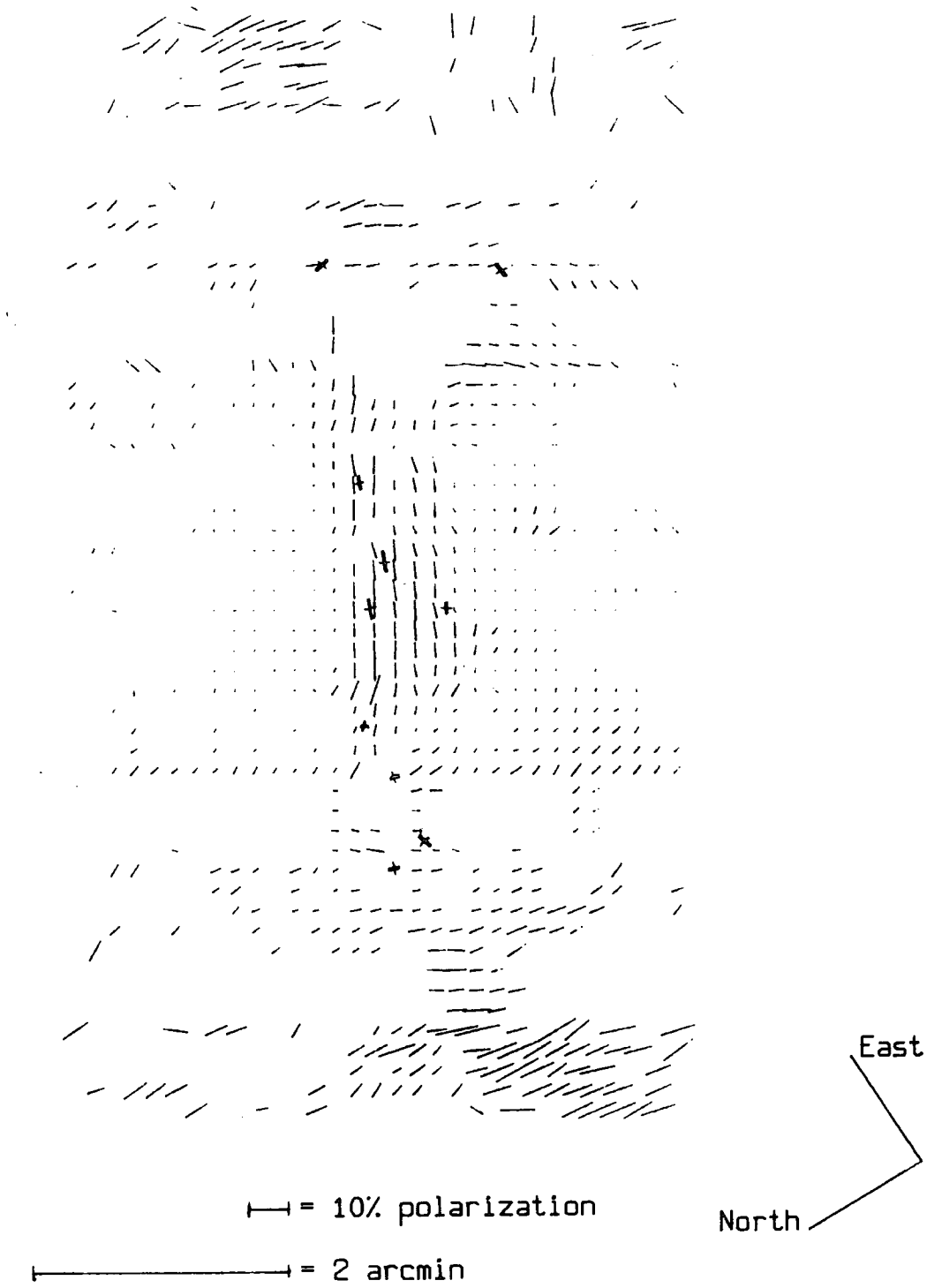

Fig. 3.2

The new polarization map of NGC5128 with the polarization vectors estimated by Elvius and Hall (1964) shown in heavy print.

outer parts of the dust lane, but valid data is sparse in these regions in the new map and what vectors there are suggest that the polarization is changing rapidly, so that close agreement between values obtained from integration areas as different as 1.7 arcsec^2 and 1250 arcsec^2 would not be expected.

3.4.6 Discussion

The existence of polarization within and parallel to the dust lane, is a feature found in several dust lane galaxies (see Visvanathan, 1974, for a review). Until recently, the cause of this polarization has generally been assumed to be extinction from non-spherical grains aligned by a large scale magnetic field, through some mechanism such as the Davies-Greenstein para-magnetic relaxation process. However, Jura (1983) has claimed that the observed polarization could be produced by scattering alone, without the need for a magnetic field. The new data presented here gives an opportunity to investigate this question further.

If one makes suitable assumptions, it is possible, at first sight, to explain the data by either method. Looking first at the scattering model, it is possible to make an estimate of the general pattern of polarization vectors which would be produced if a thin,

solid disk of optically thick dust, embedded in an extended luminosity source, was viewed from a point far distant from the disk but within the plane of the disk (i.e. with no tilt). Due to the extinction caused by the dust in the disk, a grain of dust situated within the disk will receive little illumination from other points within the disk, most of the illumination will come from the two areas of luminosity above and below the disk, since the extinction to these areas is less. Combining this observation with the fact that scattering tends to polarize light normally to the plane of scattering, we arrive at the results depicted in fig. 3.3. Each solid vector in fig. 3.3 is the sum of two vectors (shown dashed) which represent the polarization of light coming from the centroids of the two luminosity bulges. The general form of the polarization depicted in this diagram is qualitatively similar to that in the real polarization map of fig. 3.1. The polarization is parallel to the dust lane at the centre, reducing in magnitude out from the centre, until the vectors turn through 90° to become perpendicular to the dust lane and slowly increasing in magnitude from there on. Jura calculated that the polarization at the centre of a model very similar to this one, could be as high as 5% if one makes the assumptions that the light is scattered no more than once on its journey from its origin to the observer, and

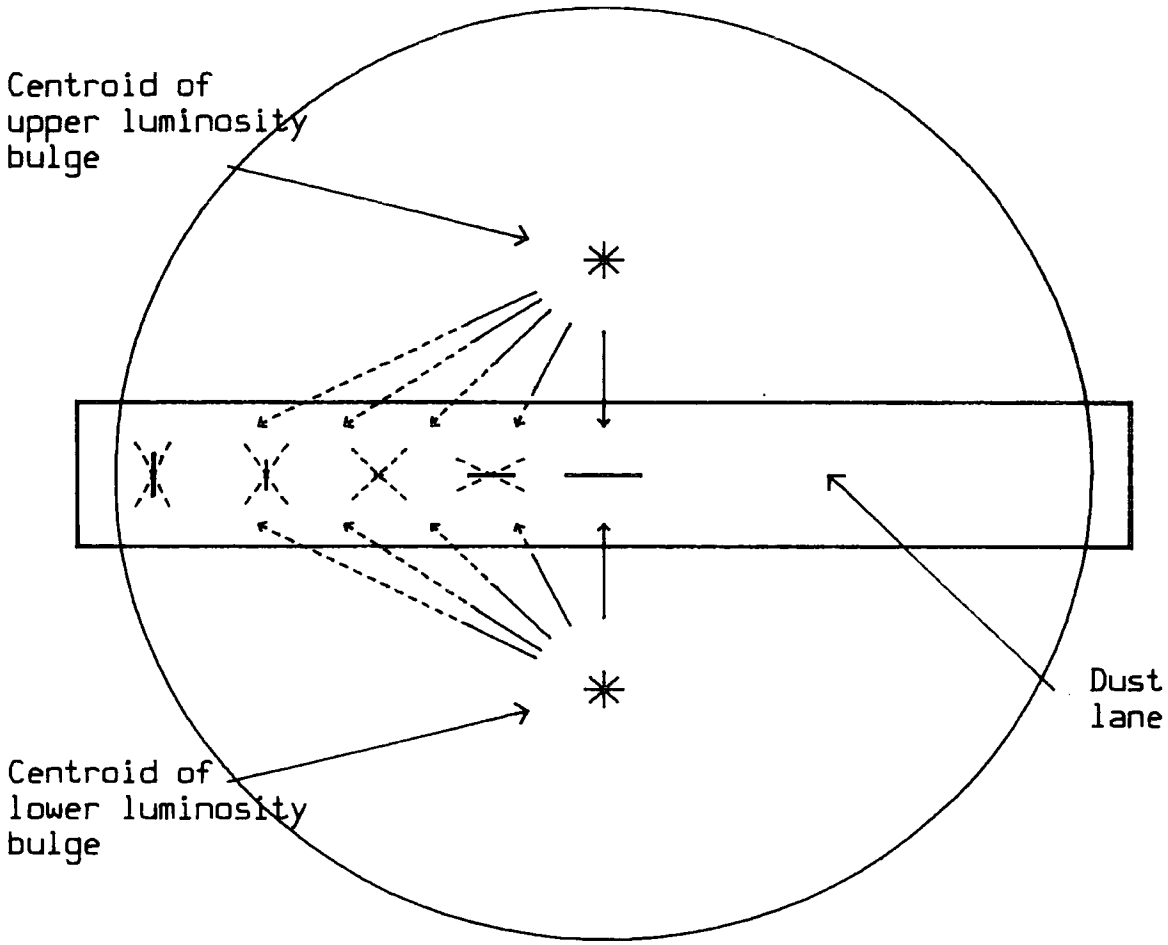

Fig. 3.3

The form of the distribution of polarization expected from single scattering within a disk of dust situated in the middle of a spherical distribution of luminosity. Each dashed vector in the dust lane represents the polarization caused by the luminosity in either the upper or the lower luminosity bulge, and the solid vectors represent the total polarization produced by adding the two dashed vectors together.

that the scatterings obey the laws of Rayleigh scattering. This figure fits in well with the value of 3 to 4% polarization found near the centre of the dust lane in the new data. Looking now at the model in which the polarization is caused by differential extinction by aligned grains, it can be seen that if one assumes a concentric field in the plane of the dust disk, then the polarization pattern produced could be similar to that produced by scattering. For polarization produced by grains aligned by the Davies-Greenstein process, the component of the magnetic field which is perpendicular to the direction of propagation of the light determines both the direction and the degree of polarization. Thus the polarization will be parallel to the disk (due to the fact that the magnetic field is parallel to the disk) and the degree of polarization will become less as the extremities of the disk are approached. This is because, as the magnetic field bends round and becomes perpendicular to the plane of the sky, the spin axis of the grains also becomes perpendicular to the plane of the sky, so that both states of polarization are absorbed equally by the grains. Of course, polarization produced by scattering will also be present, as well as that caused by extinction, and will be more important in regions far from the centre of the dust lane where the degree of polarization produced by differential extinction is small.

Thus one would expect the vectors at the ends of the dust lane to be perpendicular to the dust lane, as is in fact observed in the polarization map, and there will occur some position in the dust lane at which the polarizations produced by scattering and differential extinction will cancel each other out.

Both models mentioned above make many assumptions, not least of which is that of an orderly distribution of dust in a simple disk, but given these assumptions, they can both predict the general form of the polarization map. To arrive at a decision about which process is more likely to be the cause of the polarization, requires further investigation of these models.

The only observations which can be made immediately on the basis of the polarization map alone is that the tendency for the polarization vectors to "follow" small dust loops (as mentioned in section 3.3.1) is more easily explained by the magnetic field model. Magnetic fields tend to "bottle" dust (see Parker, 1979), so that the loops in the dust tend to be associated with loops in the magnetic field, and consequently produce polarization in which the vectors are parallel to the dust loop. The scattering model would find this structure difficult to explain, since the geometry of scattering changes little on such a small scale. However, this loop structure is

seen only in one or two places on the map and depend on very few vectors for its interpretation. It would be advantageous, therefore, if other criteria could be found to differentiate between the two models, in order to corroborate (or otherwise) the indications of this small scale structure. One possibility for differentiating between the two models is the relation between the extinction and the degree of polarization. Pictures of NGC5128 show that the dust distribution near the galactic centre is very uneven, and imply that the light coming from different locations within the dust lane suffer different amounts of extinction. The dependancy of polarization on extinction is different in the two models and so it should be possible, by obtaining the actual relationship from the data, to determine which model is more realistic.

3.4.7 The Expected Form of the Polarization-Extinction Curve

Since exact calculations of multiple scattering situations are very difficult, we shall again restrict our attention for the moment, to simple qualitative arguments.

3.4.7.1 The Scattering Model

If some area within the dust lane is free of dust, then the E component luminosity will be observed unextinguished through this "hole". Obviously there will be no polarization in this case and so the curve of polarization against extinction will go through the origin. If now a little dust is placed in this "hole", then the polarization of the scattered light from each dust grain will tend to add. This is because the "hole" is assumed to be of small size and consequently the scattering geometry is approximately the same for all grains within it. Thus for small values of the extinction the polarization will rise as the scattered light becomes a more significant fraction of the total light. As the dust density increases, the probability of light being scattered twice or more on its journey through the dust lane, also increases. the probability that the polarizations will add constructively becomes less as this happens, since multiple scatterings tend to randomize the polarizations. Consequently the rate of increase of polarization with extinction will become less at higher extinctions. At very high dust densities, the final state of polarization of light scattered by dust grains in the "hole" will be almost completely random and will thus

cancel out almost entirely.

So the general form of the polarization versus extinction curve for a scattering model will look like that in fig. 3.4. The maximum in polarization will probably occur around an extinction value of unity, due to the fact that at this value the average number of scatters experienced by the light is one. At higher values multiple scatterings will start to introduce a depolarizing effect, but at lower values much light will pass through the dust without being scattered at all.

3.4.7.2 The Aligned Grains Model

In this model, the scattered light will behave as in the previous model, but will be added to light which has been polarized by differential extinction by the aligned grains. It would be expected that this direct, unscattered light will dominate the scattered light. The polarization of the unscattered light is approximately proportional to the optical depth through which it has travelled and so one would expect the resulting polarization versus extinction curve to be roughly linear. The corresponding curve of polarization against extinction of star light in our own Galaxy shows a linear form with a gradient of about 3% polarization per magnitude of extinction (see Greenberg, 1978).

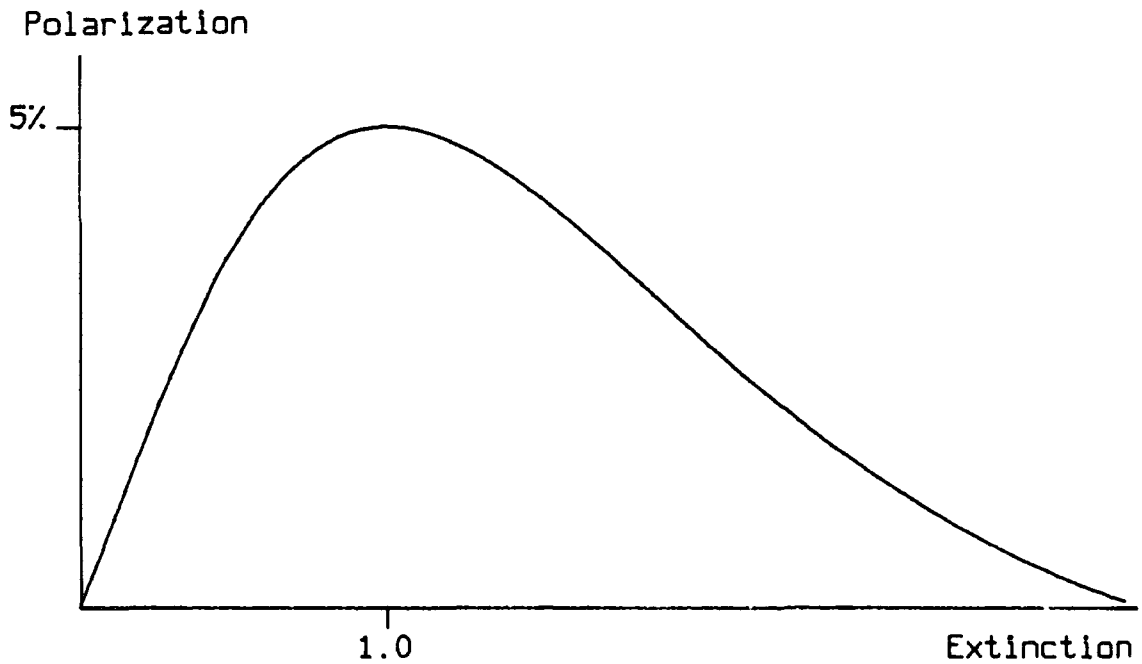

Fig. 3.4

The expected qualitative form of the polarization versus extinction curve for a simple scattering model of NGC5128. The figure of 5% for the maximum polarization was suggested by Jura (1983).

Having obtained the expected general form of the curve, we shall now look at the method used to obtain the polarization versus extinction curve from the data.

3.5 Image Processing

The end product of the reduction procedure performed on the NUMAC system was a file containing one record per pixel of the final image of NGC5128. Each record contains fourteen elements describing the polarization at that pixel, including the x and y co-ordinates of the pixel, the total intensity, and the percentage polarization. It was considered advisable to transfer this data from the NUMAC system to the new VAX 11/750 which forms the Durham node of the Science and Engineering Research Council's "Starlink" network. This computer has extensive image processing facilities and utilizes an advanced colour monitor system for interactive processes. A flexible method of data transfer between NUMAC and the Starlink VAX was developed in anticipation of a demand for such transfers, as the work of the polarimetry group at Durham moved from NUMAC to Starlink.

To evaluate the extinction caused by the dust it is necessary to know what the luminosity in the dust lane would be in the absence of dust. To do this it is necessary to fit De Vaucouleur's law to the unobscured

areas of the E component and then use the luminosity predicted by this law as the intrinsic luminosity in the obscured areas (see section 2.3).

3.5.1 Estimation of Isophotal Parameters

Before De Vaucouleur's law can be fitted, it is necessary to know several parameters which describe the geometry of the elliptical isophotes. These parameters are; their eccentricity, the orientation of their major axis, and the co-ordinates of their centre. These were estimated by finding the ellipse which gives the least squares best fit to a particular isophote. This procedure was repeated for several different isophotes and the mean values taken. It was found that the eccentricity and orientation of the best fitting ellipse changed systematically between the brightest and the faintest isophotes, the fainter isophotes having a higher eccentricity than the brighter isophotes, and being inclined at a smaller angle to the dust lane. Carter (1978) found this to be a common characteristic of elliptical galaxies. As it was more important to get a good fit in the brighter regions than the fainter regions, the actual values of the parameters adopted were estimated from the bright, inner regions. The eccentricity used was 0.39 and the major axis was taken to be tilted by

23° east of north. The centre of the elliptical isophotes was found to be situated 8 arcsec south of the nucleus found by Kunkle and Bradt (1971). Having determined values for these parameters it was possible to fit De Vaucouleur's law to the unobscured data.

3.5.2 De Vaucouleur's Law

The areas of the image which show obvious obscuration were blanked out, leaving only the unobscured regions which have been found by several people to fit De Vaucouleur's law well (see section 2.3). An image of an artificial elliptical galaxy with the isophotal parameters determined from NGC5128 was then produced in such a way that its luminosity followed De Vaucouleur's law. This galaxy was normalized to the unobscured data from NGC5128 by plotting a graph of the surface brightness of NGC5128 against the surface brightness of the artificial galaxy at the same location (fig. 3.5). It can be seen that there is a close linear fit between the luminosity of NGC5128 and that of the artificial galaxy implying that the data presented here is well represented by De Vaucouleur's law. The gradient and intercept of the best fitting straight line shown in fig. 3.5, determine the effective radius and the luminosity at the effective radius of the galaxy. The effective radius along the major axis determined by this

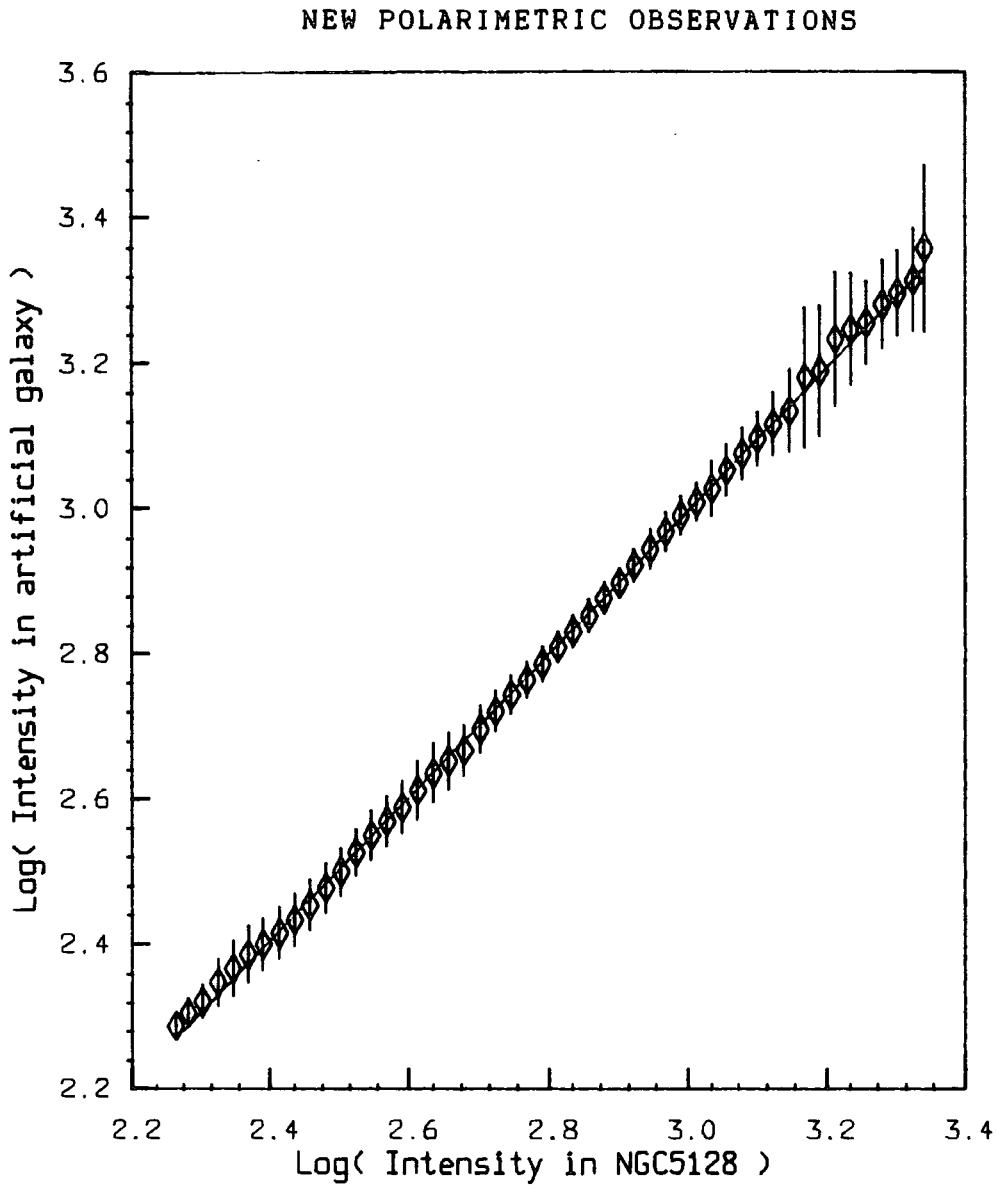

Fig. 3.5
A plot of the surface brightness in a perfect "De Vaucouleurs" elliptical galaxy (with the same isophotal parameters as NGC5128), against the surface brightness in the unobscured regions of NGC5128. The linear relationship indicates that the E component of NGC5128 follows De Vaucouleurs law well.

method was 222 arcsec which compares reasonably well with the values found by other workers, listed in section 2.3.

Having shown that the new data fits De Vaucouleur's law and having determined its parameters, it is possible to determine the intrinsic luminosity of the E component in the obscured regions of the galaxy. It is then possible, by comparing it with the actual obscured luminosity, to estimate the extinction.

3.5.3 The Extinction Image

An image was formed by subtracting the obscured surface brightness found from the data from the unobscured surface brightness as determined from the normalized artificial galaxy (fig. 3.6). The numbers in this image are a measure of the mean extinction through the obscuring dust, typical values for this extinction in the central regions of the dust lane, are 3 to 4 magnitudes. It should be noted that this is only equal to the extinction to the galactic centre if all the dust is situated in front of the luminosity (i.e. not intermingled with it), and if the scattered light is negligible compared to the direct unscattered light. However, the quantity in the image produced will be closely related to the extinction and will certainly rise as the extinction rises. In fact, the two effects mentioned both increase the brightness of the

Fig. 3.6

This image was obtained by subtracting the actual surface brightness of NGC5128 from the surface brightness of an artificial "De Vaucouleurs" elliptical galaxy, and thus provides a measure of the mean extinction through the dust lane. The brightest regions in this image correspond to 4 magnitudes of extinction.

dust lane, consequently the extinction values in the image of fig. 3.6 will always be lower than the true extinction through the dust lane to the nucleus.

3.5.4 Polarization versus Extinction

This "extinction" image can be compared directly with an image of the percentage polarization transfered from the NUMAC system and fig. 3.7 shows a scatter plot of polarization against extinction in a small region near the galactic centre where the extinction is seen to be non-uniform. It can be seen that there is some correlation between the two quantities with the polarization rising for values of extinction between 0 and 4 magnitudes. The trend appears to be linear with a gradient of 2.5% per magnitude. This data thus seems to support the claim that the polarizing mechanism is differential extinction by aligned grains. The facts that the dust in NGC5218 is thought to be similar to the dust in our own Galaxy (see section 2.4), and that the gradient of the polarization-extinction scatter plot is roughly equal to that found in our own Galaxy, imply that the magnetic field in NGC5128 is of roughly the same strength as that in our own Galaxy.

However, the scatter plot of fig. 3.7 can obviously not be presented as conclusive evidence, due to

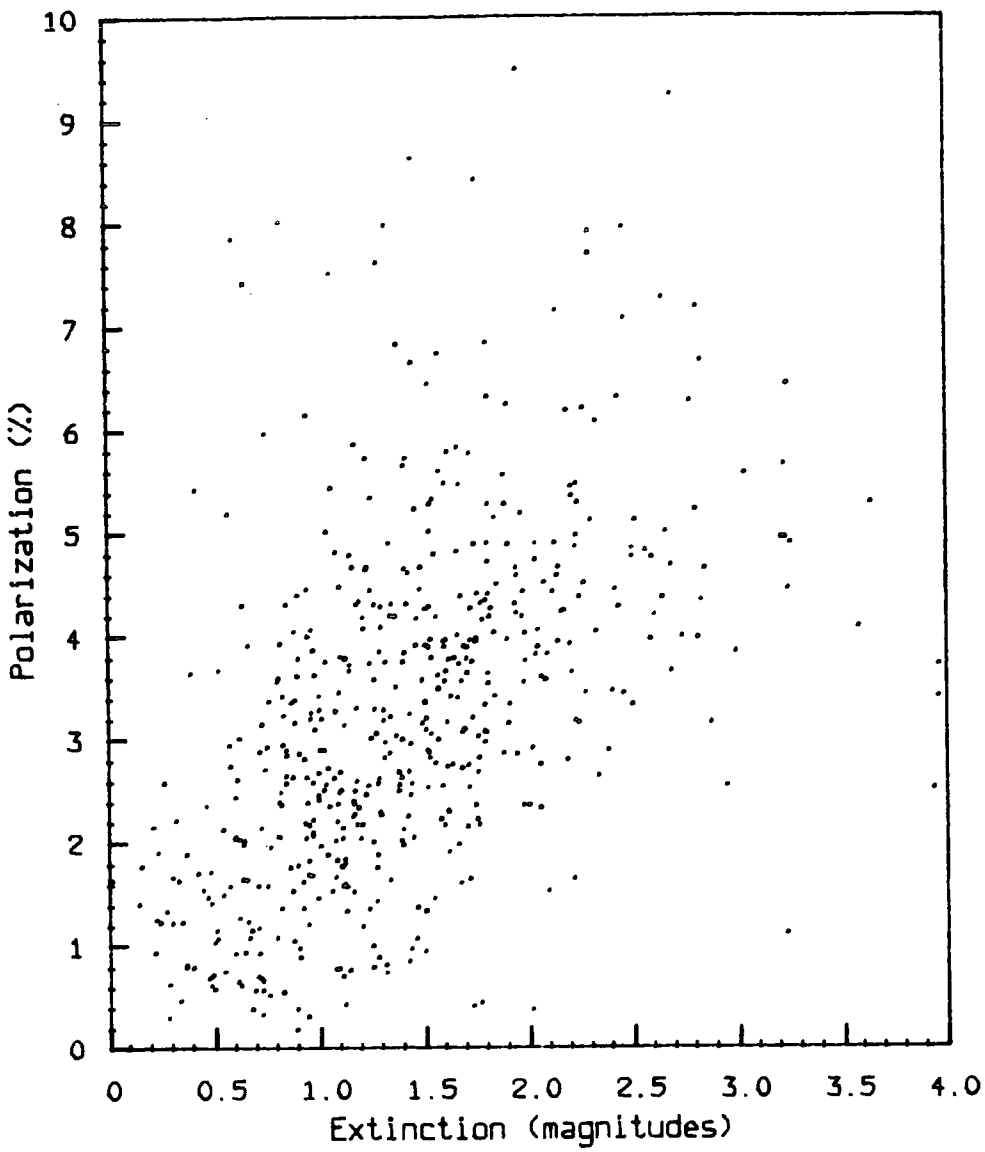

Fig. 3.7
A scatter plot of the polarization in the dust lane against the mean extinction through the dust lane (as described in section 3.5.3).

the high level of noise present. This noise is inevitable using the present polarimeter system, being a compound of the errors in total intensity and in polarization, both of which are higher than normal due to the low levels of polarization and total intensity being studied (especially in the heavily obscured regions).

3.6 Summary of Results

A new map of the polarization of NGC5128 is presented which is more extensive and is of higher resolution than previous maps of this object. The qualitative form of the map can be initially explained in terms of either a simple scattering model, or a simple model in which the dust grains are aligned by a magnetic field. Small scale structure in the map, and a possible correlation between polarization and extinction seem to imply that the magnetic field model is more likely, although the scattering model cannot be ruled out. If the magnetic field model is in fact a valid representation of the system, then the data implies that the strength of the magnetic field in NGC5128 is similar to that in our own Galaxy.

3.7 Further Work

Spectro-polarimetry of the central dust lane regions could clarify the situation further, but at the moment no such data is available. An alternative approach to the problem is to produce a more sophisticated realistic model of the system which could make quantitative, as well as qualitative, predictions. To this end, a model based on a backwards Monte-Carlo simulation of multiple photon scattering in an inclined, thick disk of Mie scatters, has been developed and will be presented in the next chapter.

CHAPTER 4

A Computer Model of NGC5128

Certain features of the data presented in the last chapter suggest that the polarization seen in the inner regions of the dust lane of NGC5128 is caused by differential extinction in a cloud of aligned, non-spherical grains. The data, however, is inconclusive, and since Jura (1982) has calculated that simple scattering from spherical or un-aligned grains could, under certain conditions, produce the observed polarizations, it would seem that this possibility cannot be ruled out. However, the validity of Jura's conclusions must be questioned, since several of the assumptions which must be made in order to arrive at his conclusion, are not tenable in the case of NGC5128. His model assumes an optically thin cloud of Rayleigh scatterers located at the centre of a thin disk,

equatorially situated in an extended luminosity source. This sort of model will produce polarizations which are higher than those possible in a more realistic model in which multiple scattering is allowed and Mie scatterers are used instead of Rayleigh scatterers. All available data on the extinction through the dust lane imply that the dust is optically thick, the data presented in the last chapter gives an extinction of more than 4 magnitudes. Thus multiply scattered light will be significant, resulting in a smaller value for the degree of polarization. The dust has been found to be similar in several respects, to that in our own Galaxy, and thus, it would be very surprising if the average size of the dust grains in NGC5128 is small enough to invoke the laws of Rayleigh scattering.

In order to see if a more realistic model supports Jura's conclusion, or if some polarizing mechanism other than scattering must be active in NGC5128, a computer model of light scattering in an NGC5128-like system has been developed. The model allows photons to be multiply scattered, using the laws of Mie scattering to describe the scatters, and uses a more realistic geometry than Jura's model.

The production of analytic models for light scattering situations is only possible in a very few simplified situations, and in general it has been found

necessary to use numerical techniques to provide more realistic models. The techniques most often used for this purpose generally use some form of Monte-Carlo simulation. The initial attempts at such models (Roark et al, 1974) required excessively large amounts of computer time to produce reasonable accuracy. Consequently the estimation of polarization was difficult since it requires the estimation of light intensities to high accuracy. With time, greater sophistication was added to these models to improve their efficiency so that now, polarization as well as total intensity can be modelled with high accuracy for certain situations, using reasonable amounts of computer time (Warren-Smith 1979,1983; Moore, 1982).

4.1 The Monte-Carlo Technique

To illustrate the principles of the Monte-Carlo technique, consider the following one dimensional definite integral

$$I = \int_a^b f(x).dx$$

There are many ways of numerically determining the value of this integral, many (known as methods of quadrature) involving the subdivision of the interval [a,b] into regular sub-intervals, and the fitting of some analytic

curve to the points within each sub-interval. The rectangle rule is one such method and provides the following estimate of the integral

$$I_{rect} = \Delta x . \sum_{n=1}^{m} f(x_n)$$

$$\text{where } \Delta x = \frac{|b-a|}{m} \quad \text{and} \quad x_n = a+(n-1).\Delta x$$

in which the integral is determined in terms of the value of the function f at a set of evenly spaced points in the interval [a,b].

It can be shown that if instead of being chosen evenly, each value of x_n is chosen randomly with a constant probability of being anywhere in the interval [a,b], then the expression given above is still an unbiassed estimator of the integral I. This is the basis of the Monte-Carlo technique of integration. Of course, such a technique has little to offer in such a simple case as the above integral, but starts to become worthwhile as the nature of the integration becomes more complex, for instance when f is a function of many variables.

If, in the above simple integral, the function f takes a wide range of values in the interval [a,b], then it is obvious that the value of the integral will be determined more by the large values than by the small values. It would be more efficient therefore if the values of x at which f takes large values could be sampled more

often (i.e. with higher probability) than those at which f takes small values. It would then be necessary to give the seldomly chosen values a larger weight than the frequently chosen values, to correct for the under sampling they have suffered. In fact, it can be shown that if x_n (n=1,m) are random samples from some distribution such that the probability of x_n having a value between x and x+dx is P(x)dx (P(x) is known as the probability density function, or PDF, of x), and if

$$\int_a^b P(x).dx = 1$$

then

$$I_{mc} = \frac{1}{m}.\sum_{n=1}^{m} \frac{f(x_n)}{P(x_n)} \qquad \text{4.1}$$

is an unbiassed estimator of the integral I (note, the |b-a| term in Δx appears within P(x) due to the normalization constraint on P(x)). If P(x) and f(x) have similar forms, then the ratio f(x)/P(x) takes nearly constant values and the random error in the estimate of the integral is reduced (Hammersley and Handscombe, 1975 - importance sampling).

4.1.1 Astronomical Aplications of Monte-Carlo

Consider a dust cloud of arbitrary shape, as shown in fig. 4.1, of constant dust density, N (m^{-3}). Let the luminosity per unit volume at each point in the cloud's co-ordinate system be $L(\underline{r})$ (Wm^{-3}), where the luminosity functon L can take the value zero. A reflection nebula will thus have a non-zero value of L only at the position vector $\underline{r}$ corresponding to the position of the illuminating star (usualy considered to be of negligble size compared to the cloud), whereas a galaxy will have a much more extensive volume of non-zero luminosity. Let the observer view the cloud in a direction parallel to the z axis, and let his instrument measure the flux $\underline{R}$ (where $\underline{R}$ is a Stokes vector with total intensity measured in Wm^{-2}), of light being emitted from an area A of the cloud's surface. The task of the computer model is to estimate $\underline{R}$ given all the parameters describing the cloud. In order to achieve this, $\underline{R}$ is broken down into seperate contributions from light which has been subject to different numbers of scatters on its journey through the cloud. Thus

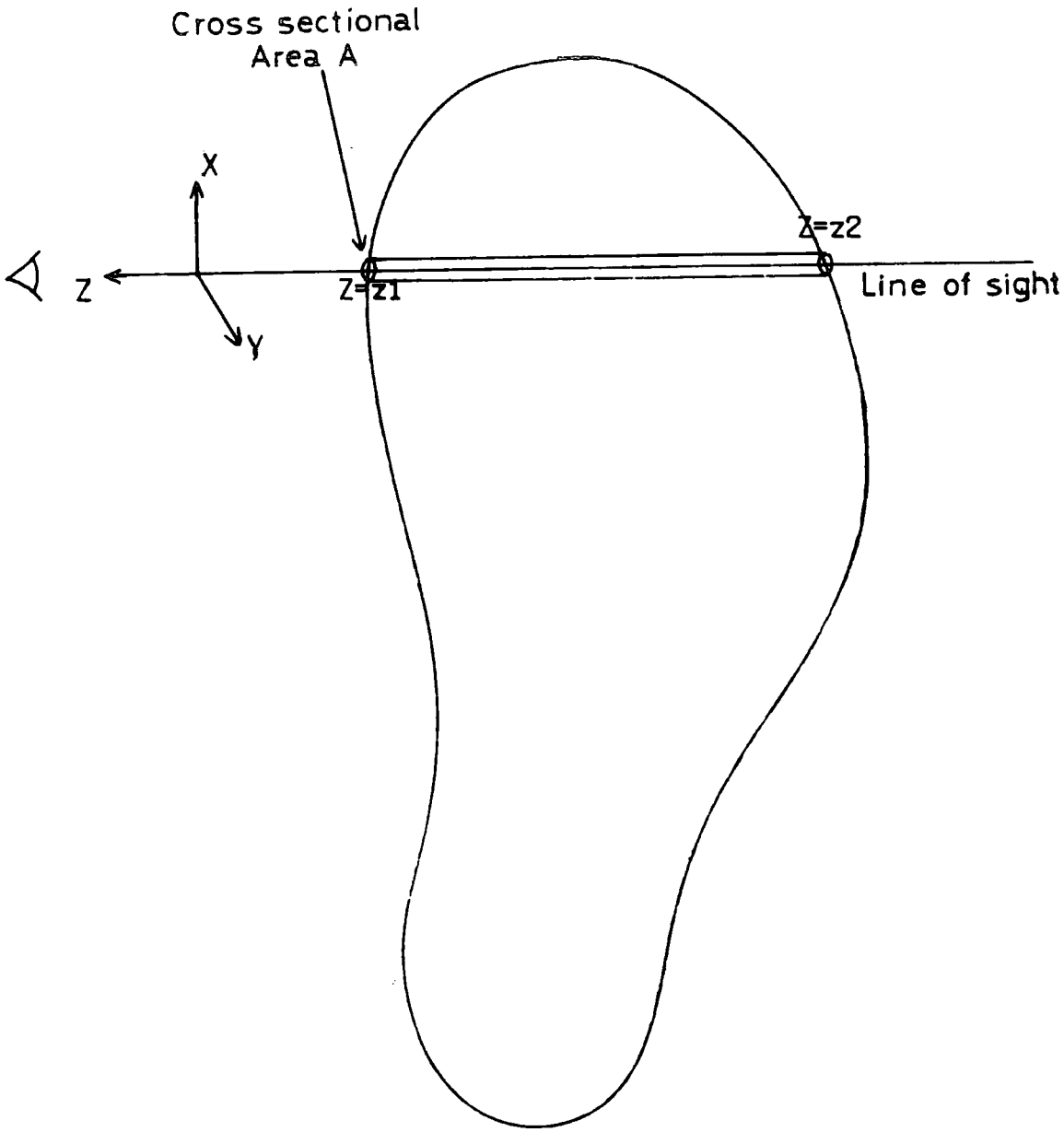

Fig. 4.1

A dust cloud of arbitrary shape.

$$\underline{R} = \sum_{j=0}^{\infty} \underline{R}_j$$

where $\underline{R}_j$ (Wm^{-2}) is the Stokes vector of light which has been scattered exactly j times.

4.1.2 The Unscattered Light

$\underline{R}_0$ corresponds to light which reaches the observer directly without being scattered even once, and so will be unpolarized (the light is considered to be initially unpolarized). Thus, in order to evaluate $\underline{R}_0$ all that must be done is to integrate the luminosity function along the line of sight, including an exponential extinction factor to account for the fact that some of the light emitted on the line of sight will be scattered out of it before leaving the cloud. So, if the distance between the cloud and the observer is d, and the dimensions of the cloud are small compared to d, then

$$\underline{R}_0 = \frac{1}{d^2}.\underline{S}_0.\int_{z1}^{z2} e^{-\tau(z)}.\frac{\underline{L}(z)}{4\pi}.A.dz \qquad \text{4.2}$$

where $\underline{S}_0 = (1,0,0,0)$, the unit unpolarized Stokes vector, and $\tau(z)$ is the optical depth from the

position z on the line of sight to the observer. This simple one dimensional integral is most efficiently evaluated using a quadrature technique.

4.1.3 The Scattered light

Light which has been scattered will, in general, be polarized. The Stokes vector of scattered light can be determined if the exact path which the light has followed through the dust is known. If the light originates within a volume element dV_0, centred at position $\underline{r}_0$ with luminosity per unit volume $L(\underline{r}_0)$, is then scattered within volume elements $dV_1, dV_2 \ldots dV_j$, centred at positions $\underline{r}_1, \underline{r}_2 \ldots \underline{r}_j$ and the final scattering angle is within a range $d\alpha$ centred at α_j (see fig. 4.2), then the final Stokes vector can be written as

$$L(\underline{r}_0) \cdot \frac{1}{4\pi} \cdot \underline{S}_j(\underline{r}_0, \underline{r}_1, \ldots \underline{r}_j, \alpha_j) \cdot \prod_{i=0}^{j} dV_i \qquad (W.Sr^{-1})$$

(where $\underline{S}_j$ is the Stokes vector produced for unit luminosity per steradian in the source volume element). If we represent the whole path by the (3*j+4) dimensional vector $\underline{P}_j$, then we can write an expression eqivalent to the above in terms of $\underline{P}_j$,

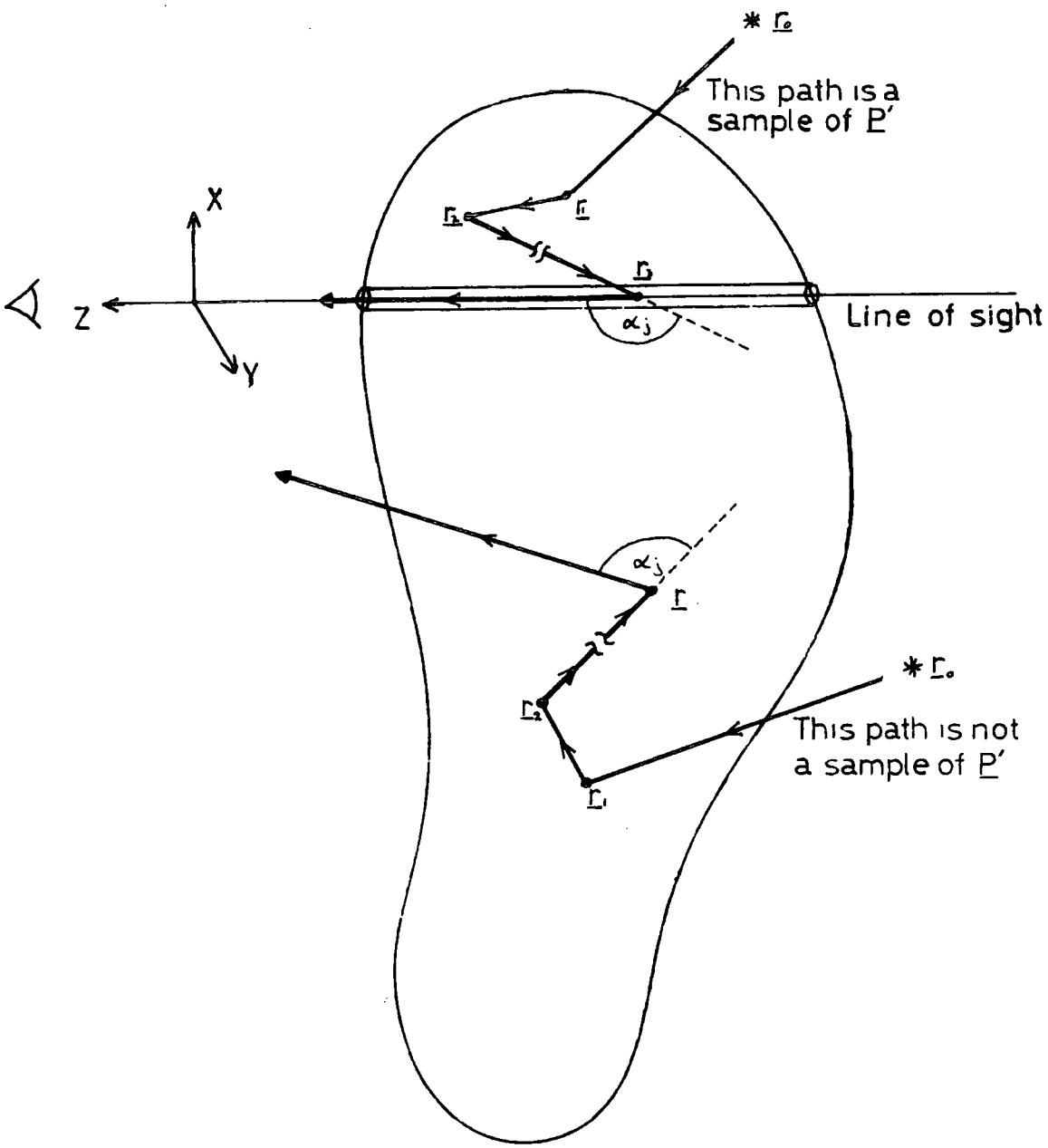

Fig. 4.2

Light paths within the dust cloud.

$$L(\underline{r}_0).\frac{1}{4\pi}.\underline{S}_j(\underline{P}_j).\prod_{i=0}^{j} dV_i \qquad (W.Sr^{-1})$$

Since light is scattered at random inside the cloud, not all of these light paths will result in light being scattered towards the observer, and so not all paths will be useful. Let those paths which do result in light being scattered towards the observer be denoted by primes, $\underline{P}_j'$. These paths must obviously have their final scattering position, $\underline{r}_j$, on the line of sight and before light following one of these paths can escape from the cloud it must avoid being scattered out of the line of sight. This results in an extinction which depends on the optical depth $\tau(\underline{r}_j)$, between the edge of the cloud and the position on the line of sight at which the light suffered its final scatter. So the Stokes vector measured by the observer for light which has followed some path $\underline{P}_j'$ through the dust will be $d\underline{R}_j$ where

$$d\underline{R}_j = \frac{1}{d^2}.e^{-\tau(r_j)}.L(\underline{r}_0).\frac{1}{4\pi}.\underline{S}_j(\underline{P}_j').\prod_{i=0}^{j} dV_i \qquad \text{4.3}$$

where $dV_j = A.dz$

What the observer would actually measure for $\underline{R}_j$ would be the sum of this expression taken over all possible light paths $\underline{P}_j'$. The Monte-Carlo method can be used to evaluate the sum of this expression if random samples of

the path $\underline{P}_j'$ can be formed with known probability and if $d\underline{R}_j$ can be evaluated for each such sample (as in equation 4.1).

4.1.4 Sampling the Light Paths

The easiest way of obtaining random samples of $\underline{P}_j'$ is to form random samples of $\underline{P}_j$ by allowing a unit of energy (referred to as a "photon") to originate at some random position anywhere within the model, and then be scattered j times at random. (Care must be taken in thinking about these "photons" since they do not correspond to real photons. The "photons" in the model are simply units of energy and can be attenuated by various means, unlike real photons.)

This method is very inefficient since very few of these samples of $\underline{P}_j$ will be samples of $\underline{P}_j'$, that is, they will not result in light being scattered towards the observer. Another source of inefficiency will arise if there are large volumes of space in which the luminosity function $L(\underline{r}_0)$ takes the value zero, since the contribution to the integral $\underline{R}_j$ of a photon originating at such a position will be zero. It is desirable therefore to use some form of sampling procedure which preferentially selects paths which are samples of $\underline{P}_j'$ and/or have their origin

at positions with non-zero luminosity. There are two basic method which can be used to achieve this known as the forward Monte-Carlo method and the backward Monte-Carlo method.

4.1.4.1 The Forward Monte-Carlo Method

In this method the point of origin of the photon path is selected from a distribution which has a probability density function (PDF) of similar form to the luminosity function, so that the bright regions are sampled more frequently than the dark regions. The bias introduced by using such a non-uniform distribution is removed by dividing the luminosity by the probabilty with which it was chosen. If the PDF is a top hat function (i.e. has the value zero everywhere except in a bounded region where it is constant) then this merely introduces a scaling factor in the final result and can be forgotten. In the case of a single point source illuminating the cloud (as in a reflection nebula) the PDF used to select the photon paths point of origin should be such a top hat function in which the volume of the bounded region tends to zero, so all paths start at the same position (the star).

Having thus determined the starting point of the photon path it is necessary to obtain a sequence of

random, independent scattering angles and path lengths to define the path. This results, of course, in the end point of the path (the jth scattering position) being randomly positioned, since it is obviously impossible to select scattering angles and path lengths independently and still constrain both the start and end of the light path. So the inefficiency introduced by not many of the samples of $\underline{P}_j$ being samples of $\underline{P}_j'$, remains. However, this can be overcome to a large extent, by the system developed by Warren-Smith (1979,1983) in which photon paths which do not form a sample of $\underline{P}_j'$ are rotated about their point of origin until the jth scattering position lies on the line of sight. The final scattering angle is then forced to take a value such that the photon travels towards the observer (see fig. 4.3). This method requires a slightly different formulation of the integral $\underline{R}_j$ in which the final scattering angle is not chosen at random. Not all photons can be thus rotated, since such a rotation may result in a scatter occuring outside the cloud, which obviously has zero probability of happening. Also the Warren-Smith method imposes limitations on the dust-luminosity geometries which can be used; there must be no chance of a photon which has left the dust, ever re-entering the dust (i.e. there must be no "holes" in the dust, or concave surfaces), and all non-zero luminosity must be situated

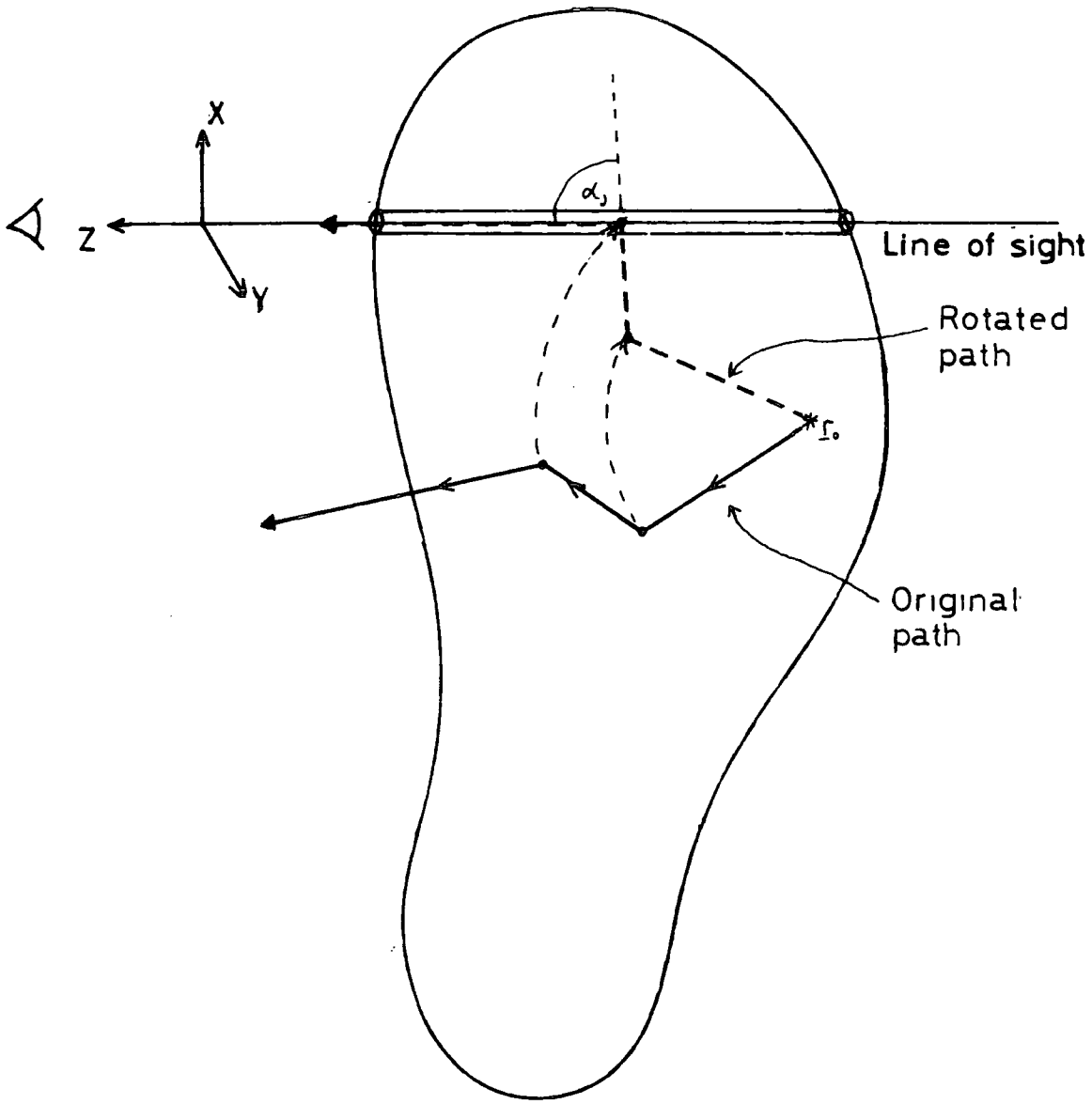

Fig. 4.3
The method of rotating the photon paths used by Warren-Smith to ensure that all photons reach the observer.

inside the cloud. Moore (1982) developed a technique to overcome the later problem by introducing a weighting factor in the photons Stokes vector to correct for the lack of extinction in the first scattering path. This method becomes very inefficient if luminosity is situated a long way from the dust (as in the case of NGC5128) . This is indicative of the fact that once one constraint has been applied to the samples (in this case, constraining the starting positions to sample the luminosity efficiently) it is difficult to apply another constraint (for example, that the dust should also be efficiently sampled) and still ensure the independance of the angles and path lengths that make up each sample.

4.1.4.2 The Backward Monte-Carlo Method

The backward Monte-Carlo method (introduced by Collins et al, 1972) constrains the end of the light path rather than the begining (as in the forward method) and thus ensures that all light paths sampled are samples of $\underline{P}_j'$. This is achieved by forcing the final scattering position $\underline{r}_j$ to be on the line of sight (the position on the line of sight is chosen at random from a distribution which samples the dust efficiently). The scattering angles and path lengths which define the light path are then chosen at random. The order in which these

angles and path lengths are chosen is, by necessity, reversed between the forward and the backward methods, and it can be shown (Carter et al, 1978) that the backward Monte-Carlo method is equivalent to a forward Monte-Carlo simulation of a time reversed scattering model (i.e. a model in which the light originates at the observer and travels towards the cloud). We shall from here on refer to the non time reversed model, so that by the "start" of the photon path we shall mean the position in the cloud at which the light was emitted, etc.

The disadvantage of the backward method is, of course, that having constrained the end of the light path, the start of the light path cannot be constrained. There is thus no control over where the lumninosity is sampled, leading to great inefficiency if the non-zero luminosity is not extensive. However, for the case of an elliptical galaxy like NGC5128, in which there is non-zero luminosity at every position within the model, the backward method is to be preferred to the forward method. This is because in an NGC5128 like model, the efficient sampling of the dust distribution is more important than the sampling of the luminosity since the luminosity is more extensive than the dust. In a reflection nebula, the position is reversed, since the luminosity is far less extensive than the dust. Consequently, it was decided to implement a backward Monte-Carlo model of NGC5128.

4.1.7 Forming the results

Having obtained samples of $\underline{P}_j'$ with known probability, the value of $d\underline{R}_j$ (equation 4.3) can now be calculated. To do this each photon is considered to start out from its point of origin (determined by the sample of $\underline{P}_j'$ being used) with a unit unpolarized Stokes vector, $\underline{S}_0=(1,0,0,0)$. If l_i is the distance travelled inside the dust between the (i-1)th and the ith scatters, then the photon will suffer an extinction of

$$e^{-\frac{l_i}{MFP}}$$

between the (i-1)th and the ith scatters, (where MFP is the mean free path of light in the dust) and so the Stokes vector of the photon when it arrives at the ith scatter will be

$$\underline{S}_{i-1}' = e^{-\frac{l_{i-1}}{MFP}} . \underline{S}_{i-1}$$

where $\underline{S}_{i-1}$ is the Stokes vector of the photon after i-1 scatters. (No modification needs to be made to the Stokes vector to account for the inverse square law, since the photons used are units of energy and do not themselves

measure light flux. The light flux is measured by the density of photons and this automatically follows an inverse square law due to the spreading out of photons as they move away from the point of origin.)

If, at the ith scatter, the photon is scattered through an angle α_i, then the Stokes vector of the scattered photon is obtained by multiplying the unscattered Stokes vector first by a matrix which rotates the reference direction of the incoming Stokes vector to the normal to the next scattering plane, T_i, and then by a scattering matrix $M(\alpha_i)$ (calculated from the Mie theory). Thus

$$\underline{S}_i' = M(\alpha_i).T_i.e^{-\frac{l_{i-1}}{MFP}}.\underline{S}_{i-1}$$

and by successive aplications of this for each scatter in the path, we obtain

$$\underline{S}_j(\underline{P}_j') = \prod_{i=1}^{j}\left(M(\alpha_i).T_i.e^{-\frac{l_{i-1}}{MFP}}\right).\underline{S}_0$$

The remaining factors in $d\underline{R}_j$ are the luminosity at the photons origin (which is easily determined), and the extinction along the path joining the final scattering position to the observer. If this path traverses a distance l^* inside the dust, then this extinction is

$$e^{-\frac{l^*}{MFP}}$$

So the final expression for $d\underline{R}_j$ is

$$d\underline{R}_j = \frac{1}{d^2}.e^{-\frac{l^*}{MFP}}.L(\underline{r}_0).\frac{1}{4\pi}.\prod_{i=1}^{j}\left(M(\alpha_i).T_i.e^{-\frac{l_{i-1}}{MFP}}\right).\underline{S}_0.\prod_{i=0}^{j}dV_i$$

The Monte-Carlo estimation of $\underline{R}_j$ (the integral of $d\underline{R}_j$) is formed by dividing this value by the probability with which the photon path was chosen, and then summing the resulting values of all the photon paths used (as in equation 4.1)

$$\underline{R}_j = \frac{1}{NPHOT}.\sum_{k=1}^{NPHOT}\left(\frac{dR_i}{PROBABILITY}\right)_k \qquad \text{---- 4.4}$$

where NPHOT is the number of photons used. since it has been ensured that all scattering angles and path lengths are chosen independently, the probability of choosing a particular path is the product of the probabilities with which the individual angles and path lengths were chosen. So if $A(\alpha_i)$ is the PDF with which α_i is chosen, and $D(l_i)$ is the PDF with which l_i is chosen, then the probability of choosing the entire path is

$$\prod_{i=1}^{j} A(\alpha_i).D(l_{i-1})$$

An additional factor in this probability expression is required, dependent on the Monte-Carlo method being used. If the forward method is being used then a factor must be included giving the probability with which the starting point of the photon path was chosen. If the backward method is being used then the extra factor needed is the probability with which the initial distance l^* was chosen, say $F(l^*)$. Thus the final estimate of $\underline{R}_j$ is (for a backward model);

$$\underline{R}_j = \frac{1}{NPHOT} \sum_{k=1}^{NPHOT} \left(\frac{\frac{1}{d^2}.e^{-\frac{l^*}{MFP}}.L(\underline{r}_0).\frac{1}{4\pi}.\prod_{i=1}^{j}\left(M(\alpha_i).T_i.e^{-\frac{l_{i-1}}{MFP}}\right).\underline{S}_0.\prod_{i=0}^{j} dV_i}{\prod_{i=1}^{j} A(\alpha_i).D(l_{i-1})} \right)_k \qquad \text{---- 4.5}$$

It is generally possible to choose the functions A,D and F such that many terms cancel in the above expression. This results in the value of $(d\underline{R}_j)/(\text{PROBABILITY})$ for each individual photon being much more similar and consequently fewer photons being needed to achieve the required accuracy.

The final values required from the model are

those of the Stokes parameters (measured by the observer) including light of all scattering multiplicities, $\underline{R}$, where

$$\underline{R} = \underline{R}_0 + \underline{R}_1 + \underline{R}_2 + \ldots \qquad 4.6$$

In general, a limit can be put on the number of terms required in this summation, due to the random walk of scattering positions away from the observers line of sight. This results in a decrease in the number of photons originating at positions of non-zero luminosity as the number of scatters the photons have suffered increases. Of course, if the dust grains have a negative imaginary part to their refractive index, then they will absorb energy from the photons at each scatter, and this will also contribute to the decrease in the importance of photons which have been scattered many times.

4.2 The New Model

The new backwards Monte-Carlo model of NGC5128 will now be described in more detail starting with the general procedure followed.

4.2.1 The General Procedure

The unscattered light contribution $\underline{R}_0$ (equation 4.2) is first evaluated using a quadrature method, and added to the final sum of equation 4.6. Test photons are then allowed to propagate backwards through the model from the observer, until each photon is "lost" (i.e. leaves the dust cloud in such a way that it never re-enters) or the specified maximum number of scatters is reached, corresponding to the truncation of equation 4.6.

As each photon travels through the dust it has associated with it a matrix which is modified according to to the extinction the photon suffers and the angles it is scattered through. This matrix represents the transformation an unpolarized Stokes vector would experience if it re-traced the photon path back to the observer. Each photon can thus be used to produce a contribution to each term in equation 4.6 (except $\underline{R}_0$) until the photon is lost. This is done by selecting an "illuminating point" after each scatter, a distance v along the new propagation direction, and allowing light from that point to travel outwards along the photon path so far defined, until it reaches the observer. The contribution it then makes to the appropriate term $\underline{R}_i$ is determined by allowing the current transformation

matrix to act on an unpolarized Stokes vector given by

$$\frac{L(\underline{r}).e^{-\tau}}{P(v)}.\underline{S_0} \qquad \text{4.7}$$

where $L(\underline{r})$ is the luminosity at the illuminating point, $P(v)$ is the probability of choosing the value v, and τ is the optical depth along the line joining the illuminating point to the first scattering point. The function P is chosen so that the luminosity is sampled efficiently.

The other probabilities required in the photons contribution to $\underline{R_j}$ (see equation 4.5) are included by dividing their values at each scatter into the matrix as they occur. For instance, if at some scatter, the value of the scattering angle is chosen to be α, then the probability with which this value was chosen (namely $A(\alpha)$) is divided into the current transformation matrix.

4.2.2 The Luminosity Function

The surface brightness of the E component of NGC5128 has been found to follow De Vaucouleur's law well (see sections 2.3 and 3.5.2) and hence it is reasonable to use a luminosity function which reproduces this law. Young (1976) tabulates the luminosity per unit volume at 124

different radii in a spherical distribution of luminosity which on integrating along the line of sight, produces a surface brightness which fits De Vaucouleur's law with an effective radius of unity. (From here on the effective radius of the surface brightness is taken as the unit of distance in the model.) The fit is found to be good from a radius of 10^{-6} effective radii to 260 effective radii. To use this function in the model the circular isophotes have been transformed into elliptical isophotes with an eccentricity of 0.39 (as found in section 3.5.1). A plot of the function, on Log-Log axes is shown in fig. 4.4. Log axes are used because of the large range of radii being used (10^{-6} to 10^{2}) and because of the very bright, narrow peak in luminosity around the origin. In the model this corresponds to a very small region of extremely high luminosity at the galactic centre. It was found to be difficult to integrate the luminosity function across this peak and so it was decided not to use lines of sight within 0.03 effective radii of the galactic centre.

The extremely large variation in luminosity function is the cause of one of the largest sources of inefficiency in the model. As was mentioned in section 4.1.4.2, the backward Monte-Carlo method cannot efficiently sample the luminosity distribution (i.e. sample the brighter regions more often) and so in cases like this where there is a large variation in luminosity

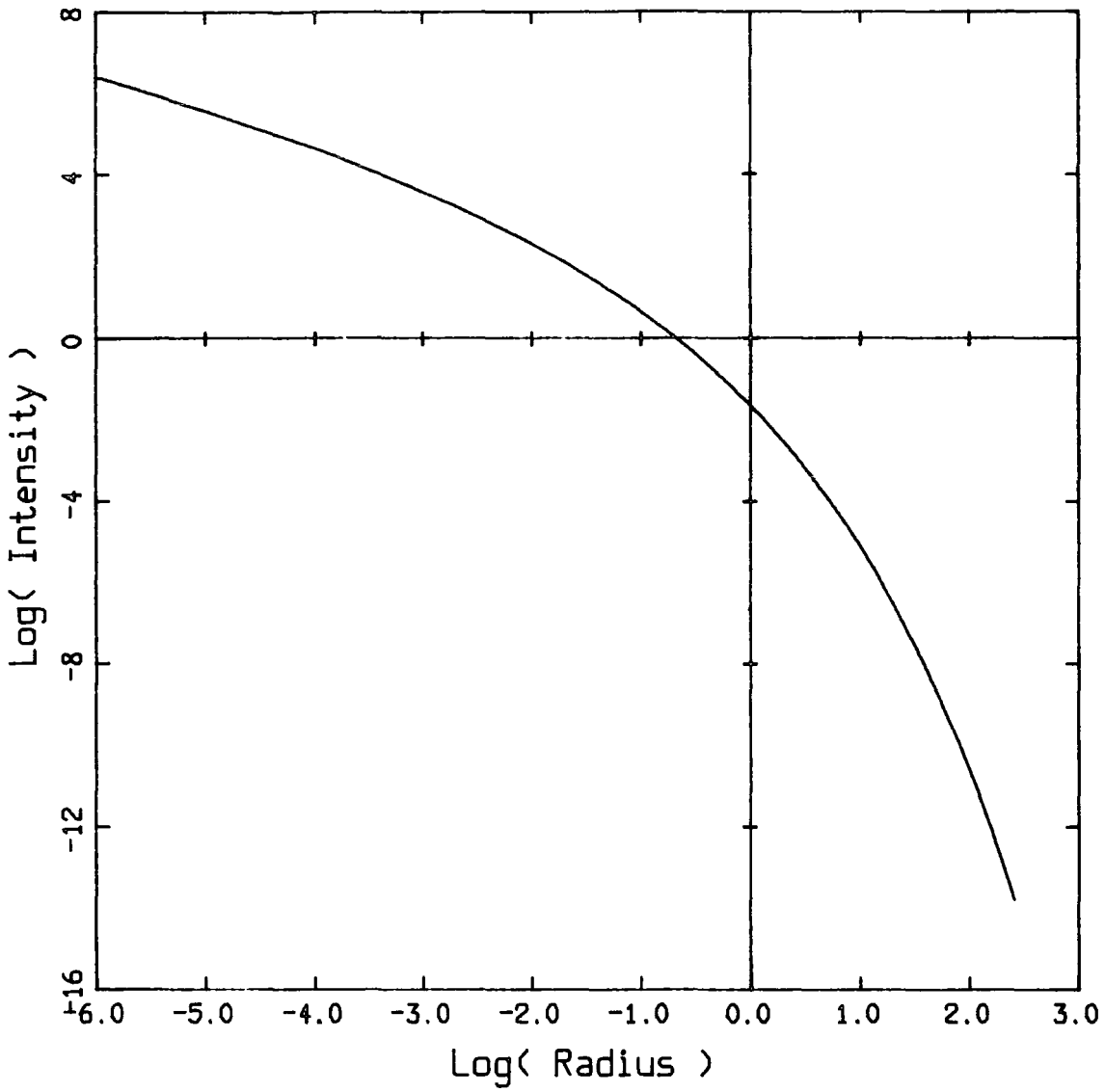

Fig. 4.4
The 3 dimensional de-projection of a De Vaucouleurs law luminosity distribution (data taken from Young, 1976). The vertical axis corresponds to the 3 dimensional density of luminosity.

(10^{6} to 10^{-14}), a high degree of inefficiency is introduced.

4.2.3 The Dust Geometry

The geometry of the dust distribution corresponding to the disk component of NGC5128, was decided on as a compromise between excessive complication and usefulness. The dust is considered to be uniformly distributed (i.e. the dust density is constant) within an annulus of finite dimensions, lying in the equatorial plane of the luminosity, as shown in fig. 4.5. All the parameters describing the dust distribution, namely the thickness of the disk, the inner and outer radii, and the dust density, are specified at the start of each run of the model. In addition to these parameters the tilt of the whole dust/luminosity system to the observers line of sight can also be specified.

This is obviously only an approximation to NGC5128. In reality the disk is warped and has various non-circular features (see section 2.4), and the dust density is certainly not constant. However, the simple geometry adopted should be able to distinguish between the available polarizing mechanisms, and is significantly more sophisticated than previous models.

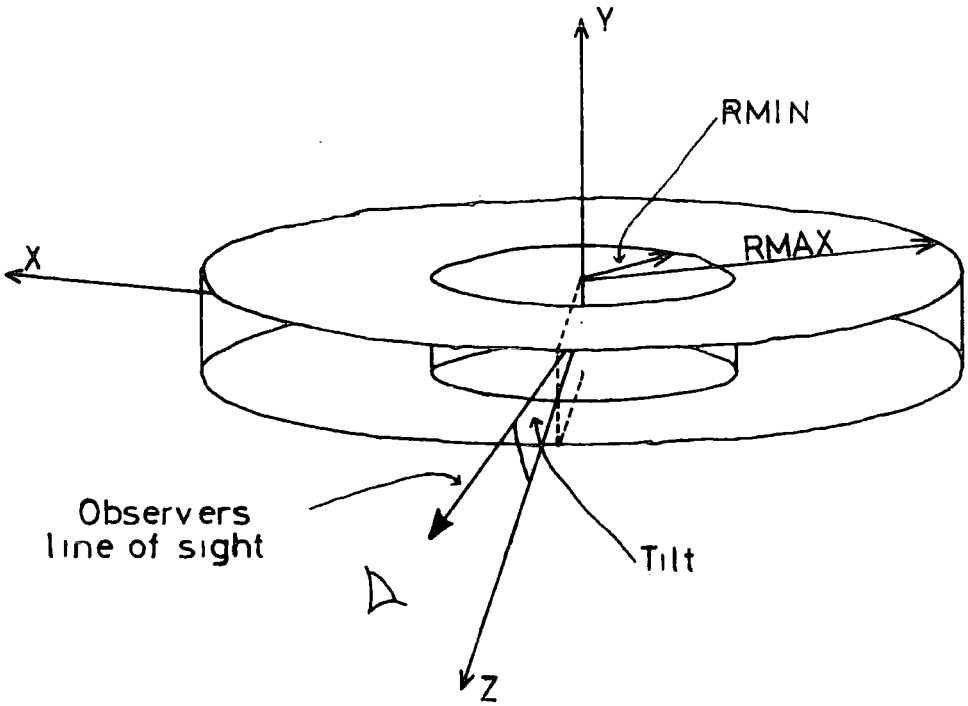

Fig. 4.5
The dust geometry used in the model. All the parameters shown, plus the thickness of the disk, can be varied easily.

4.2.4 The Scattering Matrix

The matrix which describes the transformation of an arbitrary incident Stokes vector at each scatter is derived from the Mie theory of scattering and corresponds to scattering from a cloud of spherical grains with a distribution of different grain sizes. This size distribution together with the refractive index of the grain material (which can have an imaginary part) is specified at the start of each run and can be easily changed.

The subroutines used to calculate this matrix were originally written by Dr. R.F. Warren-Smith (1979) and are described in more detail by him.

4.2.5 The Scattering Angles

The angle through which a photon is deviated at each scatter, α, is chosen randomly from a distribution with known PDF. The efficiency of the model can be increased by selecting a suitable form for this PDF such that the photons which form a greater contribution to the final result are sampled more often (importance sampling).

When light is incident on a cloud of scatterers,

it is scattered in all directions, although the amount scattered in different directions varies. If the incident light is unpolarized, the power scattered into a unit solid angles is azimuthally symetric (i.e. is independent of the angle ψ, see fig. 4.6) and depends only on the scattering angle α. However, the total solid angle corresponding to a scattering angle of α depends on the value of α being used. For instance, there is more solid angle available for scattering by 90° than by 0°. Thus if $W(\alpha)$ is the power scattered through an angle α into unit solid angle for unpolarized incident light, then the total power scattered by α is

$$W(\alpha).2\pi.\mathrm{Sin}(\alpha)$$

(The function $W(\alpha)$ can easily be calculated using the same integration routines used to obtain the scattering matrix, see Warren-Smith ,1979) Thus, ideally, the scattering angle α, should be chosen with a PDF proportional to the above expression. In fact, it is more straight-forward to select samples of $\mathrm{Cos}(\alpha)$ rather than α, since the $\mathrm{Sin}(\alpha)$ factor appears automatically due to the normalization. The probability of sampling $\mathrm{Cos}(\alpha)$ in a range $d\mathrm{Cos}(\alpha)$ from a distribution with PDF, $W'(\mathrm{Cos}(\alpha))$ is

$$W'(\mathrm{Cos}(\alpha)).d\mathrm{Cos}(\alpha) = W'(\mathrm{Cos}(\alpha)).\mathrm{Sin}(\alpha).d\alpha$$

Thus, ideally $\mathrm{Cos}(\alpha)$ should be sampled with a PDF

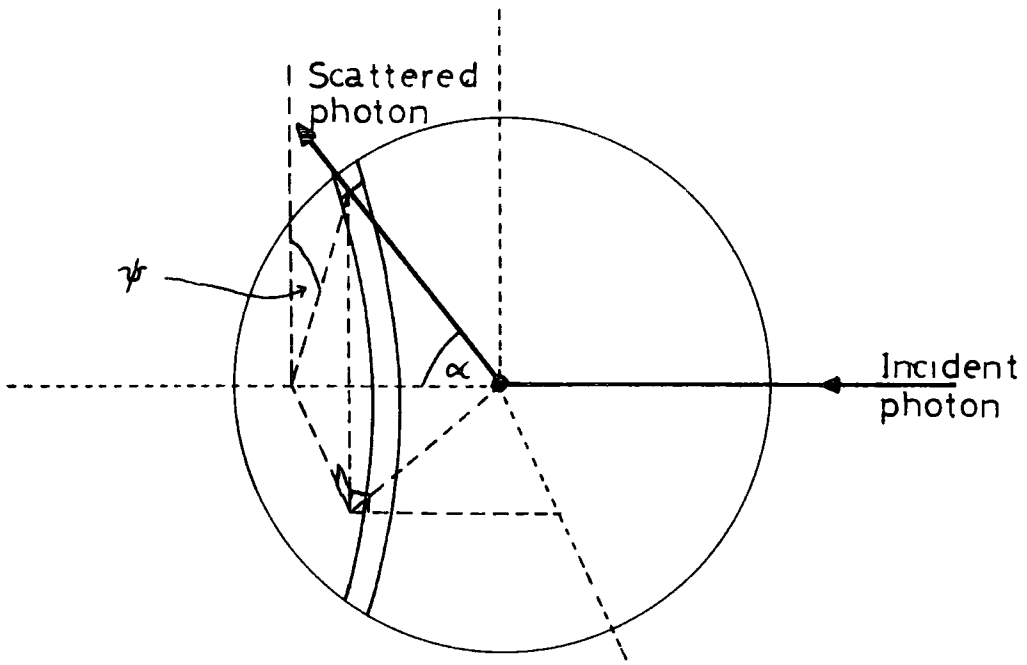

Fig. 4.6
The scattering angles.

proportional to $W'(\mathrm{Cos}(\alpha)) = 2\pi.W(\alpha)$. The above argument assumed unpolarized incident light, but if the incident light is polarized then the scattered light will not be azimuthally symetric. The present model does not attempt to sample the azimuthal scattering angle ψ, efficiently. In fact, ψ is chosen from a uniform distribution, i.e. the photons are scattered with azimuthal symetry, so the above argument still holds for the model in the case of polarized incident photons.

In previous forward Monte-Carlo models, the PDF actually used has not been $W'(\mathrm{Cos}(\alpha))$, but an analytic function with similar form. This was done because of the simplicity of producing samples with a PDF given by the analytic function, compared to the relative difficulty of producing samples with a PDF given by an arbitrary function like $W'(\mathrm{Cos}(\alpha))$. However, the inefficiency introduced by not using the correct PDF for the scattering angles was found to be considerable, due to the higher order scatters being more important in a model with extended luminosity. consequently a method was developed of producing random samples with a PDF given by an arbitrary function.

Let x be a random number between 0 and 1 chosen from a uniform distribution. The probability of x taking a value in any interval of length dx, is therefore equal to dx. Define a function G, which transforms the sample x

into a sample z from a distribution with a PDF given by the function P(z), that is

$$z = G(x)$$

Given that x has a value within some interval of length dx with a probability of dx, z will have a value within some interval of length dz with a probability of P(z)dz. These two probabilities must obviously be equal since z is a function of x, so

$$dx = P(z).dz$$

If z can take values between $z=z_0$ and $z=z_1$, then we can integrate this expression from $z=z_0$ to $z=z_2$ $(z_0 < z_2 < z_1)$

$$\int_{z_0}^{z_2} P(z).dz = \int_{G^{-1}(z_0)}^{G^{-1}(z_2)} dx$$

$$= G^{-1}(z_2) - G^{-1}(z_0)$$

If we specify that the function G must satisfy

$$G(0) = z_0 \qquad (\Rightarrow G^{-1}(z_0) = 0)$$

then

$$\int_{z_0}^{z_2} P(z).dz = G^{-1}(z_2) \qquad (= x_2)$$

If the value of the integral can be calculated, then a table of values of x_2 $(=G^{-1}(z_2))$ against z_2 can be made. After inverting this table to give z_2 against x_2, it can be used to define the function G(x), that is a sample x from a uniform distribution can be transformed into a sample z from a distribution with a PDF given by the function P(z) by looking up the value of z corresponding to the given x, in the table.

This method has been applied to obtain random samples of $\mathrm{Cos}(\alpha)$ with a PDF of $W'(\mathrm{Cos}(\alpha))$ and the scattering angles thus obtained result in much improved efficiency over the previous sampling technique.

4.2.6 The Path Lengths

The path length between scatters d_i, is chosen from some distribution with a PDF of $H(d_i)$. In the current model these paths need not lie entirely within the dust, either because the photon passes through the central "hole" of the dust annulus, or because a photon path originates outside the dust. If the distance

travelled inside the dust is l_i then the photon will suffer an extinction of

$$e^{-\frac{l_i}{MFP}}$$

along the path. Thus, photons which travel far in the dust will contribute less to the final result, and the above extinction can be thought of as being proportional to the probability of a photon traversing a distance l_i within the dust, without being scattered. For efficient sampling of the dust, l_i should be chosen from a distribution with a PDF of $D(l_i)$ where

$$D(l_i) = \frac{1}{MFP} \cdot e^{-\frac{l_i}{MFP}}$$

(the 1/MFP term ensures that $D(l_i)$ is normalized to unity), for then the probability term $D(l_i)$ cancels with the extinction term in equation 4.5. If the photon travels in such a direction that it must pass through the central "hole" in the dust annulus, then the distance travelled within the dust must be made up from two sections, one on each side of the "hole" (see fig. 4.7). In this case, the total path length d_i is made up of l_i plus the distance travelled across the hole (which can be found by simple geometry).

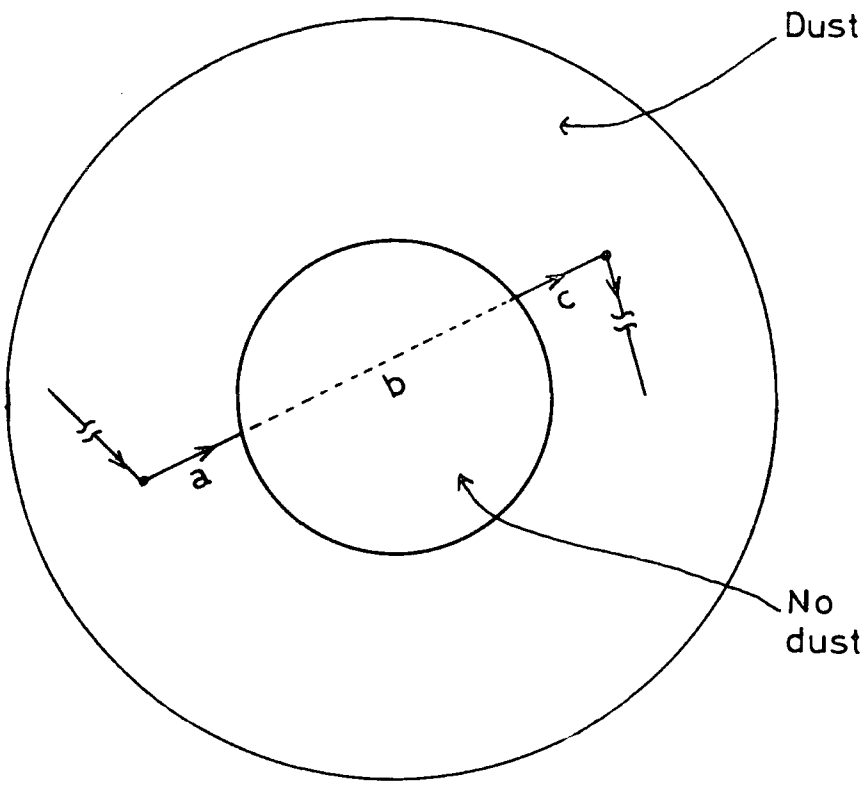

Fig. 4.7
If a photon path passes through an area with no dust then the path length between the two scatters concerned is chosen such that the distance travelled inside the dust is a sample from an exponential distribution with a mean of one mean free path.

Due to the backward nature of the model, it is not possible to determine where the point of origin of the photon is going to be, and in many cases it will not lie within the dust. If this is the case, then it is not possible to sample the distance travelled inside the dust at random; it is determined exactly by the first scattering position and the direction of travel of the photon on the first path length (see fig. 4.8). It is then necessary to sample the total path length d_i, rather than the distance travelled inside the dust l_i. The PDF with which d_i is chosen is such that the expression 4.7 converges for large d_i, that is the luminosity decreases faster than the probability.

Having described the mechanics of the model, the next chapter shall describe the results obtained by using the model.

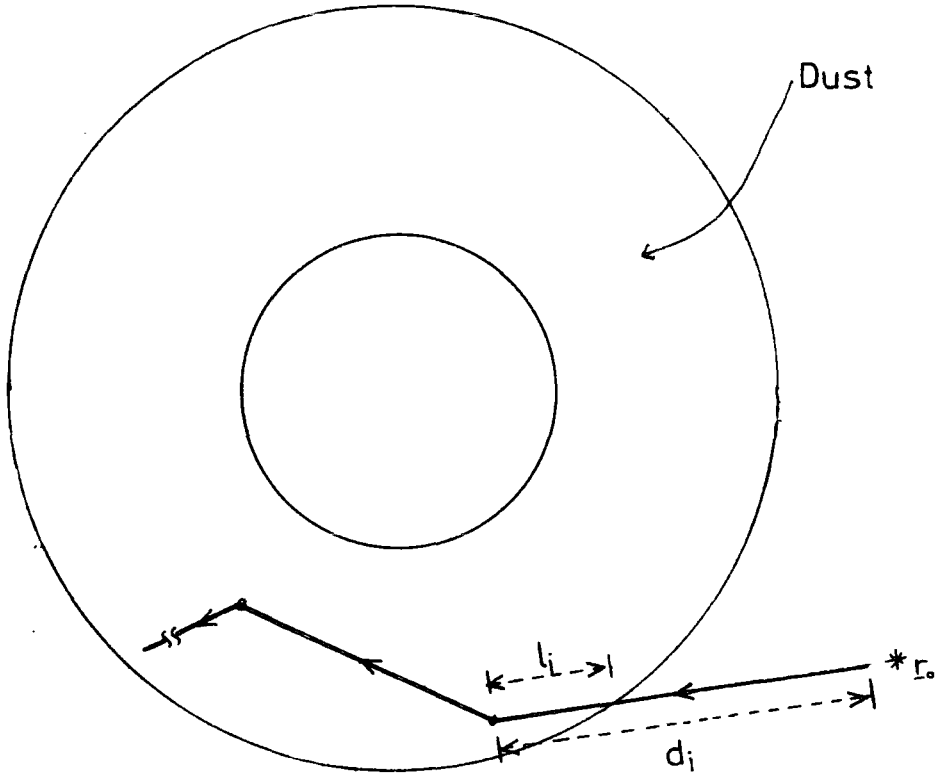

Fig. 4.8
If a photon originates outside the dust, then the distance travelled inside the dust is fixed. In this case, the total path length is chosen as a sample from a distribution which samples the luminosity well.

CHAPTER 5

TESTS AND RESULTS FROM THE MODEL

Before the results produced by the model described in the last chapter can be usefully evaluated, some evidence that the model is working correctly must be given. To this end, the tests which the model has been subjected to will be described.

5.1 Tests of the Model

It is intrinsically difficult to test the model as it stands, firstly because values of many of the required parameters are not known, but also because it is not known that scattering alone produces the observed polarization in NGC5128. All that can be done without changing the model is to perform various internal

consistency checks, and all such checks have been positive. As an example fig. 5.1 shows a log-log plot of the estimated error of the total intensity against the number of photons used. The error decreases with increasing numbers of photons, with a gradient which is asymtotically 0.5, implying that the errors decrease as $(NPHOT)^{-0.5}$ as expected. Fig. 5.2 shows a similar plot for the error on polarization. It should be noted that the errors on polarization are not normally distributed, due to the nature of the dependancy of polarization on I,Q and U. In practice, it was found by running the model several times that the error on polarization for 30,000 photons was about 0.5%, which is acceptable for the present purposes.

As a more conclusive test of the validity of the general modelling technique, it was decided to change the dust geometry, luminosity and grain properties to model a situation which could also be described analytically. Jura (1978) has obtained expressions for the total intensity and polarized intensity expected from a small cloud of Rayleigh scatterers situated at some distance from the centre of a sphere of uniform luminosity, and it was decided to reproduce this situation as a test of the backward Monte-Carlo model.

Fig. 5.3 shows plots of total intensity against radial distance of the small cloud from the centre of the

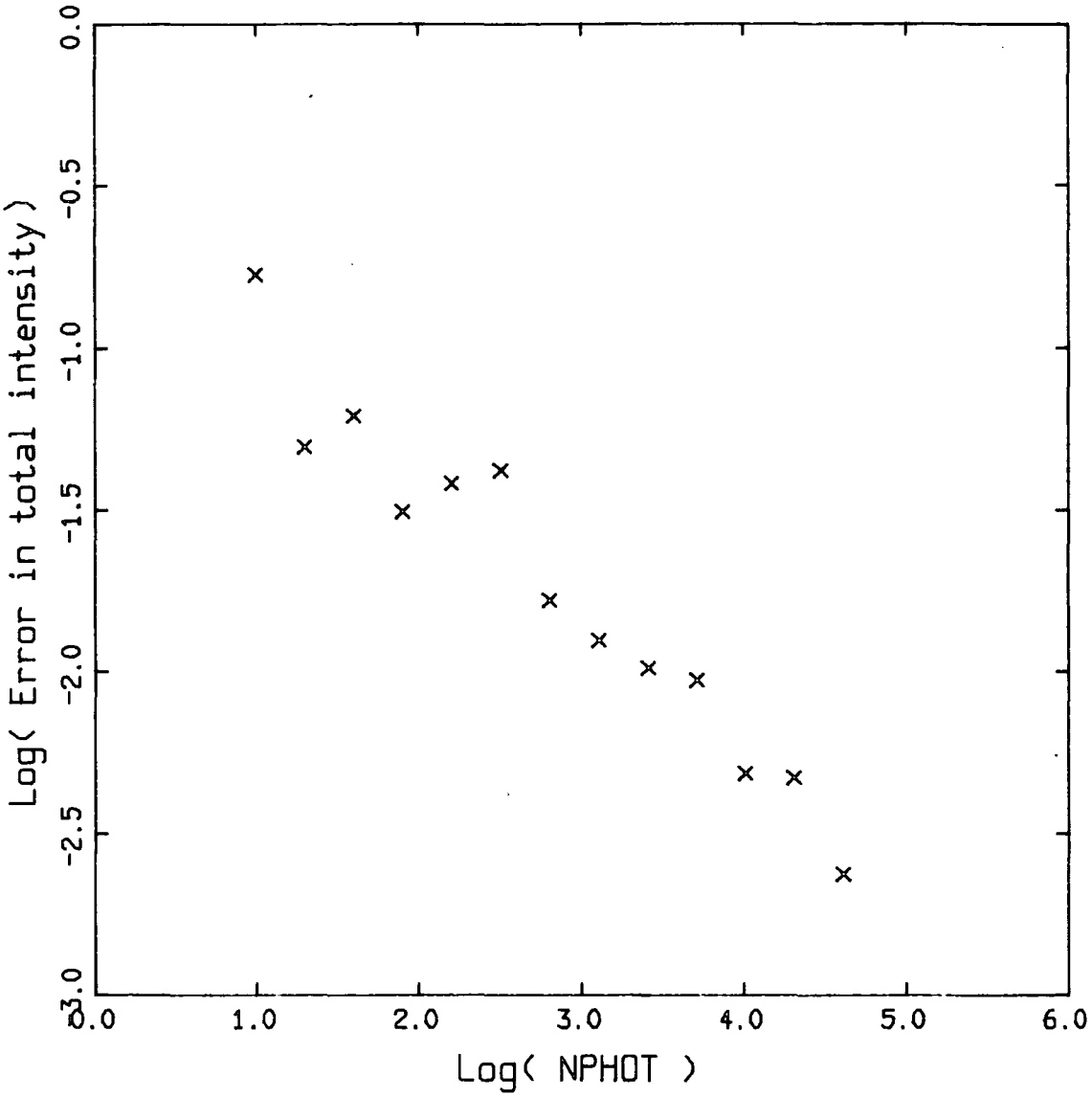

Fig. 5.1
The error in the models estimate of total intensity against NPHOT, the number of trial photons used.

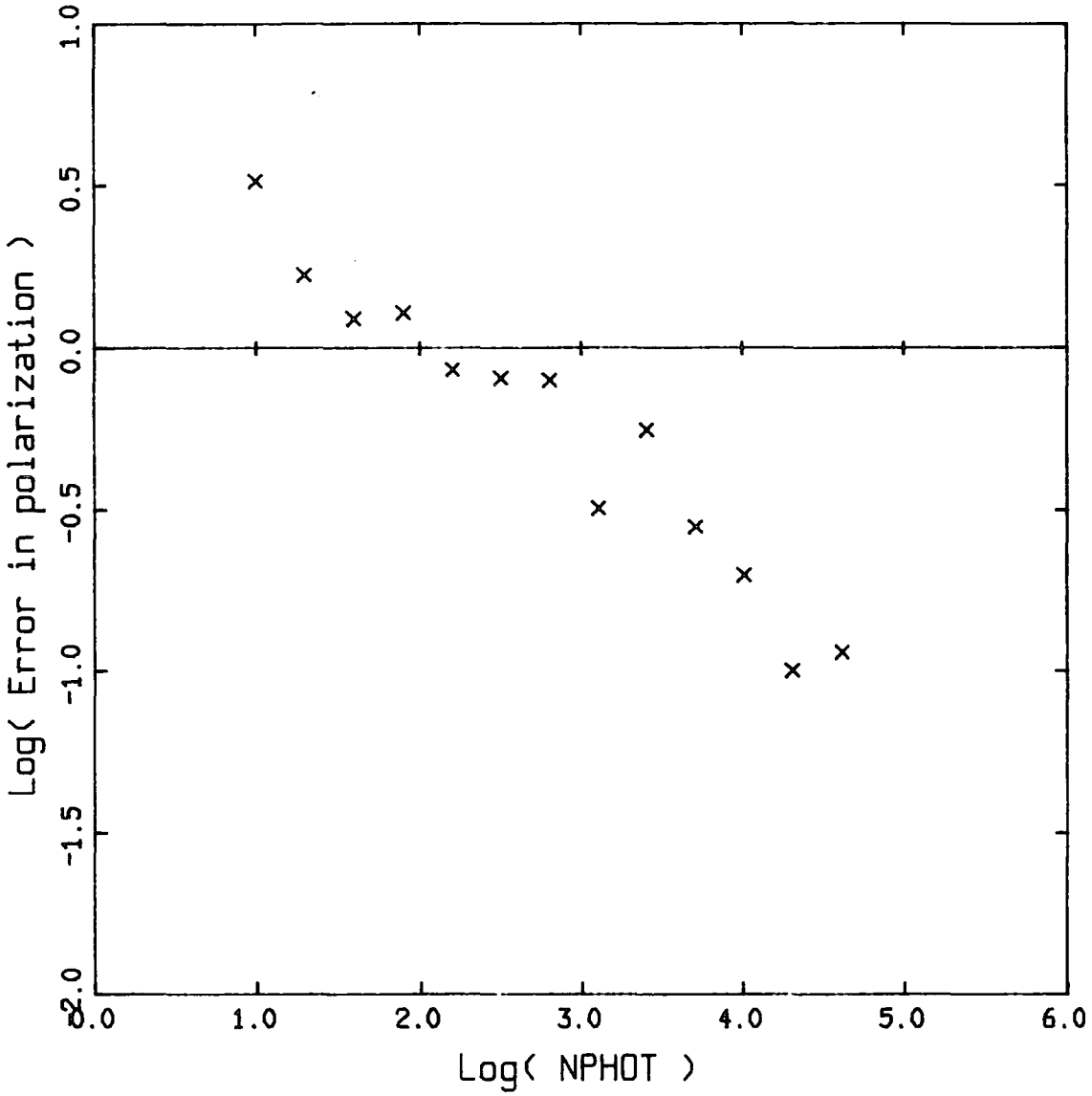

Fig. 5.2
The error in the models estimate of polarization against NPHOT, the number of trial photons used.

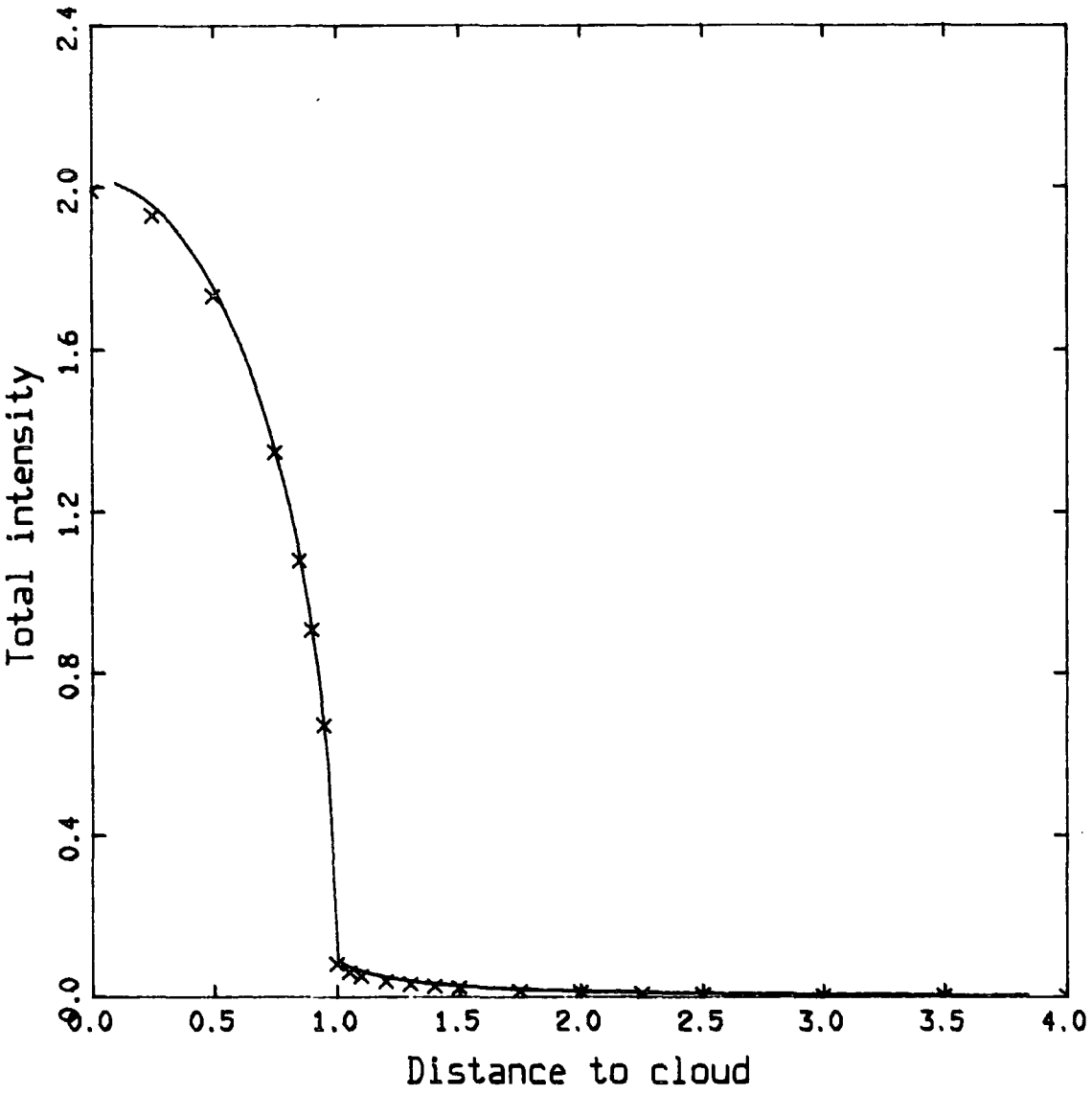

Fig. 5.3
The solid line in the above plot is the total intensity (calculated by Jura) scattered by a small cloud of Rayleigh scatterers illuminated by a sphere of uniform luminosity, (of radius 1.0) against the distance of the cloud from the centre of the luminous sphere. The crosses are the equivalent model estimates.

luminous sphere, for Jura's analytic expressions and for the new model. Fig. 5.4 shows similar plots of the polarized intensity. Between them, these two plots show that the model is functioning correctly both inside and outside the luminous sphere.

5.2 Parameter values

The model has many parameters which must be given values before it is run. The values of these parameters must be determined so that they describe NGC5128 as closely as is possible. However, due to the idealized nature of the model (for instance, in the dust geometry) and the fact that data is only available in one colour, there is not much to be gained from attempting a complex minimization procedure to determine their values. Instead, parameters will be given the most reasonable values available to begin with, and will be changed as seems appropriate. Each of these parameters, together with their initial values will now be described.

5.2.1 The Wavelength of the Observed Light

This was taken as 5500Å to match the central wavelength of the data described in chapter 3.

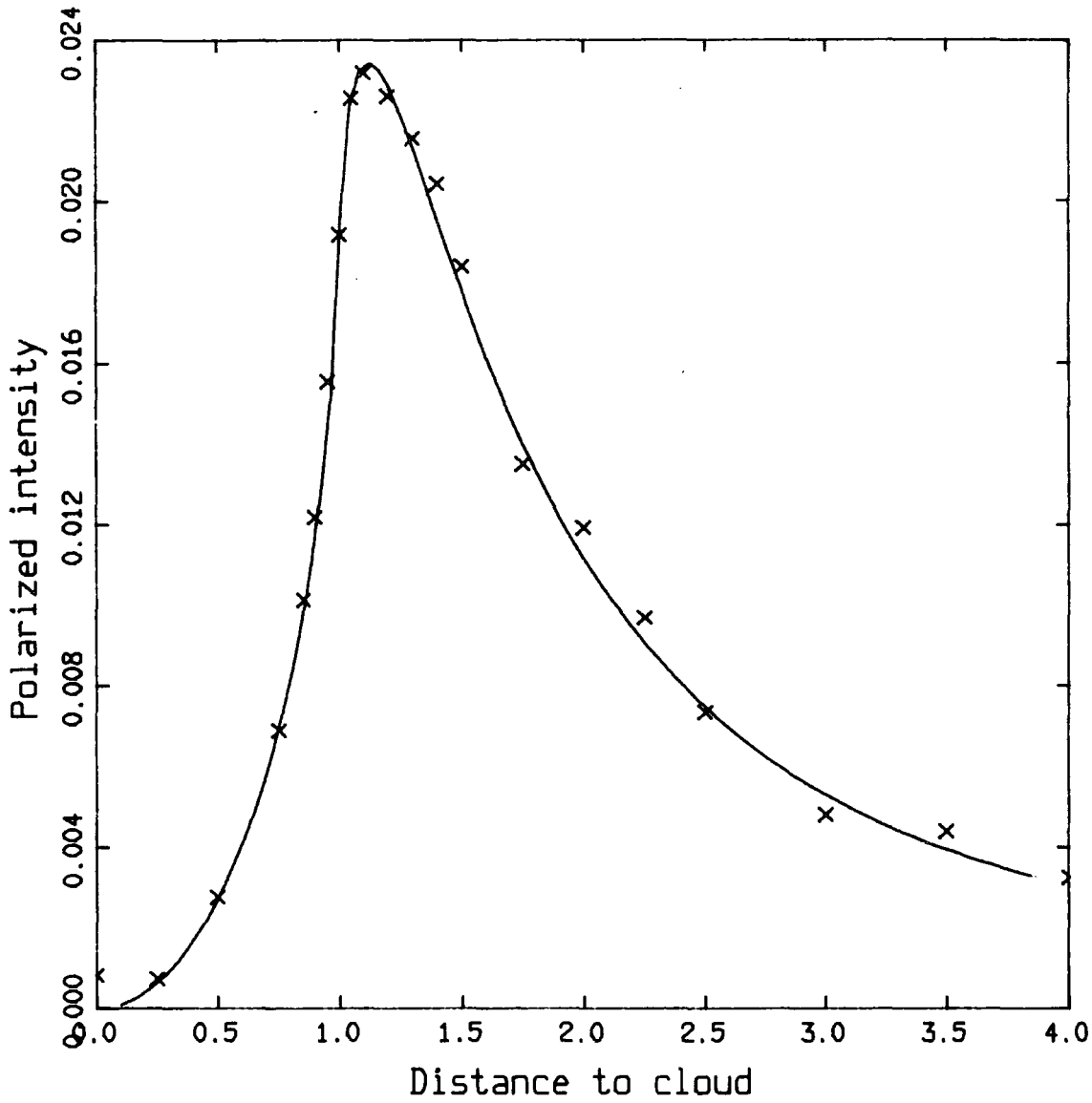

Fig. 5.4
The solid line in the above plot is the polarized intensity (calculated by Jura) scattered by a small cloud of Rayleigh scatterers illuminated by a sphere of uniform luminosity, (of radius 1.0) against the distance of the cloud from the centre of the luminous sphere. The crosses are the equivalent model estimates.

5.2.2 The Dust Parameters

The dust in NGC5128 is found to be similar in many respects to that found in our own Galaxy (see section 2.4), and so it was considered reasonable to use dust parameters typical of those found in our Galaxy. The size distribution adopted was a power law (Mathis et al, 1977; Warren-Smith, 1983) of the form

$$n(a)=a^{-\gamma}$$

where a is the grain size, n(a)da is the number of grains with sizes between a and a+da, and γ is a constant, the power law index. In order to avoid the singularity at a=0, a lower limit is put on the grain size of 70Å. The power law index of the interstellar medium in our Galaxy is found to vary with wavelength (Warren-Smith, 1983) being smaller at shorter wavelength. The value adopted for the current model is -4.25, which is consistent with the reddening law of the dust in NGC5128 found by Rodgers (1978).

The initial value of the refractive index was 1.65 with an imaginary part of -0.05, typical of silicates (Grasdalen and Joyce, 1976, have identified the 10μm "silicate" feature in NGC5128).

5.2.3 The Dust Geometry and Density

The values of the thickness and outer radius of the dust annulus were estimated from the data to be respectively 0.25 and 1.0 effective radii. The thickness of the dust lane in the central regions is quite well defined (as can be seen from the image in fig 2.1). The dust does extend further than one effective radius from the galactic centre, but is not so thick or well ordered at these distances.

To determine the tilt, the radius of the central "hole" of the dust annulus, and the mean free path within the dust (which together with the dust parameters determine the dust density), a trace of the surface brightness perpendicular to the dust lane was obtained from the data at a position near to the galactic centre. The values of the specified parameters were then varied in the model to obtain a good fit to this trace. It was found that a tilt of 5° with a mean free path of 0.125 effective radii and no hole in the middle of the dust annulus gave a reasonable fit to the data, the data trace and the corresponding model trace are shown in fig. 5.5.

The value of 5° for the tilt of the dust lane is much less than the value of 17° found by Graham (1979). Fig. 5.6 shows the data trace and the trace

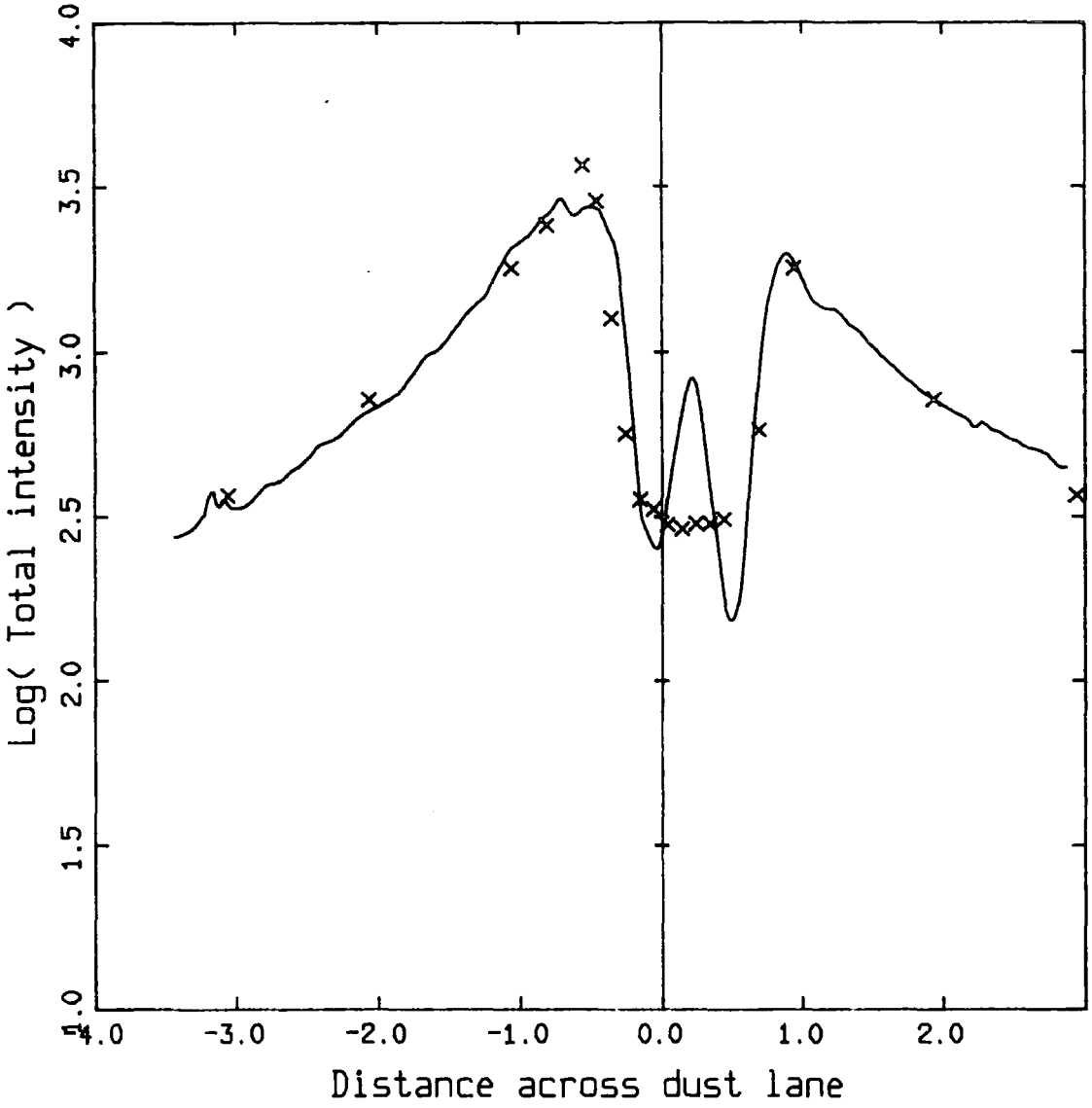

Fig. 5.5
The solid line in the above plot is proportional to the surface brightness of the observational data along a trace across the dust lane. The crosses are the equivalent model estimates using a tilt of 5 degrees, a mean free path of 0.125 effective radii, and no central "hole". The peak in the data trace in the middle of the dust lane is not reproduced by the model due to the simplified dust geometry used.

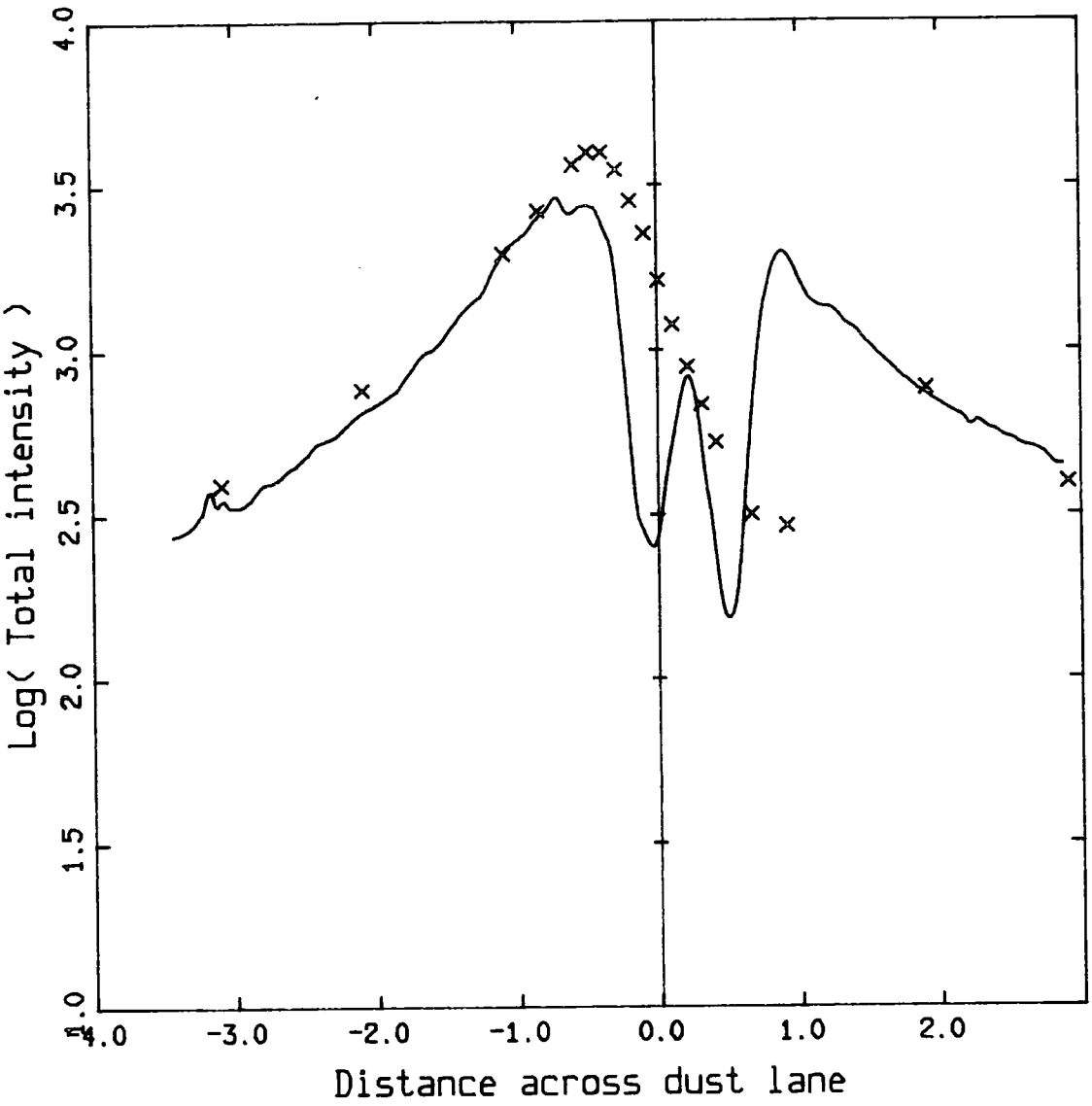

Fig. 5.6
The above plot shows the data trace of fig. 5.5 with the model estimates based on a tilt of 17 degrees. The other parameter values are the same as in fig. 5.5.

produced by the model for a tilt of 17°. It can be seen that the 17° trace does not fit the data at all, there being too great a difference between the brightness of the edges of the dust lane. Fig. 5.7 shows a similar trace for a tilt of 10° and fig. 5.8 shows a trace for a tilt of zero. The traces favour a smaller value for the tilt and the value of 5° seems to produce the best fit. The discrepency between this result and the findings of Graham could be explained if the HII regions used by Graham to find the inclination of the D component (see section 2.2) are not in the same plane as the dust.

Fig. 5.9 shows a picture of the model in total intensity, using these parameter values, including only the unscattered and the singly scattered light.

5.2.4 Other Parameters

The only remaining parameters are those describing the workings of the model, namely the number of scatters to include and the number of photons to use.

Fig. 5.10 shows a plot of the total intensity due to different orders of scattering on a line of sight close to the galactic centre, and fig. 5.11 shows a similar plot for a line of sight near the outer rim of the dust annulus. Both plots show the expected decrease of

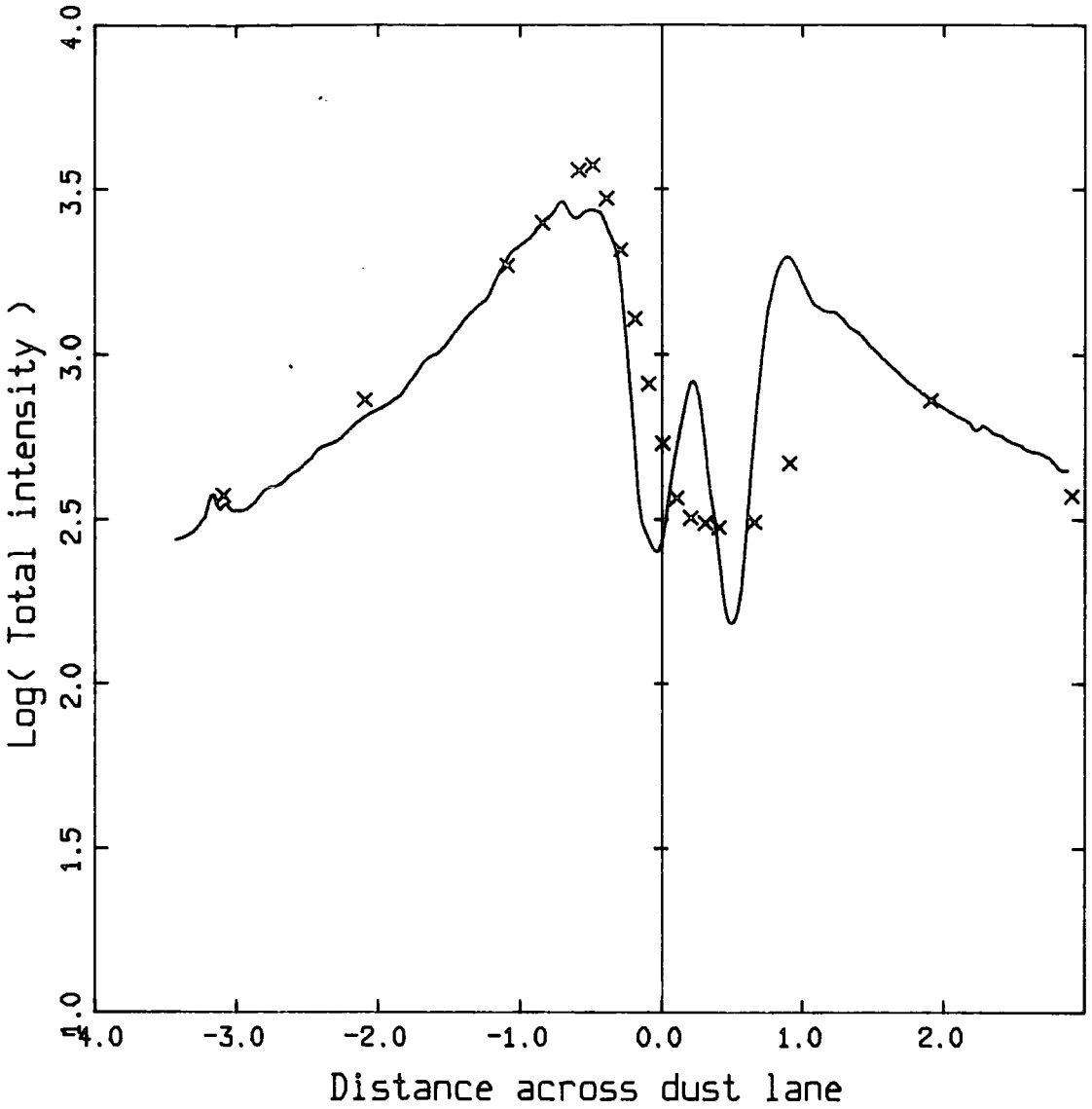

Fig. 5.7
The above plot shows the data trace of fig. 5.5 with the model estimates based on a tilt of 10 degrees. The other parameter values are the same as in fig. 5.5.

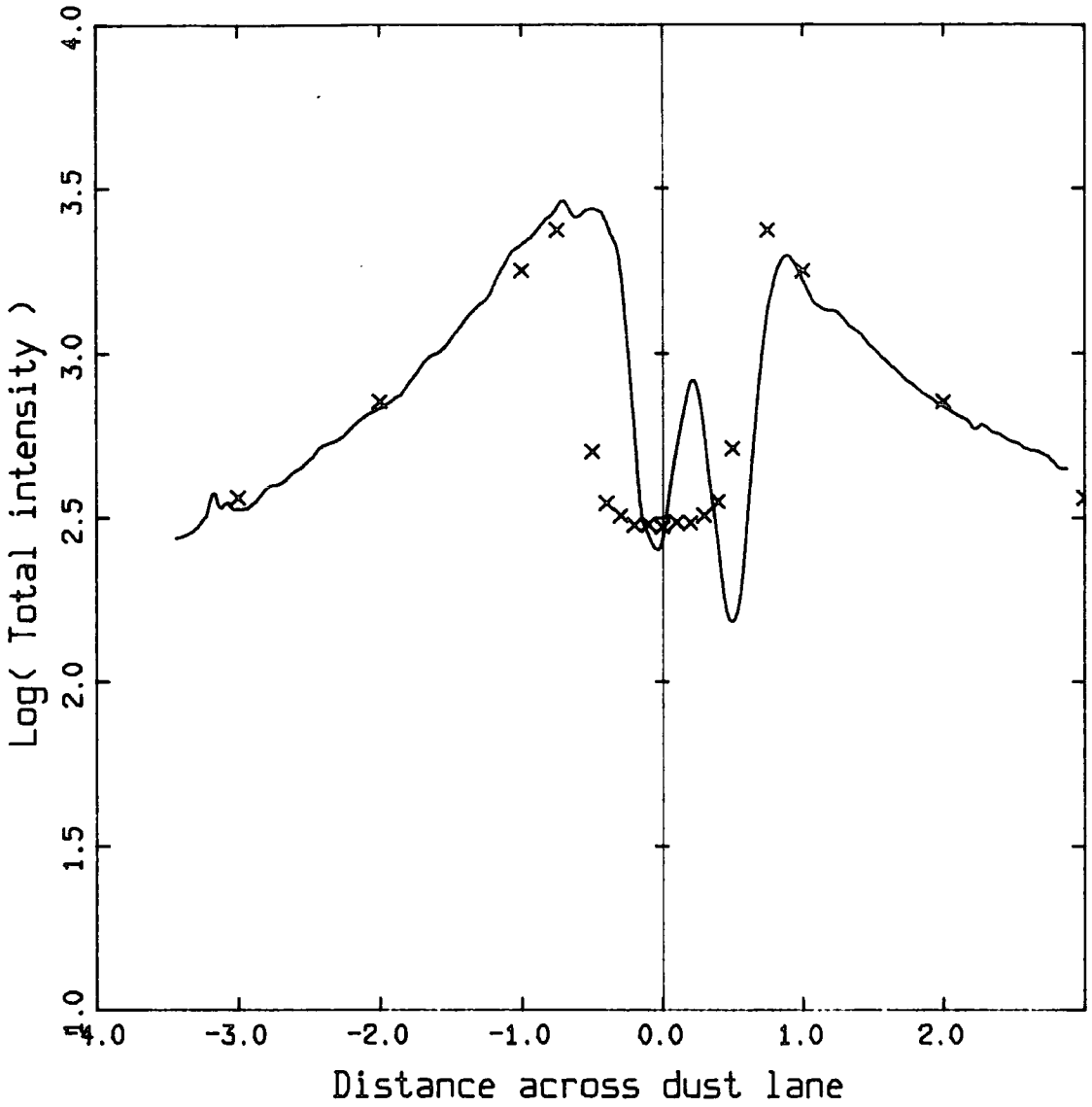

Fig. 5.8
The above plot shows the data trace of fig. 5.5 with the model estimates based on a tilt of zero. The other parameter values are the same as in fig. 5.5.

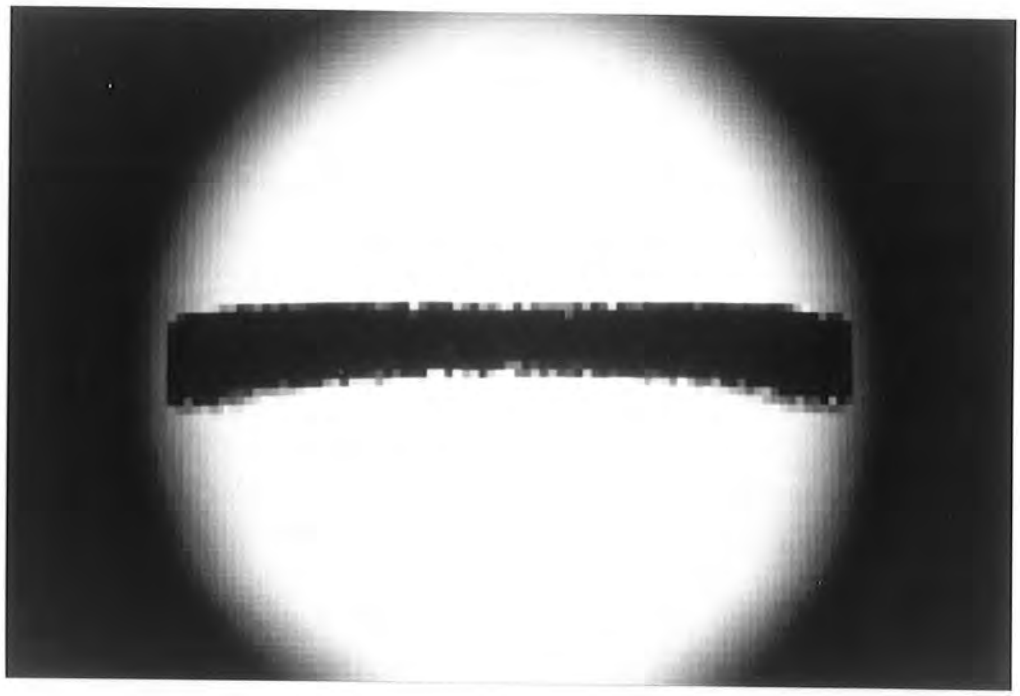

Fig. 5.9
A picture in total intensity of the model of NGC5128.
Only the unscattered and singly scattered light is included.

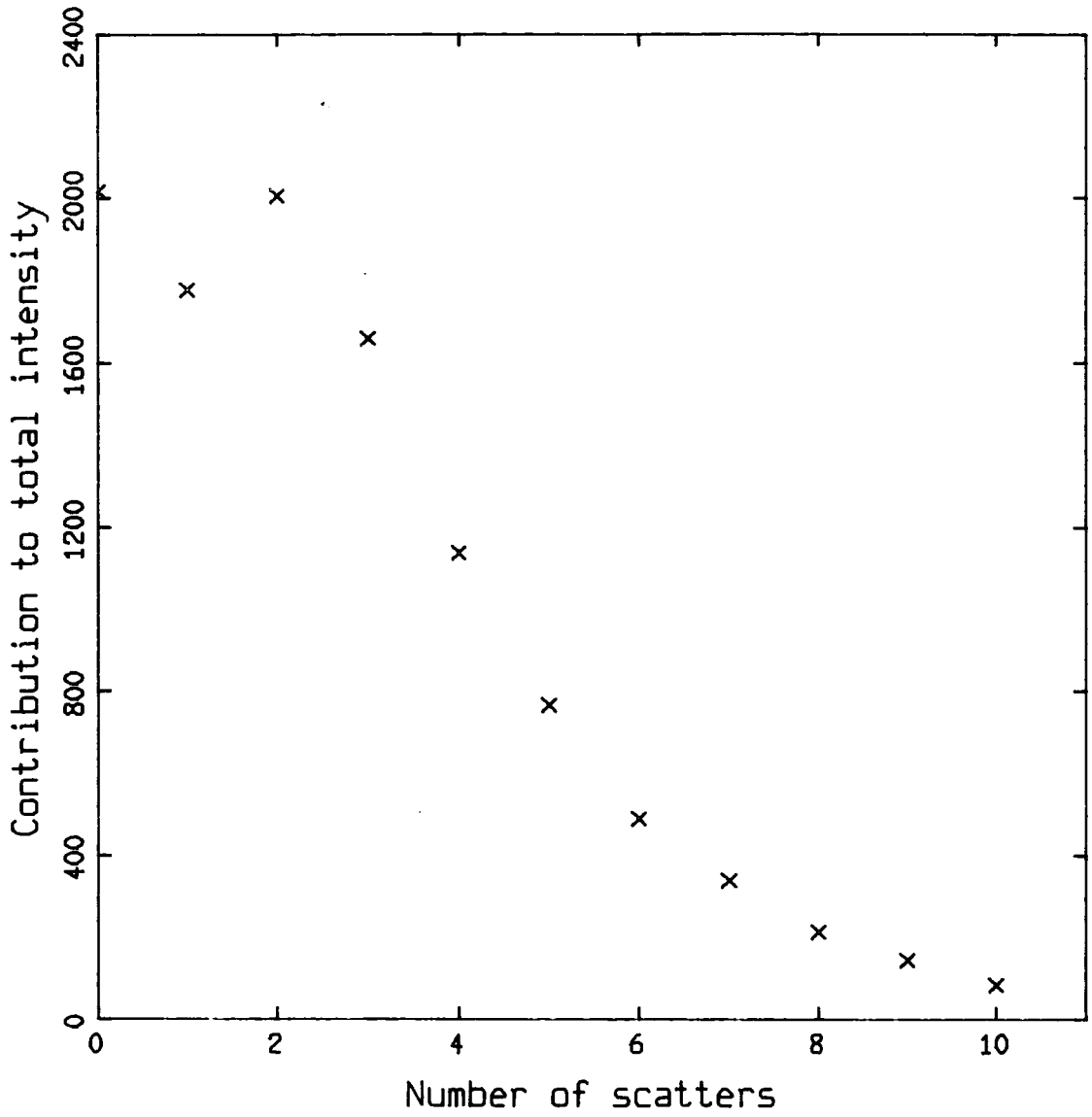

Fig. 5.10
The contribution made to the total intensity by trial photons of different scattering orders, at a line of sight near the galactic centre.

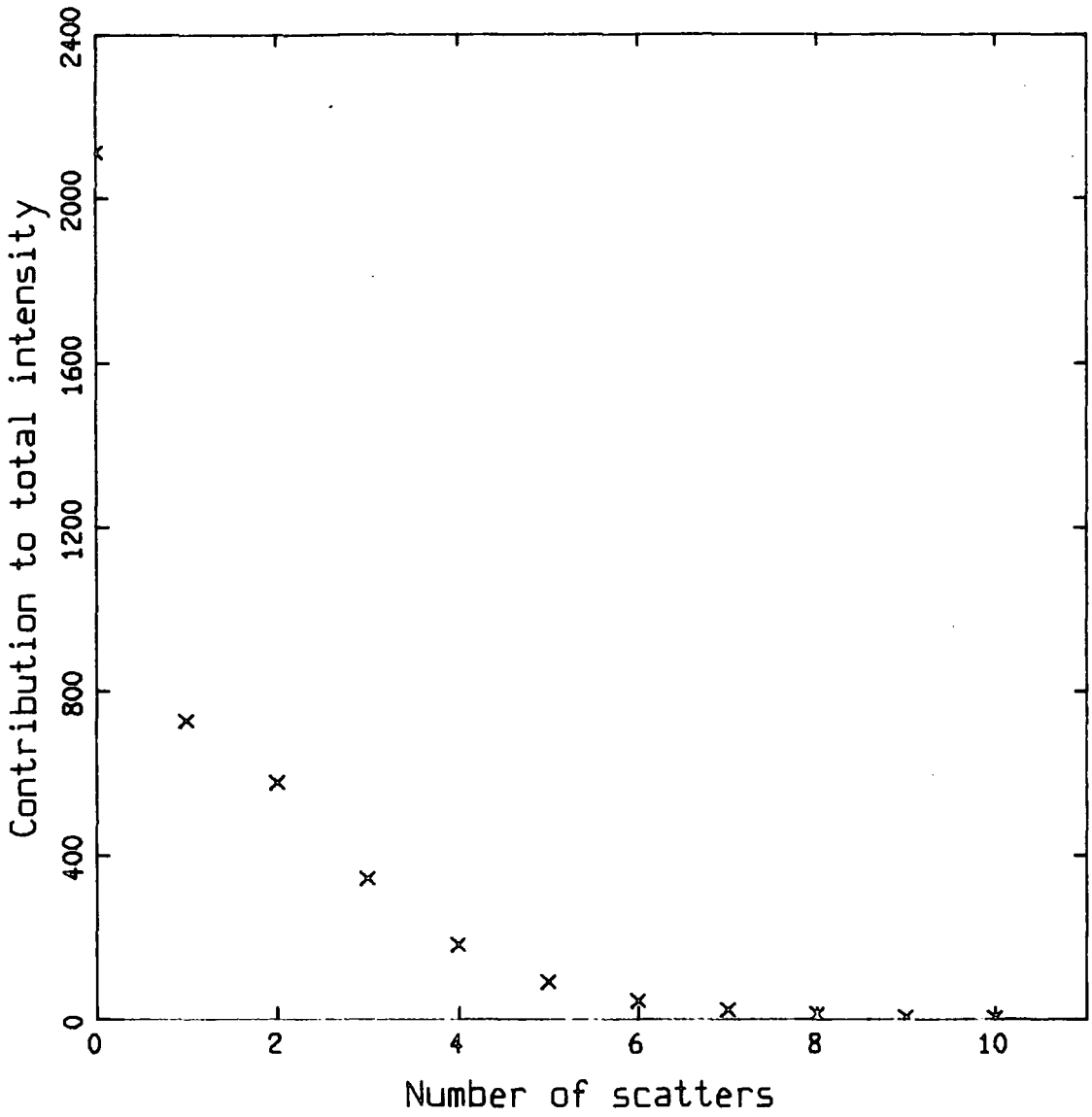

Fig. 5.11
The contribution made to the total intensity by trial photons of different scattering orders, at a line of sight near the edge of the dust lane.

total intensity with increasing numbers of scatters, and it was decided to truncate the Monte-Carlo summation (see equation 4.6) at the fifth scattering. The unscattered term due to zero scatterings is included in these plots and it can be seen that the multiply scattered light constitutes a significant fraction of the observed flux near the galactic centre. As was mentioned earlier, 30000 photons were used per line of sight and gives an accuracy of the order of 0.5%. With these parameters, the model takes 35 minutes of CPU time per line of sight, to run on the VAX 11/750 at Durham.

5.3 Results of the Scattering Model

Due to the symmetry of the model geometry, it is only necessary to consider one half of the dust lane (the other side is a mirror image of the side used), and the final model was run at twelve lines of sight at various positions.

The resulting map using the initial parameter values determined above, is shown in fig. 5.12 superimposed on a contour map of the intensity image of fig. 5.9. The polarization near the galactic centre is parallel to the dust lane and of about 1% in magnitude. At greater radial distances the vectors turn round to become perpendicular to the dust lane and increase in magnitude.

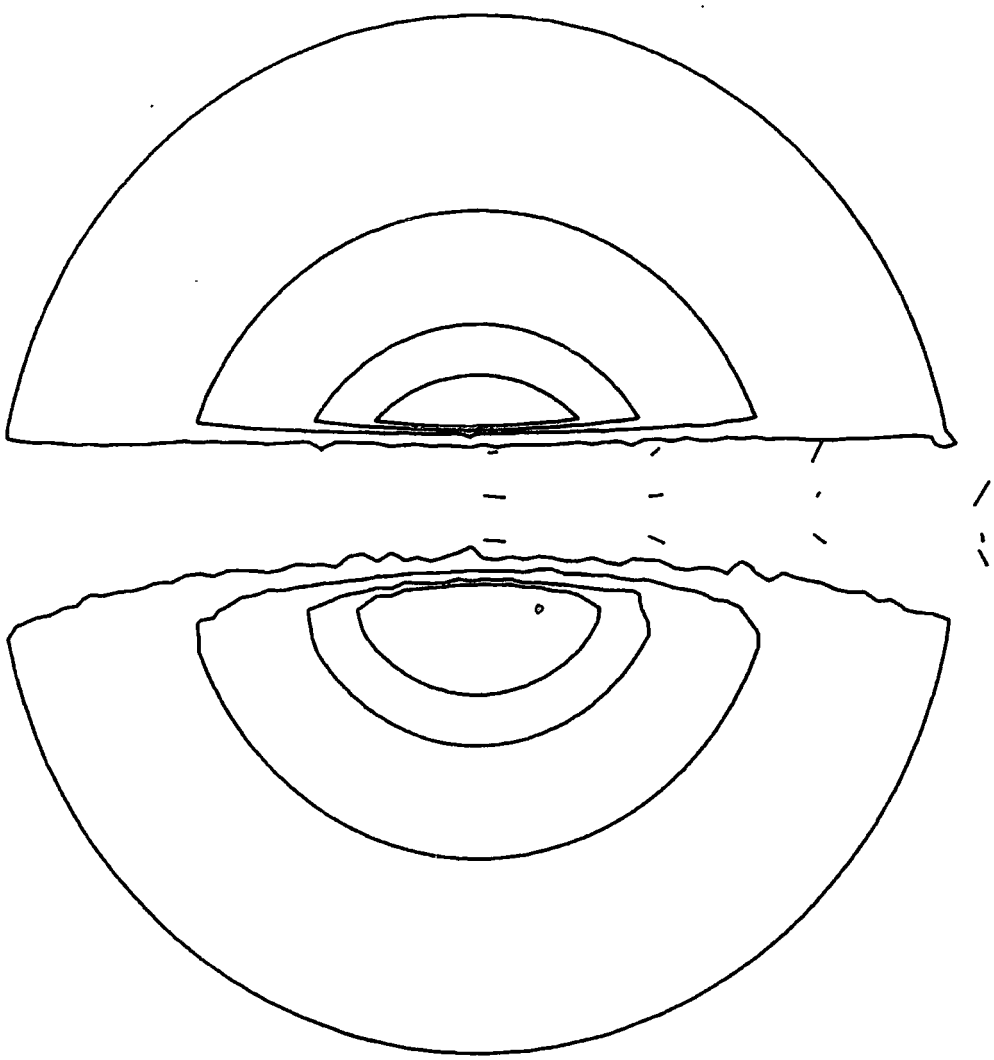

——— 5 % Polarization

Fig. 5.12
The polarization map produced by the model with all the parameters set to their initial values. The map is shown over four evenly spaced contours of the image in fig. 5.9. The degree of polarization in the middle of the dust lane is 0.8%, much less than the 4% found in the data.

The degree of polarization produced by this model in the central regions, is much lower than the 4% found in the data, and the rate at which the vectors turn round as the distance from the centre increases, is too high. Thus, either the parameter values used do not represent NGC5128 well enough or polarizing mechanisms other than simple scattering must be included.

As was mentioned earlier a sophisticated procedure of continually varying the free parameters to produce as close an agreement as possible between the model and the data, seems inappropriate due to the simplistic nature of the model geometry and the lack of multi-colour data. However, some attempt can be made to see if the polarizations can be increased by changing the parameter values appropriately, and to this end table 5.1 shows the degrees of polarization obtained by changing the parameters in turn from there initial values, while fig. 5.13 shows a plot of polarization against the log of the mean free path.

The only variations which significantly raise the degree of polarization are:

1) increasing the power law index

2) decreasing the real part of the refractive index

TABLE 5.1

		% Polarization
1)	Refractive index = 1.65-0.05i Power law index = -4.25 Inner radius of annulus = 0 Outer radius of annulus = 1 effective radius	0.4
2)	As 1) except refractive index = 1.2-0.05i	1.1
3)	" " " " " = 2.0-0.05i	0.1
4)	" " " " " = 1.65-0.0i	0.9
5)	" " " " " = 1.65-1.0i	1.9
6)	" " " power law index = -2.0	0.2
7)	" " " " " " = -5.0	1.1
8)	" " " inner radius = 0.9	0.0
9)	" " " outer radius = 1.5	0.4

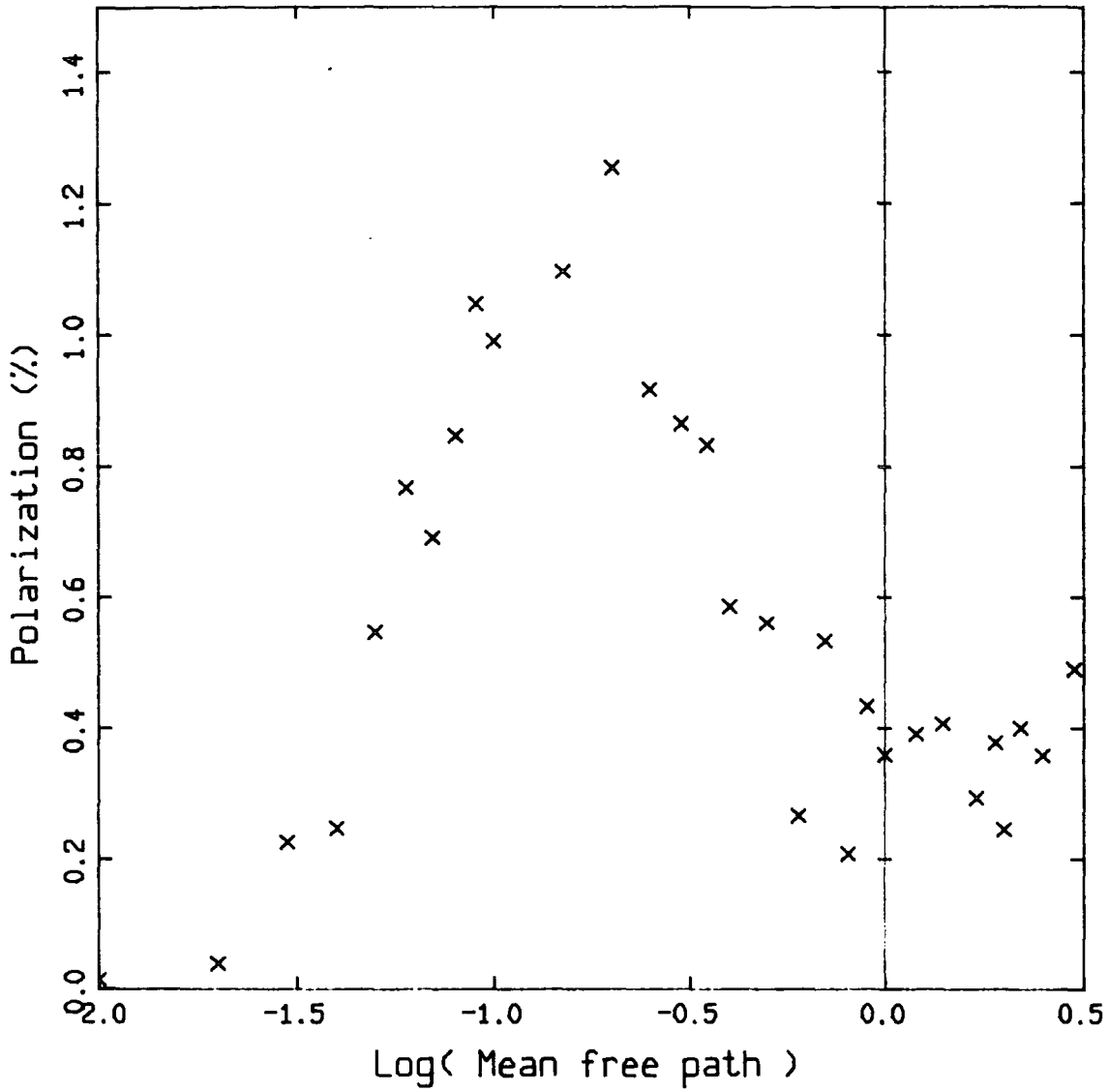

Fig. 5.13
The above plot shows the dependency of the models estimate of the polarization near the galactic centre, on the mean free path used to produce the estimate. All other parameters were kept at their initial values.

3) increasing the imaginary part of the refractive index

4) decreasing the mean free path to 0.05 effective radii

Increasing the power law index has the effect of increasing the number of very small particles relative to the larger particles, thus producing Rayleigh-like scattering functions. That this produces higher polarizations is no suprise, and it is partly to avoid the necessity of having such small grains that the current model was developed. The power law index is one of the few parameters which can be given a value with any confidence, and so it seems resonable to discount the possibility of a large power law index.

The refractive index, on the other hand, is one of the least certain of the model parameters and so it was decided to investigate the effects of varying both the real and imaginary parts to see if any combination could be found which raises the polarization to the required 4% level. Fig. 5.14 shows a plot of polarization against the real part of the refractive index and fig. 5.15 shows a similar plot for the imaginary part. It can be seen that no values approach the value of 4%. The model was also run with a refractive index real part of 1.3 and an imaginary part of -1.0 (positions of high polarization in fig.s 5.14 and 5.15) to see if higher polarization could be obtained,

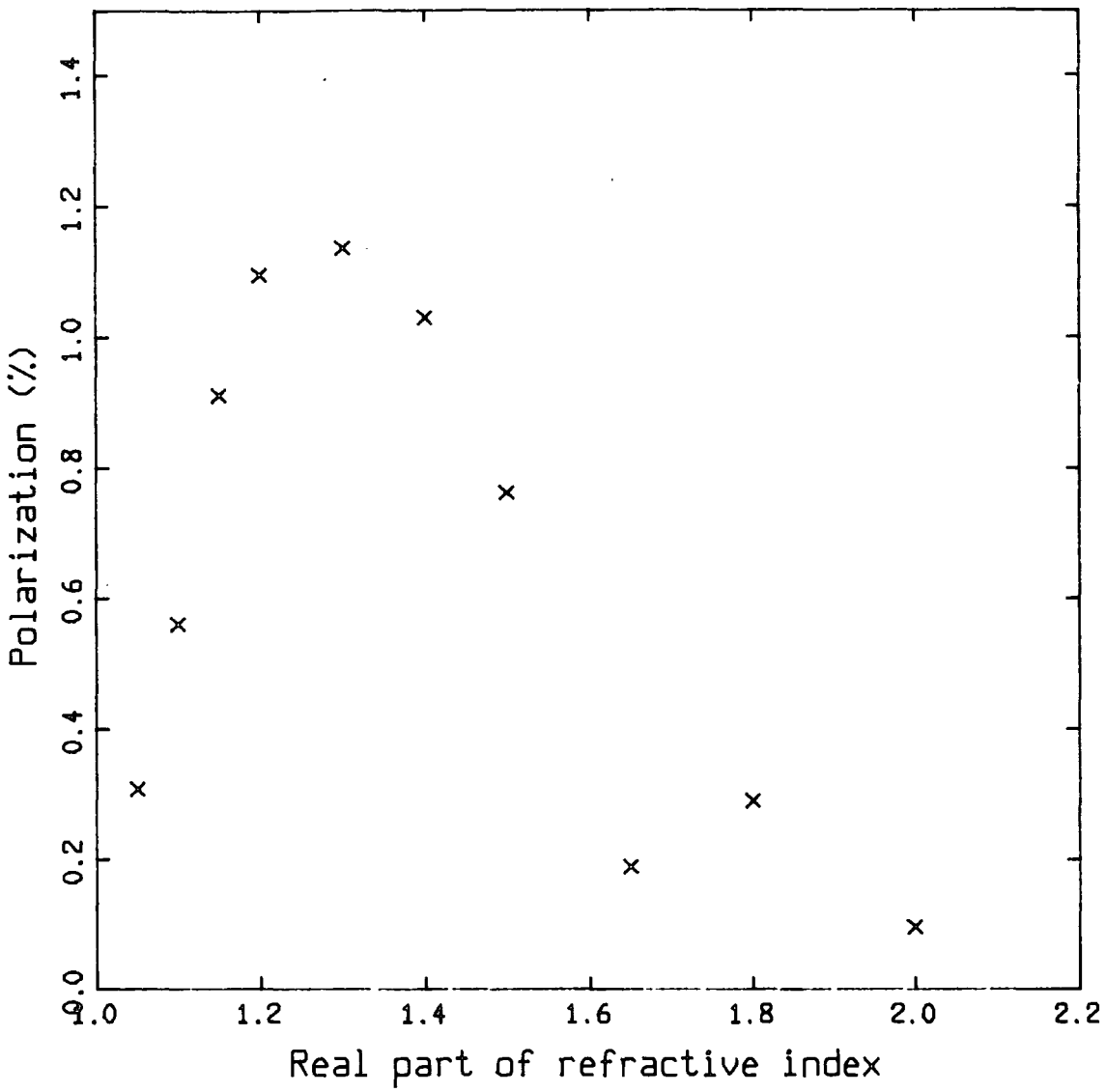

Fig. 5.14
The above plot shows the dependency of the models estimate of the polarization near the galactic centre, on the real part of the refractive index used to produce the estimate. All other parameters were kept at their initial values.

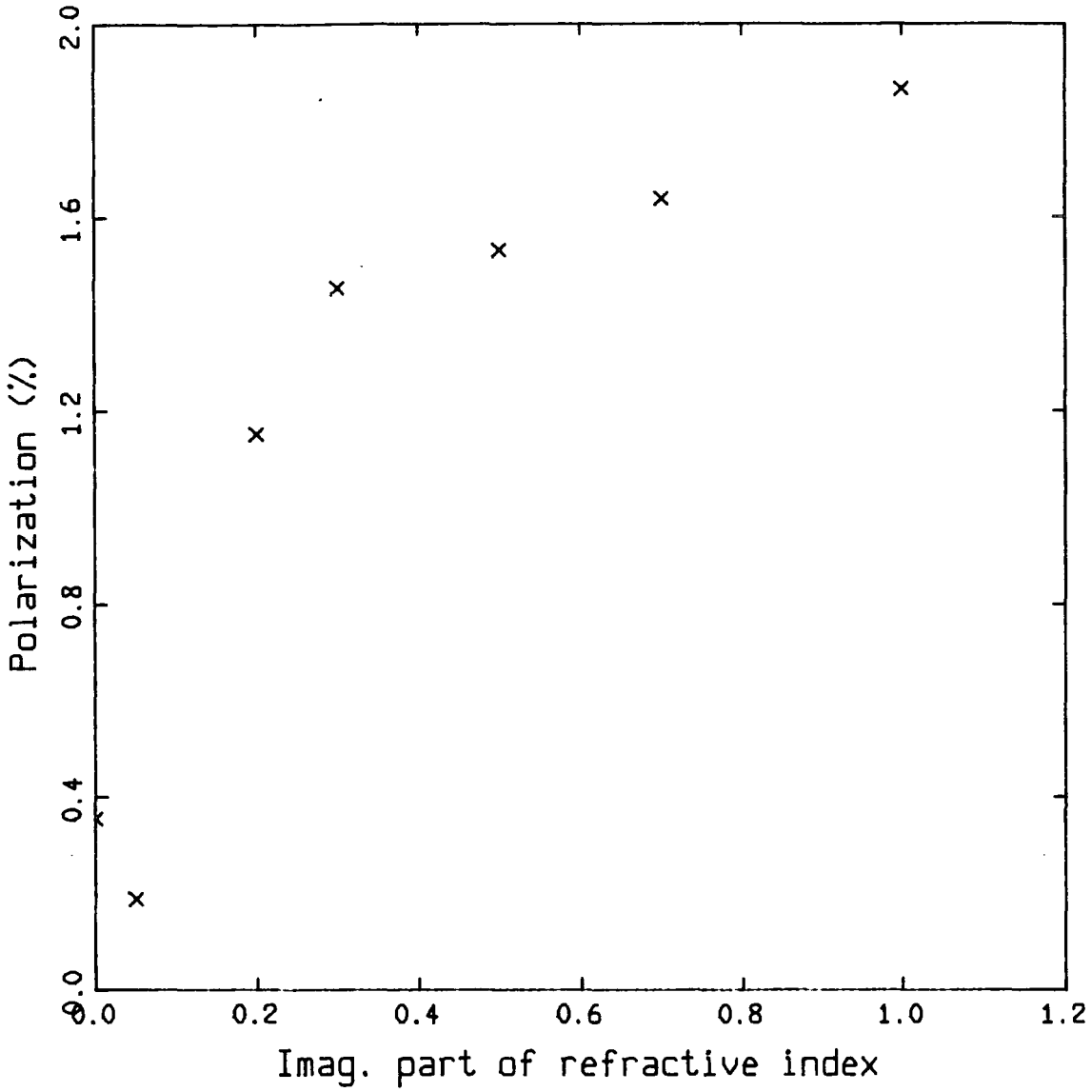

Fig. 5.15
The above plot shows the dependency of the models estimate of the polarization near the galactic centre, on the imaginary part of the refractive index used to produce the estimate. All other parameters were kept at their initial values.

but resulted in a figure of 1.8%, still much lower than the required 4%.

The mean free path has been determined by the intensity traces described in section 5.2.3 and so significant departures from the value of 0.125 effective radii found there are inprobable.

It thus seems unlikely that scattering from spherical grains can be the only polarizing mechanism at work in NGC5128, and so other effects must be included in the model.

5.4 The Magnetic Field Model

The model has been modified to simulate the passage of light through a cloud of non-spherical grains assumed to be aligned by a large scale magnetic field through some process such as the Davies-Greenstein mechanism.

5.4.1. The Modifications

The production of a scattering matrix to describe the scattering of photons by non-spherical grains is a very complicated task. In the present case, the low level of polarization (4%) suggests that the degree of alignment of the grains is small, and a simple

approximation can be made using the scattering matrix appropriate for spherical grains. The actual non-spherical grain cross sections implies that light polarized parallel to the major axis of the cross section will be scattered more than light polarized perpendicular to the major axis. This effect is equivalent to a difference in the mean free path of light in these two states. The model simulates this by resolving each photon, at every scatter, into two components, parallel to and perpendicular to the direction of the local magnetic field (which will be perpendicular to the major axis of the non-spherical cross section). The Stokes vector corresponding to each component is then given a weight to correct for the fact that, due to the different mean free paths, the extinction suffered by each component of the photon was under or over estimated (the PDF with which photon path lengths are chosen corresponds to a mean free path equal to the average of the two component mean free paths). After this correction is made, the components are re-combined (coherently) and the resulting Stokes vector is scattered according to the scattering matrix for spherical particles.

The strength of the magnetic field and the grain properties determine the degree of polarization induced by the grains per magnitude of extinction. In our Galaxy this figure is generally taken as 3% per magnitude (Greenberg, 1978), and it was decided to make this property a measure

of the field strength in the new model. The morphology of the field used was necessarily simple due to computer restrictions. A completely uniform, parallel field was used to avoid the excessively large amount of computer time needed to perform the complex integrations involved in using a varying field. It is highly unlikely that any magnetic field in NGC5128 would in fact be in the form of a completely uniform field, it is much more likely that the magnetic field would follow the dust annulus in a circular pattern. In order to produce a more realistic effect on the polarization map, the direction of the magnetic field was varied for each line of sight, so that it was parallel to the direction of a toroidal field at a position on the line of sight equivalent to the mean position of the photons final scatters (see fig. 5.16).

5.4.2 Results of the Magnetic Field Model

Fig. 5.17 shows a plot of polarization (at the same central line of sight used for the scattering model) against magnetic field (given in terms of polarization per magnitude of extinction). The refractive index used to produce this plot was 1.3-0.05i which was found to give higher polarizations in the scattering model. The plot is approximately linear with a slope of 1.3 and intercept of 1% corresponding to the polarization caused by scattering.

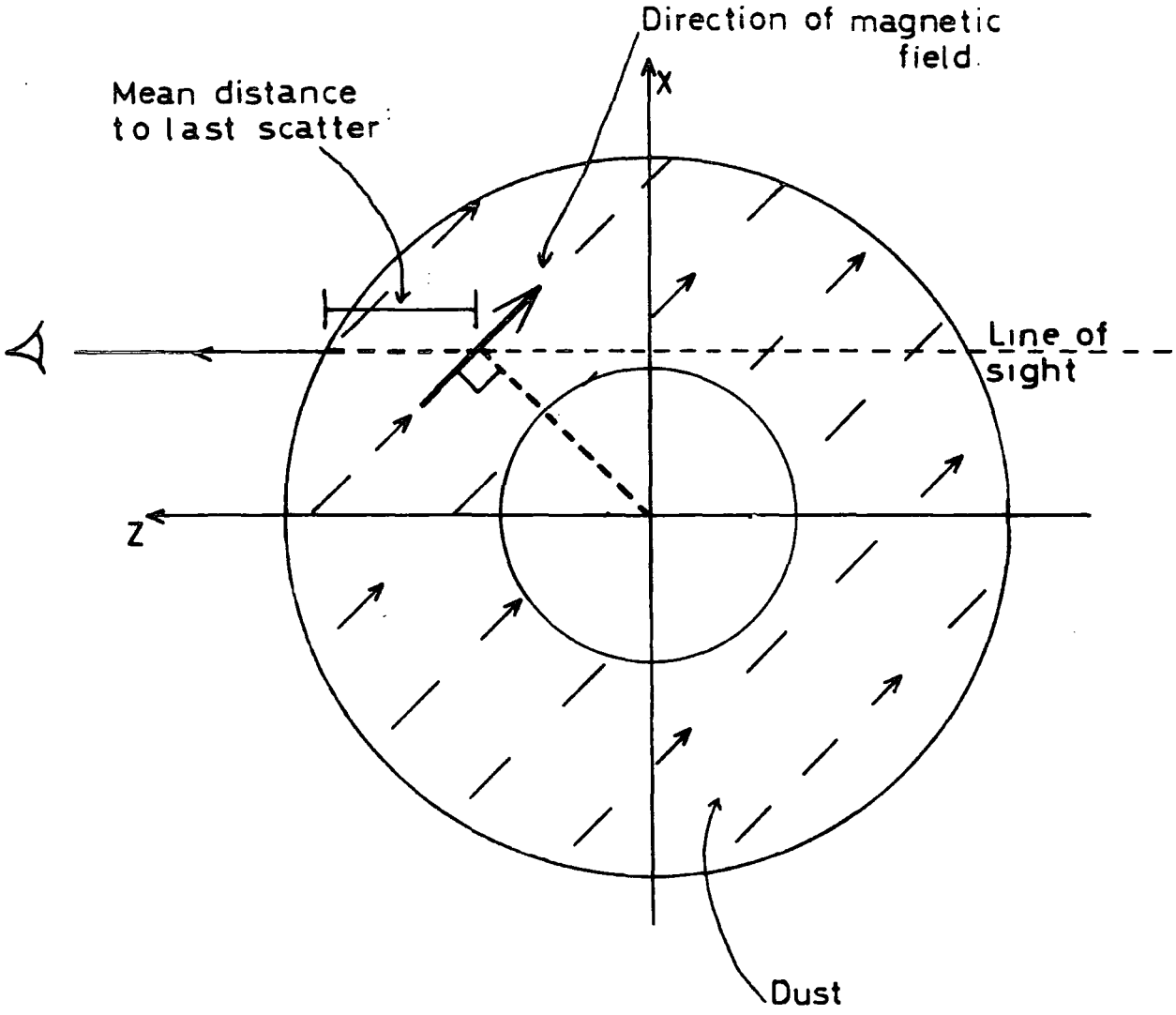

Fig. 5.16
The arrows indicate the direction of the magnetic field assumed to be responsible for the alignment of the non-spherical grains. The field is parallel throughout the model, but its direction varies with each line of sight, such that it is perpendicular to the radius vector at a position on the line of sight corresponding to the mean position of the photons final scatter, (this distance will be one optical depth for lines of sight which pass through the central regions of the dust lane).

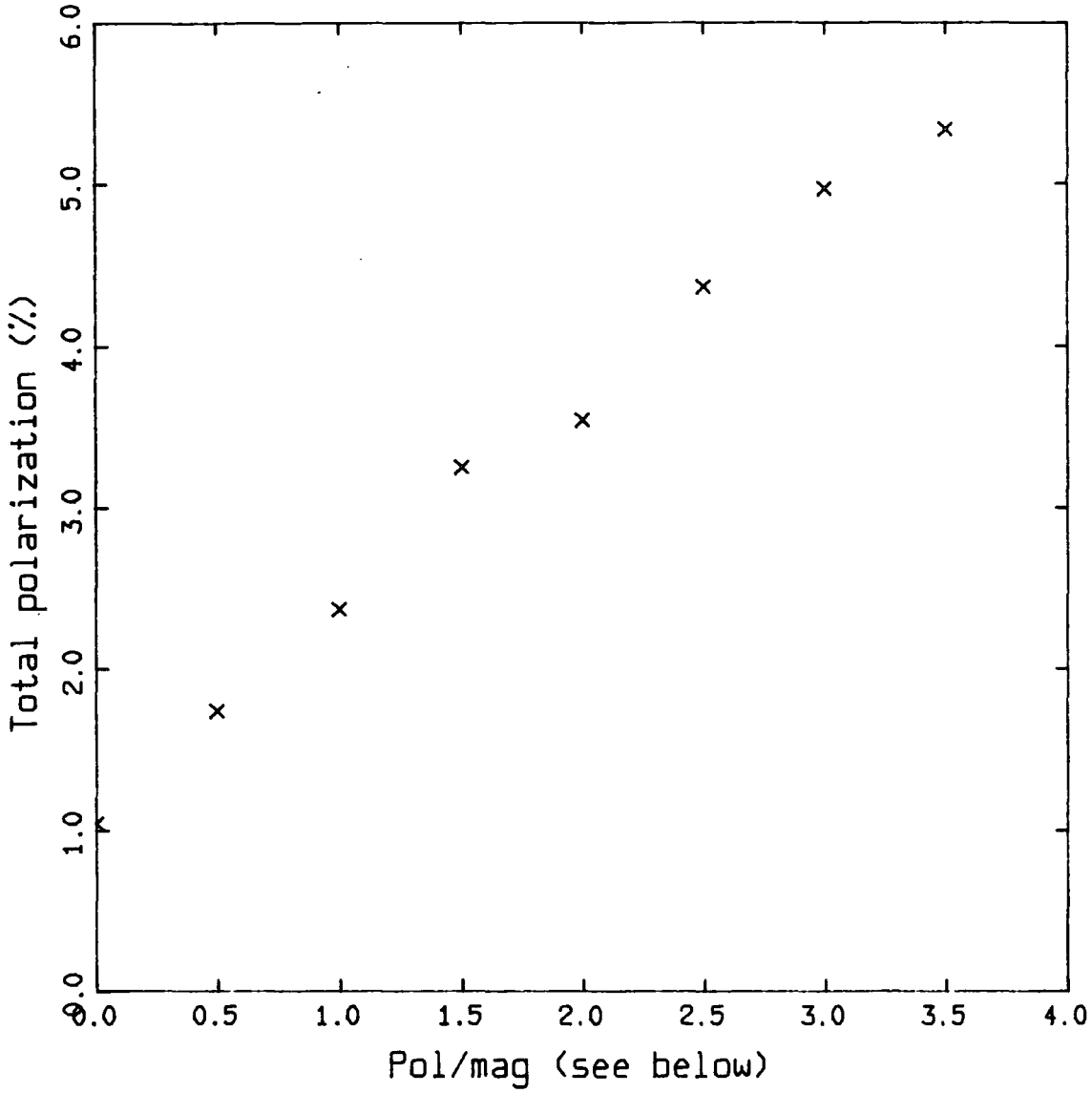

Fig. 5.17
The total polarization estimated by the model for a line of sight near the galactic centre, in terms of the magnetic field/dust grain combination (measured by the polarization produced per magnitude of extinction for unpolarized incident light). The refractive index used to produce this plot was 1.3-0.05i.

That the slope is constant and near unity is indicative of the fact that the average extinction suffered by each photon is one magnitude. To produce the required 4% polarization a field which produces 2 to 2.5 % polarization per magnitude is required. The corresponding polarization map is shown in fig. 5.18 and, for comparison, a map with the same refractive index but no magnetic field is shown in fig. 5.19. A plot of total polarization against the magnetic field, using the original refractive index of 1.65-0.05i is shown in fig. 5.20. With this refractive index a field which produces 3.5% per magnitude of extinction is required to produce a total polarization of 4% and the corresponding polarization map is shown in fig. 5.21.

5.5 Conclusion

A Monte-Carlo model of light scattering within an NGC5128-like system has been run many times with different combinations of model parameters. In the absence of aligned, non-spherical grains, none of these parameter combinations produced polarizations as high as the 4% found in the data.

The inclusion of non-spherical grains in the model, aligned by some process such as the Davies-Greenstein paramagnetic relaxation mechanism, makes

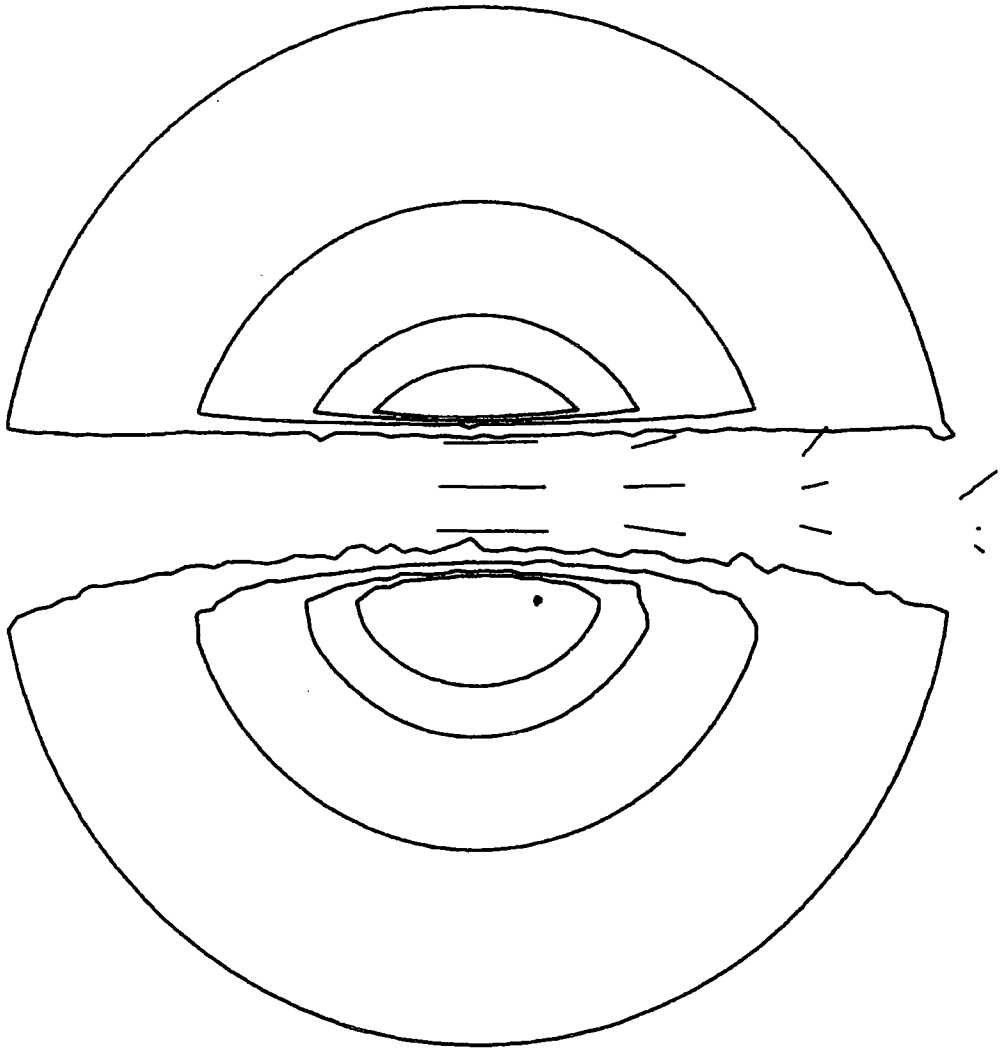

——— 5 % Polarization

Fig. 5.18
The polarization map produced by the model with a refractive index of 1.3-0.05i and with a magnetic field which produces 2.5 % polarization per magnitude of extinction for unpolarized incident light. The degree of polarization in the central dust lane region is 3.9 %.

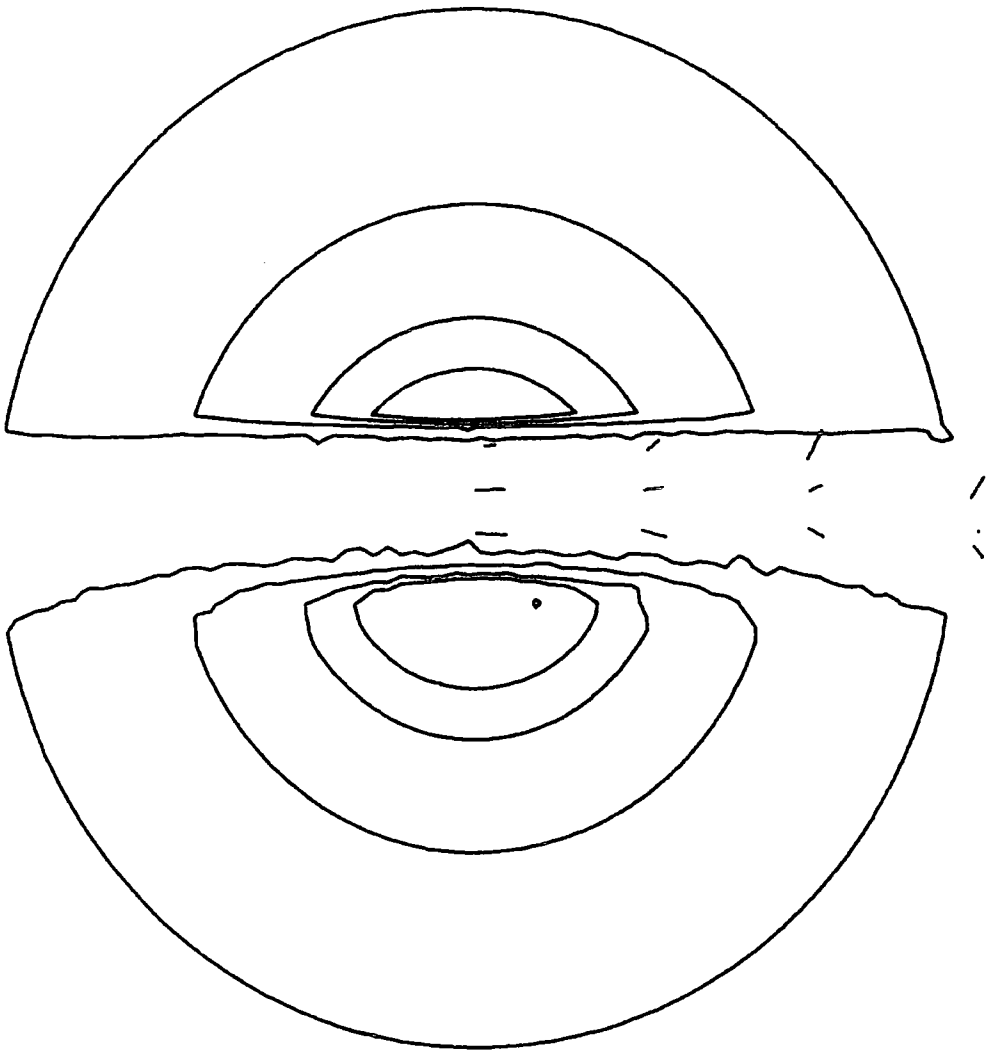

——— 5 % Polarization

Fig. 5.19
The polarization map produced by the model with a refractive index of 1.3-0.05i but with no magnetic field. The degree of polarization in the central dust lane region is 1.1%.

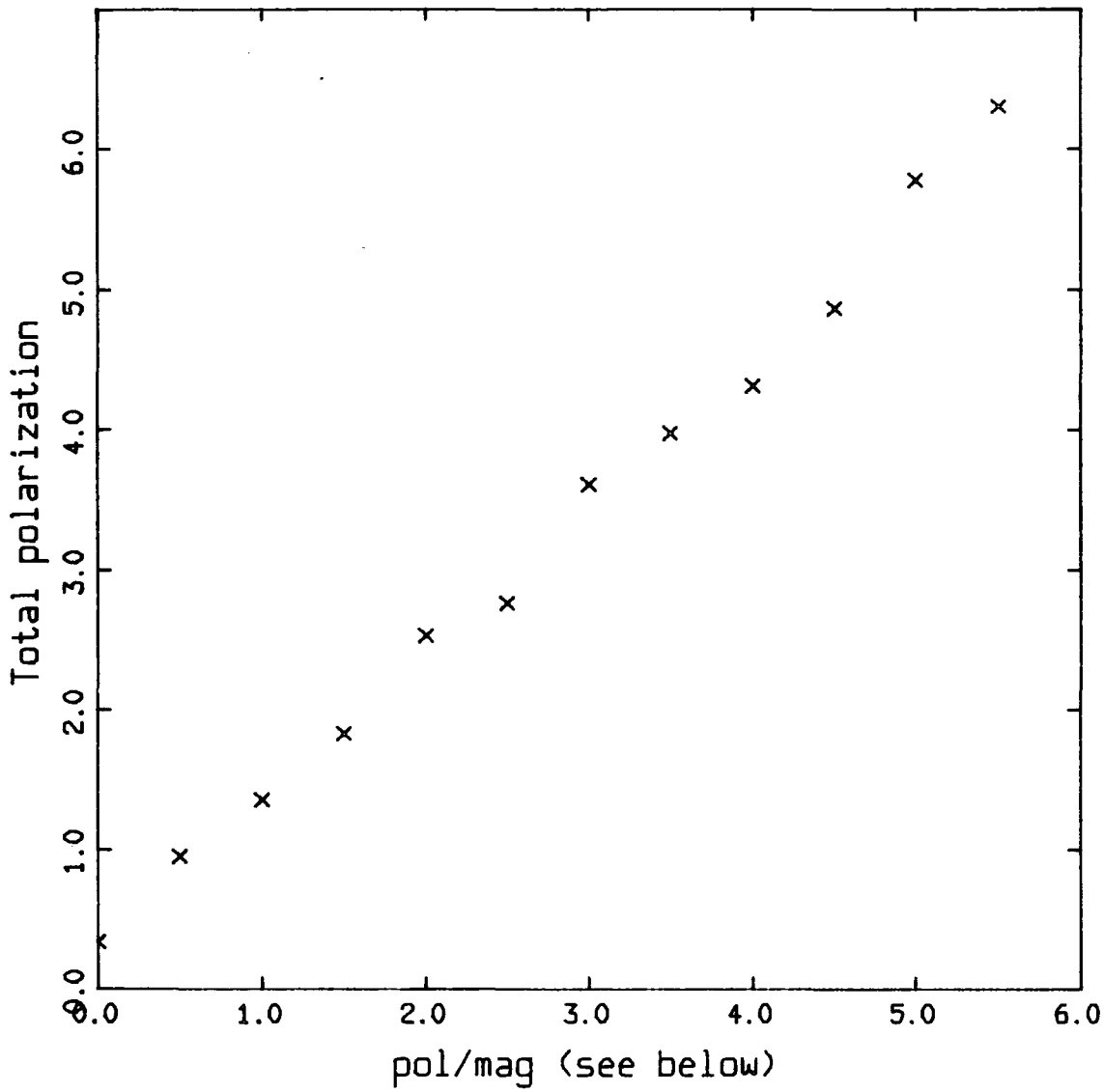

Fig. 5.20
The total polarization estimated by the model for a line of sight near the galactic centre, in terms of the magnetic field/dust grain combination (measured by the polarization produced per magnitude of extinction for unpolarized incident light). The refractive index used to produce this plot was the initial value of 1.65-0.05i.

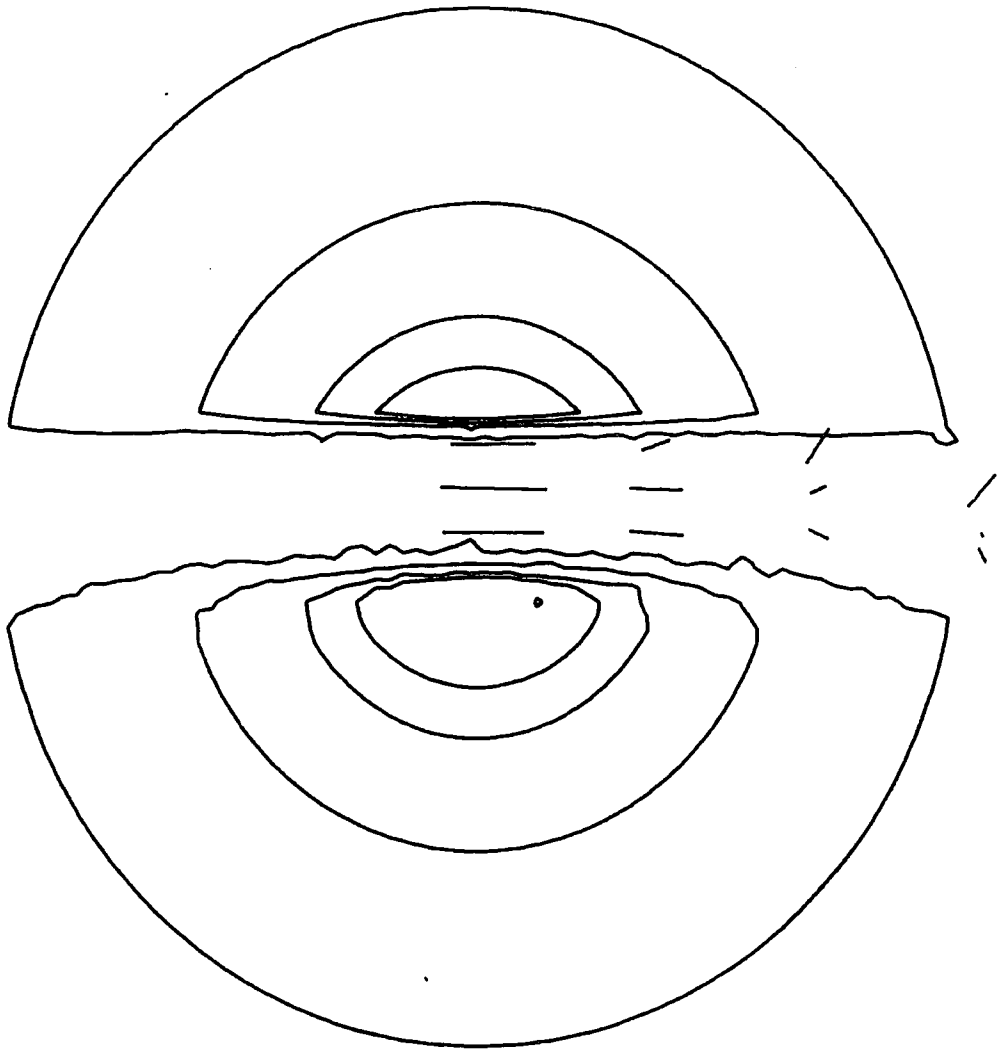

——— 5 % Polarization

Fig. 5.21
The polarization map produced by the model with the initial value for the refractive index of 1.65-0.05i and with a magnetic field which produces 3.5 % polarization per magnitude of extinction for unpolarized incident light. The degree of polarization in the central dust lane region is 3.9 %.

it possible to produce the required 4% without the need for a predominance of small particles. A field is required which produces at least 2.5% polarization per magnitude of extinction for unpolarized incident light, although if the refractive index of the grains correspond to silicates, a slightly higher value of 3% is required.

Although no extensive procedure to minimize the difference between the model results and the data by continuously varying the parameters has been attemted, all the results so far obtained from the model tend to support the evidence from the data, that the polarization is produced by extinction and scattering in a cloud of aligned, non-spherical grains, and also that if the alignment is produced by a magnetic field, then the magnetic field probably has a strength very similar to that in our own Galaxy.

CHAPTER 6

DISCUSSION

6.1 Summary

High resolution electronographic data has been used to produce a polarization map of the peculiar galaxy NGC5128. The structure of the polarization, and a correlation between the degree of polarization and the average extinction through the dust, suggest that grains aligned by a toroidal magnetic field similar in strength to that in our Galaxy, could explain the observed polarization.

A computer program using the technique of backward Monte-Carlo simulation has been developed to model the scattering of photons originating in extended

sources, such as galaxies. The program has been used to calculate the expected polarizations in an idealized NGC5128-like system, using a range of different parameter values and assumptions.

The results indicate that it is unlikely that the polarization observed in NGC5128 could be caused by simple scattering alone, and confirms the hypothesis suggested by the data, that the polarization is caused by grains aligned by a toroidal magnetic field comparable in strength to that in our Galaxy.

6.2 Dynamical Considerations

The presence of a magnetic field in the disk component of NGC5128 could have a significant effect on the dynamics of the associated gas and dust, due to the phenomenon of "Flux Freezing".

Charged particles moving in a magnetic field experience forces which tend to make the particles move in spiral paths around the magnetic flux lines. Uncharged particles do not experience this force but will also tend to move parallel to the flux lines due to the damping of other velocity components by collisions with charged particles. If the gas and dust is forced to move normally to the flux lines (by strong gravitational forces for instance) then the motion of the charged particles, which

constitutes a current, will tend to set up a magnetic field such that the flux lines appear to be dragged along with the gas. Thus the flux lines appear to be frozen into the dust and gas (the process is described fully by Parker, 1979).

The large amounts of ionizing radiation in the D component of NGC5128 (some ten times that in our own Galaxy; Ebneter and Balick, 1983) suggests that there is a high density of charged particles in the disk, and so flux freezing could well be operative.

The effects of flux freezing on the overall dynamics of the dust and gas, can be measured by the significance of the magnetic forces compared to other active forces (predominently gravity). If the magnetic field is strong, compared to the other forces, then a stress will be imparted to the gas and dust which oppose any movement perpendicular to the flux lines. Previous studies of the dynamics of the gas and dust (e.g. the computer simulations of galaxy mergers performed by Tubbs, 1980) have not included any magnetic effects, and their results could consequently be in error if the magnetic field in NGC5128 is strong enough.

To determine the overall significance of the magnetic field, the energy density of the magnetic field can be compared to the gravitational potential energy density at some position within the D component. The

magnetic energy density is

$$Em = \frac{B^2}{\mu_0} \qquad \text{(Joules/m}^3\text{)}$$

where B is the flux density in Webers/m^2 and μ_0 is the permeability of free space. The gravitational potential energy density is

$$Eg = \rho.\phi \qquad \text{(Joules/m}^2\text{)}$$

where ρ is the density of the gas and dust at some point within the disk and ϕ is the gravitational potential at that point. Given a total mass of NGC5128 of 5×10^{11} Mo (Malin, 1983) and an effective radius of 5 Kpc (derived in chapter 3, assuming a distance of 5 Mpc to NGC5128), ϕ can be calculated from the tables of functions for spherical galaxies produced by Young (1976), and is found to be 10^{12} J/Kg at a distance of one effective radius from the galactic centre. The density of the gas and dust is difficult to estimate, but assuming a mass of 2×10^9 Mo for HI and HII (Ebneter and Balick, 1983), that the mass of the dust is insignificant (Jura, 1979, estimates 0.005 for the dust to gas ratio in disk galaxies), and that the disk is 1 Kpc thick and 5 Kpc in radius, gives a density of 5×10^{-22} Kg/m^3. So

$$Eg \simeq 5 \times 10^{-10} \quad J/m^3$$

Assuming a value of 5 μG (= 5×10^{-10}) gives

$$Em \simeq 10^{-13} \quad J/m^3$$

thus

$$\frac{Em}{Eg} \simeq 10^{-3}$$

and so the magnetic field is unlikely to have a significant effect on the motion of the gas and dust. Instead, the flux lines will be dragged around with the gas due to flux freezing as described earlier. The values used in the above calculation are uncertain, but the values used have been chosen to maximise the ratio Em/Eg, and so 10^{-3} is an upper limit for the ratio of magnetic to gravitational energy.

6.3 The Origins of the Magnetic field

If one assumes that the current appearance of NGC5128 was caused by the collision of a normal giant elliptical galaxy with a small gas rich spiral (see chapter 2), than the easist possible explanation of the origin of the magnetic field is that it originally belonged to the spiral galaxy and remained frozen into the gas and dust during the collision. The existence of a magnetic field within our own Galaxy is well established (see Heiles, 1976), and the similarity of the dust and field strength in NGC5128, to those in our Galaxy, add

weight to the idea that the field originally belonged to a spiral galaxy.

One of the difficulties with this explanation is that one would expect the turbulence caused by a collision between two such galaxies to effectively disrupt and randomize the magnetic field structure, causing the large scale field to collapse. Tubbs (1980) shows that after such a collision , as the dust and gas settle into the plane of symetry, the dust and gas at larger radial distances rotate more slowly than that at smaller radial distances, consequently shearing occurs within the dust and tends to "wind up" the magnetic field due to flux freezing. Thus, after a sufficiently long length of time, a toroidal field could be developed, and thus remove the difficulty to the above explanation of the fields origin.

In previous studies of galaxy mergers, the effects of a magnetic field in determining the dynamics of the gas and dust, and the possibilities of using the present form of the magnetic field as a constraint on evolutionary models, have not been considered. Such studies could lead to significant findings concerning the origin and nature of objects such as NGC5128.

REFERENCES

Appenzeller, I. and Mollenhoff, C. 1980, Astr. and Ap., 81 ,54.

Baade, W., and Minkowski, R. 1954, Ap.J., 119 ,215.

Balick, B. and Heckman, T.M. 1982, Ann. Rev. Astr. and Ap. 20, 431.

Bertola, F. and Galletta, G. 1978. Ap.J.(letters), 226 ,L115.

Blanco, V.M., Graham, J.A., Lasker, B.M., and Osmer, P.S. 1975, Ap.J.(letters), 198 ,L63.

Brodie, J., Konigl, A. and Bowyer, S. 1983, Ap.J., 273 ,154.

Bolton, J.G., Stanley, G.J., and Slee, O.B. 1949, Nature, 164, 101.

Bowyer, C.S., Lampton, M., Mack, J. and de Mendonca, F. 1970, Ap.J.(letters), 161 ,L1.

Burbidge, E.M. and Burbidge, G.R. 1957, Ap.J., 125 ,1.

" " " " " 1959, Ap.J., 129 ,271.

" " " " " 1962, Nature, 194 ,367.

Burns, J.O., Feigelson, E.D., Schreier, E.J. 1983, Ap.J., 273, 128.

Carter, D. 1978, M.N.R.A.S, 182 ,797.

Carter, D.G., Blattner, W.G., Wells, M.B., and Horak, H.G. 1972, App. Opt., 11 ,2684.

Collins, L.L., Horak, H.G., and Sandford, M.T. 1978, Jour. Comp. Phys. 26 ,119.

Culhane, J.L. 1978, Quart.J.R.A.S., 19 ,1.

Davies, L. and Greenstein, J.L. 1951, Ap.J., 114 ,206.

de Vaucouleurs, G. 1948, Ann. d'Ap., 11 ,247.

" " " 1975, "Galaxies and the Universe" ,
Ed. A. Sandage, M. Sandage, and J. Kristian
(Chicago: University of Chicago Press)

" " " 1979, A.J. , 74 ,1270.

Dufour, R.J. and van den Burgh, S. 1978a, Sky and Telescope,
56 ,389.

" " 1978b, Ap.J.(letters), 226,
L73.

Dufour, R.J., van den Burgh, S., Harvel, C.A., Margins, D.H.,
Schiffer III, F.H., Talbot Jr., R.J., Talent, D.L.,
and Wells, D.C. 1979, A.J., 84 ,284.

Ebneter, K. and Balick, B. 1983, P.A.S.P., 95 ,675.

Elvius, A. and Hall, J.S. 1964, Lowell Obs. Bull., 6 ,123.

Elvius, A. 1978, Ap. Space Sci., 55 ,49.

Evans, D.S. 1949, M.N.R.A.S., 109 ,94.

Graham, J.A. 1979, Ap.J., 232 ,60.

Graham, J.A. and Price, R.M. 1981, Ap.J., 247 ,813.

Grasdalen, G.L. and Joyce, R.R. 1976, Ap.J., 208 ,317.

Greenberg, J.M. 1978,in "Cosmic Dust" (Ed. McDonnell)
(Wiley,Chichester)

Gregory, C.C.L. 1921, Helwan Obs. Bull., 21 ,201.

Grindlay, J.E. 1975, Ap.J., 199 ,49.

Grindlay, J.E.W., Helmken, H.F., Hanbury-Brown, R., Davies, J.
and Allen, L.R. 1975, Ap.J.(letters), 197 ,L9.

Gunn, J.E. and Gott, J.R. 1972. Ap.J., 176 ,1.

Hall, J.S. 1949, Science, 109 ,166.

Hammersley, J.M. and Handscombe, D.C. 1975, "Monte-Carlo Methods" (London: Methuen)

Harding, P., Jones, T.J., and Rodgers, A.W. 1981, Ap.J., 251 ,530.

Hawarden, T.G., Elson, R.A.W.., Longmore, A.J., Triton, S.B., and Corwin, Jr., H.G. 1981, M.N.R.A.S., 196 ,747.

Heiles, C. 1976, Ann. Rev. Astr. and Astrophys. , 14 ,1.

Herschel, J.F.W. 1847, "Results of Astronomical Observations at the Cape of Good Hope" (London:Smith, Elder),pp.20,105.

Hiltner, W.A. 1949, Science, 109 ,471.

Hubble, E.,1922, Ap.J., 56 ,162.

Illingworth, G.D. 1977, Ap.J.(letters), 218 ,L43.

Johnson, H.M. 1963, Pub. Nat. Radio Astron. Obs., 1 ,251.

Johnson, P.E. 1982, Nature , 295 ,371.

Jura, M. 1978, Ap.J., 223 ,421.

" " 1979, Ap.J., 229 ,485.

" " 1982, Ap.J., 258 ,59.

Kellerman, K.I., Clarke, B.G., Niell, A.E., and Shaffer, D.B., 1975, Ap.J.(Letters), 197 ,L113.

Kunkel, W.E. and Bradt, H.V. 1971, Ap.J.(letters), 170 ,L7.

Longair, M.S. "High Energy Astrophysics" (Cambridge University Press).

Malin, D.F., Quinn, P.J., and Graham, J.A. 1983, Ap.J., 272 ,L5.

Mathis, J.S., Rumpl, W. and Nordsieck, K.H. 1977, Ap.J., 217 ,425.

McLean, I.S., Aspin, C. and Reitsema, H. 1983, Nature, 304 ,243.

Mercelin, M., Boulestix, J., Courtes, G., and Milliard, B. 1982,

Nature, 297 ,38.

Mie, G. 1908, Ann. Physik, 25 ,377.

Mills, B.Y. 1952, Nature, 170 ,1062.

Mollenhoff, C. 1981, Astr. and Ap., 93 ,248.

Nandy, K. 1965, Pub. Roy. Obs. Edinburgh, 5 ,13.

Ostriker, J.P., and Hausman, M.A. 1977, Ap.J.(letters), 217 ,L125.

Parker, E.N. 1979, "Cosmical Magnetic Fields" (Clarendon, Oxford)

Phillips, M.M. 1981, M.N.R.A.S., 197 ,659.

Purcell, E.M. and Spitzer, L. 1971, Ap.J., 167 ,31.

Quinn, P.J. 1982a, Dissertation, Australian Nat. Obs.

" " 1982b, in "Internal Kinematics and Dynamics of Galaxies, I.A.U. Symposium No. 100, E. Athanassoula, ed. (Dordrecht: Reidel), P.347.

Lord Rayleigh 1871, Phil. Mag., 41 ,107,274,447.

Roark, T., Roark, B., and Collins, G.W. 1974, Ap.J., 190 ,67.

Rodgers, A.W. 1978, Ap.J.(letters), 219 ,L7.

Rodgers, A.W. and Harding, P. 1980, Ap.J.(letters), 236 ,L17.

Sandage, A.R. 1973, Ap.J., 183 ,731.

Sandage, A.R., and Tammann, G.A. 1974, Ap.J., 194 ,551.

Scarrott, S.M., Warren-Smith, R.F., Pallister, W.S., Axon, D.J. and Bingham, R.G. 1983, M.N.R.A.S., 204 ,1163.

Schweizer, F. 1980, Ap.J., 237 ,303.

Sersic, J.L. 1958, Observatory, 78 ,24.

" 1969, Nature, 224 ,253.

" 1982, "Extragalactic Astronomy", (Dordrecht:Reidel)

Telesco, C.M. 1978, Ap.J.(letters), 226 ,L125.

Tubbs, A.D. 1980, Ap.J. , 241 ,969.

van Albada, T.S., Kotanyi, C.G., and Schwarzchild, M. 1982, M.N.R.A.S., 198 ,303.

van den Burgh, S. 1976, Ap.J., 208 ,673.

van de Hulst, H.C. 1957, "Light Scattering by Small Particles", (New York: Wiley).

Visvanathan, N. 1974, in "Planets, Stars and Nebulae studied with photopolarimetry" (University of Arizona Press, Tucson)

Warren-Smith, R.F. 1983, M.N.R.A.S., 205 ,349.

" " 1979, Thesis (University of Durham)

Webster, B.L., Goss, W.M., Hawarden, T.G., Longmore, A.J., and Mebold, U. 1979, M.N.R.A.S., 186 ,31.

Wickramasinghe, N.C. 1973, "Light Scattering Functions For Small Particles With Applications In Astronomy", (Hilger, London)

Young, P.J., 1976, Ap.J., 81 ,807.

ACKNOWLEDGEMENTS

The author would like to thank his academic supervisor, Dr. S.M. Scarrott for his continued support over the period of this research. A great debt of thanks is also owed to Dr. R.F. Warren-Smith, for his lucid explanation of simulation techniques and his patience with the many questions put to him by the author concerning the use of both NUMAC and Starlink computers. Dr. J.V. Shirt and the other members of the Durham Polarimetry group should also be thanked for their friendship and encouragement over the course of this research.

Thanks are due also to the staff of the NUMAC and Starlink computer systems, and especially the manager of the Durham Starlink node, Mr. A.P. Lotts.

The Science and Engineering Research Council, and the University of Durham are thanked for their financial support, both while in Durham and during observing trips abroad.

Finally, the author would like to thank his wife, Carol, both for her help in proof reading this text, and for her moral support during the research.

APPENDIX A

A.1 Rotation of the Reference Direction of a Stokes Vector

Let a light beam be described by a Stokes vector $\underline{S}=(I,Q,U,V)$ with respect to some reference direction, where the Stokes parameters are given by equation 1.5 (see section 1.1.4.1)

$$\begin{aligned} I &= a^2 \\ Q &= a^2.\mathrm{Cos}(2\beta).\mathrm{Cos}(2\alpha) \\ U &= a^2.\mathrm{Cos}(2\beta).\mathrm{Sin}(2\alpha) \\ V &= a^2.\mathrm{Sin}(2\beta) \end{aligned} \qquad \text{a.1}$$

Here, α is the angle between the reference direction and the major axis of the ellipse describing the polarization. If the reference direction is changed, then the Stokes vector is changed to $\underline{S}'$, where

$$\underline{S}' = R.\underline{S}$$

and R is a 4x4 matrix to be derived in this section of the appendix. The effect of a rotation of the reference direction is to change α by some amount θ equal to

the angle through which the reference direction is rotated. So the Stokes parameters of $\underline{S}'$ can be calculated from equation a.1 by replacing α by $(\alpha+\theta)$, so:

$$I' = a^2$$

$$Q' = a^2.\mathrm{Cos}(2\beta).\mathrm{Cos}(2\alpha+\theta)$$

$$U' = a^2.\mathrm{Cos}(2\beta).\mathrm{Sin}(2\alpha+\theta)$$

$$V' = a^2.\mathrm{Sin}(2\beta)$$

Therefore

$$I' = a^2$$

$$Q' = a^2.\mathrm{Cos}(2\beta).(\mathrm{Cos}2\alpha.\mathrm{Cos}2\theta - \mathrm{Sin}2\alpha.\mathrm{Sin}2\theta)$$

$$= Q.\mathrm{Cos}(2\theta) - U.\mathrm{Sin}(2\theta)$$

$$U' = a^2.\mathrm{Cos}(2\beta).(\mathrm{Sin}2\alpha.\mathrm{Cos}2\theta + \mathrm{Sin}2\theta.\mathrm{Cos}2\alpha)$$

$$= Q.\mathrm{Sin}(2\theta) + U.\mathrm{Cos}(2\theta)$$

$$V' = a^2.\mathrm{Sin}(2\beta)$$

$$= V$$

and so

$$R = \begin{pmatrix} 1 & 0 & 0 & 0 \\ 0 & \mathrm{Cos}2\theta & -\mathrm{Sin}2\theta & 0 \\ 0 & \mathrm{Sin}2\theta & \mathrm{Cos}2\theta & 0 \\ 0 & 0 & 0 & 1 \end{pmatrix}$$

A.2 The Action of an Ideal Polarizer

To simplify the derivation of the matrix which describes the action of an ideal polarizer, the reference

direction of the incident Stokes vector is first rotated by an angle θ so that the new reference direction is parallel to the axis of the polarizer. This results in a Stokes vector $\underline{S}'$, where $\underline{S}'=R(\theta).S$. An ideal polarizer completely removes the component of the incident E vector which is perpendicular to the polarizers axis. Thus, if the Stokes vector before passing through the polarizer is (from equation 1.4):

$$I' = a_y^2 + a_x^2$$

$$Q' = a_y^2 - a_x^2$$

$$U' = a_y . a_x . \mathrm{Cos}\delta$$

$$V' = a_y . a_x . \mathrm{Sin}\delta$$

then the Stokes vector of the beam after passing through the polarizer will be $\underline{S}''$, obtained from $\underline{S}'$ by setting $a_x=0$ in the above equations. So

$$I'' = a_y^2 = 0.5*(I'+Q')$$

$$Q'' = a_y^2 = 0.5*(I'+Q')$$

$$U'' = 0$$

$$V'' = 0$$

This transformation can be described by the matrix

$$0.5*\begin{pmatrix} 1 & 1 & 0 & 0 \\ 1 & 1 & 0 & 0 \\ 0 & 0 & 0 & 0 \\ 0 & 0 & 0 & 0 \end{pmatrix}$$

APPENDIX A

After considering the polarizer, the final step in the derivation is to rotate the reference direction of $\underline{S}''$ through an angle $-\theta$, back to the original direction. So the total transformation is

$$R(-\theta)*0.5*\begin{pmatrix} 1 & 1 & 0 & 0 \\ 1 & 1 & 0 & 0 \\ 0 & 0 & 0 & 0 \\ 0 & 0 & 0 & 0 \end{pmatrix}*R(\theta)$$

which is equivalent to

$$0.5*\begin{pmatrix} 1 & \text{Cos}2\theta & -\text{Sin}2\theta & 0 \\ \text{Cos}2\theta & \text{Cos}^2 2\theta & -\text{Sin}2\theta.\text{Cos}2\theta & 0 \\ -\text{Sin}2\theta & -\text{Sin}2\theta.\text{Cos}2\theta & \text{Sin}^2 2\theta & 0 \\ 0 & 0 & 0 & 0 \end{pmatrix}$$